THE INVESTIGATION OF THE GENETIC AND PHARMACOLOGICAL INHIBITION OF STRIATAL-ENRICHED PROTEIN TYROSINE PHOSPHATASE (STEP) AND ITS ROLE IN HIPPOCAMPAL EXCITABILITY AND SEIZURE PROPENSITY

BY

JENNIFER M. WALTERS

DISSERTATION

Submitted in partial fulfillment of the requirements
for the degree of Doctor of Philosophy in Neuroscience
in the Graduate College of the
University of Illinois Urbana-Champaign, 2022

Urbana, Illinois

Doctoral Committee:

Associate Professor Hee Jung Chung, Chair and Director of Research
Associate Professor Catherine A Christian-Hinman
Associate Professor Daniel A Llano
Associate Professor Lori T Raetzman

ABSTRACT

Temporal Lobe Epilepsy (TLE) is the most common form of focal-onset epilepsy in adults and accounts for 60% of epileptic patients [1]. In mesial TLE, seizures often begin in the hippocampus and progressively worsen over time. Current anti-seizure drugs are ineffective for approximately 75% of the patients with advanced mesial TLE, leading to severe consequences including hippocampal sclerosis, high mortality rate, cognitive decline, depression, and temporal lobe resection [1]. Furthermore, dysregulation of intrinsic excitability and synaptic transmission has been widely thought to underlie hippocampal hyperactivity that drives the development of spontaneous seizures in TLE [2], underscoring a critical need to identify the underlying mechanisms and novel therapeutic targets. STriatal-Enriched protein tyrosine Phosphatase (STEP) is a brain-specific tyrosine phosphatase – membrane-bound $STEP_{61}$ is the only isoform expressed in the hippocampus and cortex. Genetic deletion of STEP enhances excitatory synaptic currents and long-term potentiation in the hippocampus. However, whether $STEP_{61}$ affects seizure susceptibility is unclear. The goal of this dissertation is to investigate the effects of STEP inhibitor TC-2153 and genetic STEP knockout (KO) on seizure propensity and hippocampal excitability. **Chapter 1** covers a comprehensive review of STEP and its effect on neuronal excitability and synaptic regulation, as well as the therapeutic potential of STEP inhibition for patients experiencing detrimental neurological disorders. **Chapter 2** presents our manuscript [3] published in *Epilepsia* journal investigating the role of TC-2153 on hippocampal network excitability and seizure severity. By combining techniques such as *in vivo* kainate-induced seizure modeling using a murine system, GCaMP6s calcium imaging, and electrophysiology, our study revealed that TC-2153 treatment significantly reduced kainate-induced seizure severity, with greater effects seen in females. Ovariectomy of females abolished the TC-2153-induced decrease in seizure severity. TC-2153 application significantly decreased overall hyperexcitability of acute hippocampal slices from both sexes. Surprisingly, TC-2153 treatment also hyperpolarized resting membrane potential and decreased firing rate, sag voltage, and hyperpolarization-induced currents of cultured hippocampal pyramidal neurons *in vitro*. **Chapter 3** discusses our project investigating the effects of spontaneous recurrent seizure development using a repeated, low-dose kainate injection model in a homozygous STEP KO strain. We also demonstrate that STEP expression changes in the hippocampus upon neuronal injury using a cortical controlled impact (CCI) model to induce

traumatic brain injury (TBI), which is known to cause epilepsy. In **Appendix A**, I included the contributions I made to the manuscript our lab published in *Neurobiology of Disease*, which investigate the impact of epileptic encephalopathy mutations on $K_v7.2$ expression. **Appendix B** includes a paper published in *Scientific Reports* from one of my first projects involved in looking at the effects of kainate-induced stress on PC2 expression in the hippocampus. **Appendix C** covers our preliminary results investigating how the application of TC-2153 impacts the potassium chloride-evoked activity of neurons and astrocytes derived from mouse neural progenitor stems cells. Our lab's goal for this project is to advance our collaboration with Dr. Jack Parent at the University of Michigan and examine the effects of TC-2153 on a human iPSC-derived model of differentiated neurons.

ACKNOWLEDGEMENTS

Foremost, I would like to thank my advisor, Dr. Hee Jung Chung, for her constant support and guidance throughout my PhD journey. She is truly passionate for her work and for her students; she wants to see everyone succeed. Over the last five years, Dr. Chung has not only prepared me with the skills necessary to prosper in research, but she has also taught me valuable lessons in life that I will never forget.

I would also like to thank my past and present colleagues in Chung lab: Dr. Jiaren Zhang, Dr. Eung Chang Kim, Dr. Brian Baculis, and Gregory Tracy. I sincerely miss our outings together on campus to find some (seriously) spicy ramen and boba tea. I will always cherish the conversations we had and the way we encouraged and supported each other through the failed experiments, exam preparations, and crazy life happenings. To that end, I am obliged to have had the pleasure of mentoring several wonderful undergraduate and graduate students: Allison Houghton, Braesen Raeder, Archit Bajaj, and Emma Bridgeman. It was a wonderful experience to watch their confidence grow as researchers.

I would like to thank my committee members, Drs. Catherine Christian-Hinman, Daniel Llano, and Lori Raetzman, for their keen insights and suggestions on my research projects and scientific manuscripts. I would also like to thank the MBM program, specifically Dr. Martha Gillette, my co-advisor Dr. Hyunjoon Kong, and our program manager Anne McKinney for providing me with such a wonderful opportunity to be exposed to new, cutting-edge research and supporting the latter half of my journey through graduate school. In addition, I would like to sincerely thank Stephanie Pregent and Sam Beshers from the Neuroscience Program, two incredible individuals who care so much for the students of their program. They provided me with immense support through my PhD, and I will always be grateful for their kindness.

I would also like to thank Dr. Rhanor Gillette, my previous undergraduate research advisor, for instilling in me the belief that anything is possible if you are willing to work hard enough for it.

Importantly, I would like to thank my husband, Austin Walters, for providing me with his endless support, love, and home-cooked meals after arduous experiments and late nights. He is my rock, and I could not have done any of this without the compassion and encouragement from him and my three children. I would also like to thank my parents and my in-laws for their personal support as well as tending to the care of our children.

Finally, I would like to thank and commemorate my uncle, Julius Eric Friedman, for being my role model through life. After developing what began as petit mal seizures as a young child, over time his seizures progressed to be devastating, debilitating, and drug-resistant until adulthood. He was enthralled with life and never let his circumstances bring him down. He ultimately obtained his Juris Doctorate and eventually opened his own law practice. At the age of 34, he passed away from Sudden Unexpected Death in Epilepsy. He always believed in the unity of people and that everyone has instilled within them the potential for goodness. My uncle brought happiness to everyone in his life – he will always be celebrated, and never forgotten, for the impacts he made on this world.

DEDICATION

In memory of my uncle, Mr. Julius Eric Friedman, J.D.

TABLE OF CONTENTS

CHAPTER 1: THE ROLE OF STEP IN SEIZURES AND NEURONAL NETWORK EXCITABILITY

1.1 Introduction

STriatal-Enriched protein tyrosine Phosphatase (STEP) is a central nervous system-rich protein that is associated with and implicated in numerous neurological disorders involving neurodegeneration, impaired memory, and disruption of synaptic function. STEP downregulates key substrates glutamate receptors N-methyl-D-aspartate (NMDA) and α-amino-3-hydroxyle-5-methyl-4-isoxazolepropionic acid (AMPA) by dephosphorylating designated tyrosine residues, thus internalizing them. STEP also inactivates extracellular signal-regulated kinases 1 and 2 (ERK1/2), p38 mitogen-activated protein kinase, Fyn and Pyk2 kinases by dephosphorylation. Many of these substrates are necessary for synaptic strengthening and glutamatergic receptor trafficking. Emerging evidence implicates STEP's role in hyperexcitability disease. Recent work from my thesis research and other laboratories suggests that STEP reduces seizure susceptibility and neuronal intrinsic excitability in acute seizure models of both acute pharmacological inhibition and genetic knockout models of STEP. High levels of STEP are present within patients and models of Alzheimer's Disease and schizophrenia, as well as animal models of fragile X syndrome – all of which exhibit hyperexcitable phenotypes and synaptic dysfunction. This chapter will provide a comprehensive review on STEP function and its regulation and discuss STEP's contribution to brain hyperexcitability and the underlying potential mechanisms.

1.2 STEP Structure and Expression

STriatal-Enriched protein tyrosine Phosphatase (STEP) is a brain-specific tyrosine (Tyr) phosphatase that is highly expressed in the central nervous system, except for the cerebellum and is encoded by the *PTPN5* gene [4] (Fig. 1.1). Similar to other protein tyrosine phosphatases (PTPs), STEP contains a catalytically active signature consensus sequence [I/V]HCxAGxxR[S/T]G at its C-terminus [5 6]. Downstream from this catalytic sequence is the Kinase Interacting Motif (or KIM domain), which is involved in binding to all of STEP's known substrates [5 7 8]. The *PTPN5* gene is alternatively spliced to produce four main isoforms of STEP – $STEP_{38}$, $STEP_{20}$, $STEP_{46}$, and $STEP_{61}$. The first two isoforms, $STEP_{38}$ and $STEP_{20}$, do not contain the signature consensus

sequence – thus, these isoforms are catalytically inactive [9 6 10 11]. The remaining two isoforms, $STEP_{46}$ and $STEP_{61}$, are considered the main STEP variants (Fig. 1.1).

Both $STEP_{46}$ and $STEP_{61}$ isoforms contain this critical signature consensus sequence for catalytic activity and are differentially expressed in various brain regions and at developmental times [6 12 13]. Specifically, $STEP_{61}$ is found in multiple brain regions, notably the hippocampus, neocortex, striatum, and central nucleus of the amygdala, whereas $STEP_{46}$ is mainly expressed in the striatum, nucleus accumbens, and amygdala and optic nerve [10 14]. Additionally, $STEP_{61}$ contains a 172 amino acid sequence at its N-terminus, which contains two hydrophobic domains required to tether $STEP_{61}$ to the endoplasmic reticulum and, importantly, the postsynaptic density of dendritic spines [12 15]. $STEP_{61}$ also contains two proline-rich regions which contribute to (along with the KIM domain) substrate binding and specificity – the first region is required for binding to Fyn [16], while the second is necessary for binding to Pyk2 [17] (Fig. 1.2). Importantly, both STEP isoforms are found in excitatory as well as inhibitory neurons [18], in addition to glia [14 19].

In terms of developmental expression, $STEP_{61}$ is expressed abundantly through the lifespan from birth to adulthood, while $STEP_{46}$ is not expressed until postnatal day 6, continues to increase throughout the first postnatal month, and finally plateaus to adult levels [13 20]. Recently, it was found that PTPN5 is expressed specifically within the murine pituitary in a developmental manner, where expression significantly increases during the 8^{th} and 16^{th} week of development. PTPN5 expression is shown to heavily reduce after ovary removal [21].

1.3 STEP Regulation and Function

The main function of catalytically active STEP isoforms is to remove the phosphate groups from specific tyrosine residues of the main substrates of STEP, which leads to their internalization or deactivation. STEP itself is regulated via phosphorylation by protein kinase A (PKA) in two separate ways – the first is by the direct phosphorylation of $STEP_{61}$ and $STEP_{46}$ at regulatory serine (Ser^{221}) within the KIM domain [22], which provides steric hindrance, in turn preventing STEP from binding to its substrates. PKA also phosphorylates DARPP-32, which is a potent inhibitor of protein phosphatase 1 (PP1) – PP1 dephosphorylates STEP at its regulatory serine residue. This results in the indirect inhibition of STEP by PKA, since the inhibition of PP1 by DARPP-32

maintains STEP phosphorylation and reduces the overall level of active STEP in the system [23](Fig. 1.3).

1.4 Main STEP substrates

Foremost, both active isoforms $STEP_{61}$ and $STEP_{46}$ dephosphorylate two members of the mitogen-activated protein kinase (MAPK) family: the extracellular signal-regulated kinases 1 and 2 (ERK1/2) [24 25] are dephosphorylated at Tyr^{187} or Tyr^{204}, respectively [26 27] and p38 [28 29 30] at Tyr^{182} [31 28]. When phosphorylated, ERK1/2 activates transcription factors CREB and Elk1 [26], while p38 requires dual phosphorylation of Thr^{180} and Tyr^{182} in order to initiate cell death pathways, activate proapoptotic proteins, and regulate transcription factors [32]. The phosphate removal at designated Tyr residues by STEP ultimately results in the inactivation of these substrates by limiting their ability to initiate transcription (Fig. 1.2).

Both N-methyl-D-aspartate receptors (NMDARs) and α-amino-3-hydroxyle-5-methyl-4-isoxazolepropionic acid receptors (AMPARs) mediate excitatory synaptic transmission based on their levels of postsynaptic expression [33], and STEP is a regulator of the Tyr phosphorylation and surface density of both excitatory receptors [34 35 36 37]. Dynamic changes in postsynaptic levels of NMDARs and AMPARs that affect excitatory synaptic transmission also mediates the expression of homeostatic synaptic plasticity. NMDAR subunit GluN2B [38] and AMPAR subunit GluA2 [34] are also critical, as their dephosphorylation results in receptor internalization from the postsynaptic membrane) [39 36 35 34 40]. Specifically, $STEP_{61}$ regulates the phosphorylation of the GluN2B subunit of NMDARs at Tyr^{1472} using two pathways: directly by the dephosphorylation of GluN2B and indirectly by the inactivation of nonreceptor tyrosine kinase Fyn that phosphorylates GluN2B at that site [16, 39]. Once dephosphorylated by $STEP_{61}$, Tyr^{1472} residue of GluN2B binds to clathrin adaptor proteins and promotes the internalization of GluN1/GluN2B receptors [38]. Additionally, $STEP_{61}$ dephosphorylates the GluA2 subunit of AMPARs at Tyr^{869}, Tyr^{873}, and Tyr^{876} (3Tyr), which results in their internalization [34] (Fig. 1.2).

A recent study investigating and isolating the $STEP_{61}$ interactome has also shown that this particular variant interacts with numerous binding partners, including (but not limited to): cytoskeleton and motor proteins (e.g. MAP2, α-actinin, Arp2/3 complex), vesicle trafficking proteins (e.g. AP-2, Rab3a), kinases and phosphatases (e.g. Fyn, PKA, PP1, PP2A), and ion

channels (e.g. GluN2B, GluA2, mGluR5), as well as a variety of scaffolding proteins (e.g. PSD-95, GPCR signaling proteins, ATPase/ATP synthase, ubiquitin enzyme proteins (e.g. Nedd4), and cell adhesion proteins [41]. Numerous of these identified interactions with STEP are its main binding proteins (i.e., GluN2B, GluA2, and Fyn). It has also been recently identified interactor that PSD-95 is an interactor of STEP by inducing its degradation via the proteasome, in turn stabilizing surface NMDARs [42](Fig. 1.2). Various other proteins modulate STEP activity specifically, such as PKA and PP1. In addition, E3 ubiquitin-protein ligases, such as Nedd4, RNF14, and KCMF1, were isolated within the STEP interactome, which remains consistent with previous studies demonstrating $STEP_{61}$'s ubiquitination [35, 42].

1.5 Role of STEP in Synaptic Plasticity via NMDA and AMPA Receptor Regulation

The $STEP_{61}$ isoform expressed in the hippocampus and cortex [12] plays a large role in glutamatergic synaptic transmission. The current model of STEP function is that it typically opposes synaptic strengthening by dephosphorylating its key synaptic substrates. The $STEP_{61}$ isoform has an extra 172 amino acids at its N-terminus, which contains two hydrophobic domains required for its targeting to the endoplasmic reticulum and postsynaptic density of dendritic spines [12, 15]. Notably, it is the dephosphorylation of Tyr residues by $STEP_{61}$ and the surface density of glutamatergic NMDA and AMPA receptors that associates it with the postsynaptic density [34, 36, 37]. $STEP_{61}$ dephosphorylates main glutamate receptors, the NMDA receptor subunit GluN2B at Tyr^{1472} and AMPA receptor subunit GluA2 at $Tyr^{869/873/876}$ (3Tyr), which results in their internalization [34, 38](Fig. 1.2). STEP has a significant effect on NMDAR function – for instance, high levels of STEP decrease NMDAR-mediated postsynaptic currents (EPSCs) and prevents high-frequency stimulation LTP from occurring [43]. NMDAR-mediated EPSCs are enhanced and LTP is blocked using a monoclonal antibody against a portion of STEP located outside of the catalytic domain [12], which was also shown to inhibit the function of STEP, but not other protein tyrosine phosphatases (PTPs) [43]. Administering non-competitive NMDAR agonist dizocilpine (MK801) and a Src family kinase inhibitory peptide also prevents the enhancement of NMDAR-mediated EPSCs, suggesting that STEP has a role of being a "tonic brake" on LTP by opposing Src family kinase-mediated enhancement of NMDAR activity [43].

AMPA receptors are also implicated in synaptic strengthening and memory consolidation – AMPARs are ligand-gated ion channels composed of subunits GluA1 to GluA4. They regulate

fast synaptic transmission that depolarizes postsynaptic membranes and activates NMDARs [44, 45]. AMPAR internalization occurs in LTD and seems to be regulated by STEP [34, 46, 47]. It was found that STEP regulates the Tyr dephosphorylation of the GluA2 subunit, which leads to the internalization of GluA1/GluA2 receptor complexes post-mGluR stimulation [34]. Activation of mGluRs by agonist DHPG also increases local translation of STEP, which results in tyrosine dephosphorylation of GluA2 and internalization of GluA1/GluA2 receptor complexes [34]. DHPG also induces the dephosphorylation of GluA2 and the internalization of AMPARs – this is decreased by the substrate-trapping protein TAT-STEP (C to S). It has been shown that STEP knockout (KO) neuronal cultures do not undergo DHPG-mediated AMPAR endocytosis while this endocytosis is restored by adding wild-type TAT-STEP protein to STEP KO cultures. This ultimately suggests that STEP activated by mGluR stimulation dephosphorylates GluA2, thus promoting their internalization [34, 48]. Recently, by utilizing mass spectrometry, more light has been shed on the interlinkages of the $STEP_{61}$ interactome, specifically on $STEP_{61}$'s relation to AMPARs. It has been shown that $STEP_{61}$ binds to the C-termini of GluA2 and GluA3, as well as endogenous AMPARs in the hippocampus. Specifically, within the STEP KO mouse brain, synaptic expression of both GluA2 and GluA3 subunits is increased. Further, it was shown that the knockdown of STEP in hippocampal slices increases AMPAR-mediated currents, whereas $STEP_{61}$ overexpression reduced synaptic expression of AMPARs. $STEP_{61}$ also regulates synaptic AMPARs by modulating lysosomal degradation. These findings define $STEP_{61}$'s critical role in organizing synaptic AMPARs [41].

To test if $STEP_{61}$ serves as a key modulator of these glutamatergic receptors during homeostatic synaptic plasticity, our laboratory first investigated if $STEP_{61}$ expression and/or activity is regulated during the induction of this plasticity. Jang et al. showed that prolonged hippocampal network activity blockade for 48 hours using sodium channel blocker tetrodotoxin (TTX) induced synaptic scaling in dissociated hippocampal cultured neurons and reduced $STEP_{61}$ mRNA and protein expression compared to control treatments. TTX treatment for 36-48 hours also enhanced Ser^{221} phosphorylation indicated decreased $STEP_{61}$ activity. In contrast, prolonged activity enhancement for 48 hours using $GABA_A$ receptor antagonist bicuculline (BC) increased $STEP_{61}$ protein levels. BC treatment for 36-48 hours reduced Ser^{221} phosphorylation, which indicated increased $STEP_{61}$ activity [40].

Jang et al. further showed using mEPSC recording that these prolonged alterations of hippocampal network activity, using either TTX or BC bidirectionally, regulate Tyr-phosphorylation of GluN2B and GluA2 subunits of NMDA and AMPA receptors, respectively. Overall, this study revealed that homeostatic scaling occurs in a STEP-dependent manner. Prolonged TTX treatment increased the amount of Tyr^{1472}-phosphorylated GluN2B (GluN2B-pY1472) and 3Tyr-phopshorylated GluA2 (GluA2-p3Y), which was consistent with the decreased level of $STEP_{61}$ activity seen due to TTX treatment. On the other hand, prolonged BC treatment decreased the levels of GluN2B-pY1472 and GluA2-p3Y, as well as increased $STEP_{61}$ level and activity. Enhancing STEP activity by administering TAT-STEP WT versus TAT-myc prior to the TTX-induced recording revealed that increased STEP blocks synaptic scaling – the TTX-induced synaptic scaling was abolished by the TAT-STEP WT preincubation [40].

Intriguingly, the BC-induced activity enhancement increased $STEP_{61}$ and decreased the Tyr-phosphorylation of GluN2B and GluA2, but did not induce synaptic down-scaling [40]. It may be that $STEP_{61}$ upregulation internalizes extrasynaptic GluN2B and GluA2. Previous studies have shown that activity-dependent AMPAR endocytosis occurs extrasynaptically [49] and requires GluA2 [50] and that GluN2B-containing NMDARs are extrasynaptically enriched and undergo endocytosis [38, 51, 52]. Jang et al. hypothesize that this $STEP_{61}$-dependent decrease in GluA2 and GluN2B abundance due to BC-induction may be an additional homeostatic mechanism in place to limit or prevent overstimulation and excitotoxicity [40].

1.6 Role of STEP in Synaptic Plasticity via MAPK, Fyn, or Pyk2 Inactivation

$STEP_{61}$ also dephosphorylates main substrates that are members of the mitogen-activated protein kinase (MAPK) family, such as extracellular signal-regulated kinases 1 and 2 (ERK1/2) and p38. $STEP_{61}$ dephosphorylates the regulatory Tyr^{204} or Tyr^{187} residues within the respective activation loops of ERK1/2, therefore resulting in their inactivation (Fig. 1.2). This is critical regarding its effect on glutamatergic synaptic transmission since ERK1/2 activation is necessary for the development of synaptic strengthening. Specifically, it's implicated in synaptic plasticity and memory formation through its role in stabilizing dendritic spines, initiating local protein synthesis in dendrites and spines, and its involvement in nuclear transcription [26, 27]. P38, on the other hand, is dephosphorylated and deactivated by $STEP_{61}$ within its activation loop at Tyr^{182} [28, 31]. It is involved in regulating cell death pathways and NMDAR-mediated excitotoxicity [53, 54]. When there

is increased glutamate signaling, extrasynaptic NMDARs are engaged and promote calpain cleavage of $STEP_{61}$ within its kinase interacting motif (KIM) domain, resulting in the production of $STEP_{33}$ which is unable to bind to substrates. This extrasynaptic stimulation and the subsequent cleavage of $STEP_{61}$ into $STEP_{33}$ ultimately activates p38 and cell death pathways. When a peptide that corresponded to the calpain cleavage site was used to prevent this $STEP_{61}$ cleavage, neurons were significantly protected from glutamate-mediated excitotoxicity [28].

$STEP_{61}$ has also been shown to directly dephosphorylate and inactivate nonreceptor tyrosine kinase Fyn at Tyr^{420} [16], which phosphorylates the GluN2B subunit of NMDARs at the same phosphorylation site that $STEP_{61}$ regulates (Tyr^{1472}) [16, 39](Fig. 1.2). Lastly, $STEP_{61}$ regulates proline-rich tyrosine kinase 2, or Pyk2, which is a member of the focal adhesion kinase family that is highly expressed in the brain [55] and plays a role in synaptic plasticity and the induction of LTP [56]. $STEP_{61}$ directly binds and dephosphorylates Pyk2 at Tyr^{402}, which ultimately leads to its inactivation, as well as its downstream signaling pathways, such as Pyk2's phosphorylation and activation of Src and Fyn (Fig. 1.2), as well as Pyk2's role as a docking site for the SH2 domain of each of these kinases [57, 58]. In addition, Pyk2 activation results in its postsynaptic translocation and association with the SH3 domain of PSD-95, which is critical for LTP [56]. It has been previously shown that STEP KO mice displayed enhanced phosphorylation of Pyk2 at Tyr^{402} and its substrates paxillin and ASAP1, confirming that the removal of STEP (and thus removal of its ability to dephosphorylate Pyk2) exerts a functional downstream effect of Pyk2 [17].

1.7 Role of STEP in Learning, Memory, and Behavior

Utilizing a genetic STEP knockout (KO) murine model has revealed novel data on the role of STEP in behavior and neurological disorders. A seminal study published by Venkitaramani et al. found that a double homozygous knockout model of STEP maintained typical neuroanatomy relative to wild-type (WT) littermates – notably in the striatum, hippocampus, and amygdala – and expressed virtually no STEP protein. Mice that were heterozygous for the STEP gene expressed approximately 50% of what was expressed by WT littermates. Surface expression of GluN1/GluN2B receptor complexes is also increased in STEP knockout (KO) mice [59].

In comparison to WT littermates, STEP KO mice display normal behavior by performing baseline locomotor activity in terms of distance traveled in open field tests as well as during rotarod

performance, which is a test designed to assess motor coordination. STEP KO mice show significantly enhanced hippocampal memory, such as improved spatial memory during the Morris water maze test as well as reference memory during radial-arm water maze tests. They elicit normal social behavior in social discrimination tasks, yet differ in that STEP KO mice exert significantly higher levels of dominance compared to WT [48]. However, STEP KO mice display significant deficits in pre-pulse inhibition (PPI), which is a measure of the startle reflex response and sensory motor gaiting. PPI is an autonomic inhibition system that regulates sensory input by filtering out irrelevant or distracting stimuli and is found to be deficient in patients with schizophrenia [60, 61]. Conflicting reports have found that in the elevated zero maze and light/dark test, STEP KO mice experience both anxiogenic-like phenotype compared to WT controls [62]. Overall, no significant difference in behavior is shown [63].

Previous literature investigating the effects of STEP KO on acute seizure models demonstrates that there is a reduced sensitivity to pilocarpine-induced seizures [64] and a diminished response to acutely administered NMDAR antagonist, MK-801 (0.6 mg/kg, i.p.) [65]. However, there is counterevidence offered by one study that found hypersensitivity of STEP KO mice to in response to acute administration of MK-801 (0.178 mg/kg, i.p.) and pentylenetetrazole (PTZ)-induced seizures (80 mg/kg, i.p.) [63], suggesting that STEP KO mice are more susceptible to acute seizures. To address this, it is important to note that pilocarpine-induced seizures and PTZ operate using two different mechanisms of seizure onset. Pilocarpine is a cholinergic muscarinic agonist and induces seizures in rodents after systemic or intracerebral administration. The amygdala, thalamus, olfactory cortex, hippocampus, neocortex, and substantia nigra are the most sensitive regions to epilepsy-related damage produced by pilocarpine [66], whereas PTZ is a GABA antagonist . The difference in results could also be age-dependent, as the former study tested the effects of MK-801 in mice 6-8 months of age (around 24-32 weeks old) [65], whereas the latter study tested mice that were 4-5 months of age (16-20 weeks old) [63] (Table 1.1).

Furthermore, it is theorized that BDNF level in AD patients is associated with reduced cortical cholinergic synapses, where BDNF dysregulation may affect cholinergic synapses and overall impact synaptic plasticity [67]. Altering BDNF expression or the BDNF/TrkB signaling pathway may go on to induce synapse loss and overall synaptic function [68], and the early downregulation of BDNF in AD is associated with severity of cognitive impairments [69]. In contrast, the

upregulation of BDNF/TrkB mRNA expression, specifically within the hippocampus, is associated with improved memory [70]. Interestingly, it has been shown that when there is a downregulation in BDNF, STEP levels reciprocally increase in vivo, as observed in in BDNF(+/-) mice and after acute BDNF knockdown in cortical cultures [71] – while BDNF signaling has been shown to reduce STEP levels in murine primary cortical neurons and promotes ubiquitin-proteasome system (UPS)-mediated degradation of $STEP_{61}$ in protein extracts obtained from primary cortical cultures [72]. Pharmacologically inhibiting STEP was also shown to reverse motor abnormalities in BDNF(+/-) mice, in which treatment with acute STEP inhibitor TC-2153 (10 mg/kg, i.p.) significantly attenuated increased locomotor activity of these mice in an open-field chamber at 1 hour post-injection, while the locomotion of wild-type mice were not affected. Additionally, TC-2153 administration reversed biochemical abnormalities in BDNF(+/-) mice by increasing phosphorylated levels of STEP substrates GluN2B, Pyk2, and ERK1/2, in synaptic membrane fractions of the frontal cortex [71]. Phosphorylated GluN2B and ERK1/2 have also been shown to increase in neuronal cultures during post-treatment of BDNF or TrkB activation [72]. The culmination of these findings demonstrates that increased STEP in AD patients, as well as animal models, may reflect alterations in BDNF/TrkB signaling.

1.8 Role of STEP in Hyperexcitability Disorder

Many diseases are suggested to be affected by STEP dysregulation. Up-regulation of STEP protein contributes to the pathophysiology of diseases such as Alzheimer's disease (AD) [73], schizophrenia [65], fragile X syndrome (FXS) [62], pilocarpine-induced acute seizure onset [64, 74], and alcohol-induced memory loss [75, 76](Tables 1.1 and 1.2). In contrast, having too little STEP and/or STEP activity has been associated with Huntington's disease [77], drug abuse [23, 78], stroke/ischemia [79], inflammatory pain [62, 80] and thermal hyperalgesia (altered perception of temperature in which normal stimuli may be perceived as pain) [81] – though interestingly, elevated STEP levels and decreased phosphorylation of proteins involved in nociception transduction in hippocampi is observed in APP mice [82]. Specifically, there is emerging evidence that suggests STEP may be a critical molecular target for treating seizures. Deletion of the *PTPN5* STEP gene results in resistance to pilocarpine-induced seizures in a murine model [64] as well as reverses the audiogenic seizure phenotype observed in the FXS mouse model [83]. In the same vein, acute pharmacological inhibition using selective STEP inhibitor TC-2153 is shown to reverse cognitive deficits in a 3xTg

mouse model of AD [73] – these mice are documented to display hippocampal hyperactivity and spontaneous seizures [84, 85]. Aspects of AD observed in human patients and animal models strongly coincide symptomatically with the Temporal Lobe Epilepsy (TLE), the most common form of focal-onset epilepsy in adults accounting for approximately 60% of epileptic patients [1]. In mesial TLE, seizures typically originate in the hippocampus and progressively worsen over time [1]. AD and TLE share several main features related to cognitive dysfunction, pathological and neuroimaging features [86], one of the hallmarks being hippocampal sclerosis [87], or the scarring and hardening of the hippocampal tissue. Notably, patients with drug resistant TLE who experience a higher frequency of seizures have an increased likelihood of having such cognitive comorbidities [88]. Current antiseizure drugs are ineffective for ~75% of patients with advanced mesial TLE, which ultimately leads to severe outcomes, including depression, significant memory loss, cognitive decline, hippocampal sclerosis, temporal lobe resection, and high mortality rate [1, 86]. Ultimately, these disorders – in addition to FXS, schizophrenia –display hyperexcitability phenotypes both in recapitulative models of the disease as well as in diagnosed human patients, and exhibit significantly upregulated STEP expression. We will continue to elaborate on the role of STEP in these diseases as our prime area of focus.

1.9 STEP and its Role in Acute Seizures and TBI

Mesial temporal lobe epilepsy (TLE) is a hyperexcitability disease, in which seizures often begin in the hippocampus and progressively worsen over time [89, 90] to cause hippocampal sclerosis, cognitive decline, and drug-resistant seizures [1]. High levels of $STEP_{61}$ in the hippocampus and cortex are implicated in hyperexcitability disease – one such disorder being epileptogenesis. It is apparent that $STEP_{61}$ weakens excitatory synaptic strength in the hippocampus [36, 43, 47] – thus, seizure susceptibility and propensity would theoretically increase after genetic ablation or pharmacological inhibition of STEP.

However, this is not what is seen in STEP KO mice between 6-8 weeks of age (males and females combined, weight 18-22 g). These mice end up displaying resistance to pilocarpine-induced seizures, associating with higher seizure thresholds when compared to wild-type mice. Furthermore, significantly fewer STEP KO mice develop seizures that progress to the stage of *status epilepticus* (SE) [64], which is generally defined in experimental models as the time between chemoconvulsant administration and the end of behavioral seizure activity [91]. In humans and

rodents alike, this severe period of SE is critical since even a single event can result in breakthrough spontaneous recurrent seizures (which typically occur after a latent period ranging from weeks to years) [92]. It was also found that by electrically stimulating the hippocampal-entorhinal cortical pathway in STEP KO hippocampal slice, there is less activation of the dentate gyrus granule cell layer (GCL) – however, there is *greater* activation of the hilus, compared with heterozygous slices (Table 1.1). These results are intriguing, considering GABAergic hilar neurons expressing STEP undergo excitotoxic cell death (one of the events that occurs during TLE development) following pilocarpine-induced SE. Disrupting STEP function in these neurons via calcineurin inhibitor FK506 to block STEP activity (calcineurin is an upstream activator of STEP [24]) leads to decreased SE-induced hilar interneuron cell death [74] (Table 1.2). Briggs et al. addressed the question of whether the ablation of STEP, specifically in hilar interneurons, will increase resistance to SE development in a pilocarpine model. Their work concludes that a genetic knockout model of STEP demonstrates a seizure-resistant phenotype, and thus propose that the mechanism behind such resistance lies within the reduced excitability of GCL neurons in STEP KO mice. These results raise the question: if the genetic deletion of STEP increases resistance to pilocarpine-induced SE, would the acute pharmacological inhibition of STEP produce a similar phenotype?

Interestingly, wild-type (C57Bl/6J) mice and $SOD^{+/-}$ mice (a model low antioxidant capacity, which contributes to oxidative stress) also show decreased synaptic formation of NMDARs, decreased NMDAR-dependent synaptic current, and increased $STEP_{61}$ activity after being exposed to a traumatic brain injury (TBI) protocol using a controlled frontal impact device [93]. $SOD^{+/-}$ mice also show alterations in cognitive performance. This suggests that $STEP_{61}$ may contributes to neuropathological progression post-TBI and could potentially be used as a biomarker for synaptic damage in traumatic lesions. TBI is a significant trauma to the brain and can lead to the onset of post-traumatic epilepsy and development of TLE, also referred to as post-traumatic TLE [94]. Similarly, the induction of *status epilepticus* (SE) is a form of traumatic injury, particularly achieved by using systemic or focal injection of a chemoconvulsant (e.g. kainate or pilocarpine). It has been shown that loss of GABAergic hilar neurons prominently occurs in excitotoxic cell death during the development of TLE by induction of SE [95]. High levels of STEP have been reported in vulnerable somatostatin-immunoreactive hilar interneurons, and in vivo disruption of STEP activity allows the activation of the MAPK pathway, leading to immediate-early gene expression and significant rescue from cell death after pilocarpine-induced seizures [74].

1.10 Effects of Genetic and Pharmacological Inhibition of STEP on Seizures and Excitability

Acute, selective pharmacological STEP inhibitor TC-2153 (8-(trifluoro-methyl)-1,2,3,4,5-benzopentathiepin-6-amine-hydrochloride) was originally targeted to be a small-molecule inhibitor following the validation of STEP as a possible target for drug discovery [96]. Amino-substituted benzopentathiepin derivatives, such as TC-2153, were shown to maintain reasonable solubility in aqueous solution [97, 98] and TC-2153 itself was shown to have reportedly low levels of acute toxicity (LD 50.1,000 mg/kg) [99]. To determine whether TC-2153 modified the active cysteine residue of STEP, high-resolution tandem mass spectrometry was performed on WT STEP and a catalytic cysteine-to-serine (C to S) STEP mutant for comparison. In the absence of TC-2153, the catalytic Cys^{472} of STEP revealed a disulfide bridge between Cys^{465} and Cys^{472}, which was not present in the STEP (C to S) mutant. The incubation of WT STEP with TC-2153 showed the presence of a *de novo* trisulfide bond within the bridge connecting Cys^{465}/Cys^{472}, which was not observed in WT STEP or mutant STEP alone – ultimately, this analysis suggested that the active cysteine site is modified by TC-2153 and that the sulfur(s) from the benzopentathiepin core is retained, and concluded STEP activity (in the hippocampus and frontal cortex, specifically) to be potently inhibited by TC-2153 [73](Table 1.2).

Pharmacological inhibition of STEP using TC-2153 significantly reduced seizure severity in wild-type mice of both sexes, and subsequent ovariectomy (OVX) rescued the TC-2153-induced seizure reduction in females. TC-2153 application had significantly decreased the overall excitability of acute hippocampal slices from wild-type mice of both sexes, as well as decreased the intrinsic excitability and hyperpolarization-induced currents of cultured hippocampal neurons *in vitro* [100](Table 1.2). These findings ultimately suggest that the antiseizure effects of TC-2153 are mediated by its unexpected action on suppressing neuronal intrinsic excitability. Considering this potential novel mechanism of action, TC-2153 may prove to be a worthy candidate for patients with epilepsy, since there is a critical need for new therapeutic drugs.

1.11 Genetic Ablation of STEP Exerts Age- and Sex-Dependent Effects on Seizure Severity

Since $STEP_{61}$ weakens excitatory synaptic strength in the hippocampus, seizure susceptibility should increase in STEP KO mice which deletes all STEP isoforms [35] (Table 1.1). However, Briggs et al. previously showed that STEP KO mice (at 6-8 weeks of age and of combined sex) are resistant to pilocarpine-induced seizures [64]. STEP KO females at 6-7 weeks and 8-12 weeks of age

show decreasing trends in seizure severity [100] (Table 1.1), which demonstrate that genetic ablation of STEP, especially catalytic $STEP_{46}$ and $STEP_{61}$, most likely affects seizure severity in an age- and sex-dependent manner. It is important to highlight that in rodents 6 to 8 weeks of age, puberty onset coincides with significant changes in sex hormone-dependent synapse formation and circuit maturation in the brain, specifically within the hippocampus and cortex [101, 102]. The 8th week of age in particular designates the end of puberty and the adolescence period [101]. During this time, critical changes in the hippocampal circuitry and synapse formation as a result of fluctuating sex hormone levels may dictate the overall sensitivity to chemoconvulsant, specifically kainate and pilocarpine, which utilize different pathways for inducing limbic seizures [103, 104]. This may explain the age-dependent switch in seizure susceptibility of STEP KO mice observed between the two models.

1.12 Anti-Seizure Effect of the STEP Inhibitor TC-2153

TC-2153 treatment decreased hippocampal excitability and the severity of KA-induced seizures [100] that arise mostly from the hippocampus where KA subtype glutamate receptors are highly expressed, especially in the CA3 region [103]. It is known that TC-2153 inhibits two catalytically active STEP isoforms, $STEP_{46}$ and $STEP_{61}$, though only $STEP_{61}$ is expressed in the hippocampus and neocortex [12]. Thus, most of the anti-seizure effect of TC-2153 is likely mediated by inhibition of $STEP_{61}$ in the hippocampus, though the possibility of inhibiting both catalytically active STEP isoforms in other brain regions contributing to this decreased excitability cannot be excluded.

Particularly, females displayed a greater trend in anti-seizure effect of TC-2153 compared to males – this marked difference was ultimately abolished by OVX [100]. This is not anomalous, since greater anti-seizure potency in females has also been reported for neurosteroids in various acute seizure models [105]. Estrogen has also been shown to exacerbate seizures in women with epilepsy [106] and both estrogen and testosterone increase seizure susceptibility in rodent KA models [107,108]. In contrast, seizure frequency in mice and women with epilepsy is reduced by high progesterone level [106,109]. The potential role of ovarian-derived hormones in seizure susceptibility is interesting since prevalence, frequency, and semiology of focal seizures and TLE have been reported to differ by sex in both clinical patient populations and preclinical animal models due to their neurobiological actions [110].

Excitability of hippocampal slices from both sexes was also reduced following TC-2153 application [100], even after circulating gonadal hormones had washed away while acclimating the slices in ACSF [111]. This suggests that gonadal hormone cannot fully explain the subtle sex difference in the response to TC-2153. Considering that women display higher drug concentration in blood and longer duration for drug metabolism and clearance than men [110], a greater trend in anti-seizure effect in females may arise from higher brain concentration of TC-2153 in females than males. Alternatively, the enhanced seizure severity in OVX females compared to naïve females may also contribute to the diminished efficacy of TC-2153 in OVX females. Future studies shall evaluate ADME properties of TC-2153 in both sexes and use gonadectomy in combination with hormone replacement to confirm whether TC-2153 decreases KA-induced seizure severity by altered pharmacokinetics of TC-2153 or suppressing proconvulsant actions of estrogen or testosterone, and/or potentiating anti-convulsant actions of progesterone.

1.13 Decrease in Hippocampal Intrinsic Excitability as a Proposed Mechanism for Anti-Seizure Effect of TC-2153

TC-2153 application markedly decreased intrinsic excitability of cultured hippocampal pyramidal neurons [100]. This suggests a compelling possibility that $STEP_{61}$ may regulate ionic currents critical for intrinsic neuronal excitability and action potential (AP) waveform, in contrast to its well-known role in weakening synaptic transmission. It is known that the $STEP_{61}$ interacts with various proteins, including ion channels, ion transporters, and signaling proteins important for neuronal excitability and synaptic transmission [41]. In addition, hyperpolarized RMP and decreased R_{in} in TC-2153-treated hippocampal neurons suggest the opening of potassium channels [100]. Among major potassium currents in hippocampal pyramidal neurons [112], fast activating and inactivating I_A and fast activating and slowly inactivating I_D delay the onset of firing and contribute to AP repolarization and firing rate [112, 113]. Slowly activating and inactivating I_K mediates AP repolarization [113], whereas slowly activating and non-inactivating I_M hyperpolarizes resting membrane potential (RMP) and suppresses repetitive firing of APs without affecting their latency [114]. Calcium-activated I_C contributes to fAHP and regulates AP repolarization, firing rate, and half-width [115]. The effects of TC-2153 on ISI, AP rise and decay times, AP half width, and fAHP amplitude [100] suggest that one or more of these potassium currents may be regulated by TC-2153 to control intrinsic excitability and AP waveform.

1.14 I_h as a novel target of TC-2153

TC-2153 treatment is shown to decrease I_h, which contributes to sag voltage and rebound potential evoked by membrane hyperpolarization. The role of I_h in hippocampal neuronal excitability is complex, as I_h exerts both excitatory and inhibitory effects on the ability of an excitatory postsynaptic potential (EPSP) to trigger an AP [116]. HCN1 and HCN2 are preferentially enriched in the distal dendrites of hippocampal CA1 pyramidal neurons [116], where I_h decreases EPSP summation [117], but dendritic excitability can be enhanced or reduced by I_h [118, 119]. I_h can also increase AP firing rate by depolarizing RMP and decreasing R_{in} [120]. Therefore, TC-2153-induced I_h reduction may contribute to hyperpolarized RMP and decreased excitability seen in TC-2153-treated neurons [100].

Finally, the mechanism underlying how TC-2153 decreases I_h is unknown. Activation kinetic of HCN2 channel is regulated by Src phosphorylation of its Tyr^{476}, whereas the receptor-like protein-tyrosine phosphatase-alpha can dephosphorylate HCN2 and decrease its surface and current expression [121], raising the possibility that $STEP_{61}$ may dephosphorylate HCN2, and its inhibition by TC-2153 may ultimately modify HCN2 channel function or expression. Alternatively, TC-2153 may directly bind to and decrease current expression of HCN1 and/or HCN2 channels (Fig. 1.4). The mechanism underlying inhibitory actions of TC-2153 on I_h warrants future studies.

1.15 STEP and its Role in Alzheimer's Disease

Alzheimer's disease (AD) is a chronic, progressive, age-dependent neurodegenerative disorder associated with memory loss and the leading cause of dementia [122] It is characterized by two main pathological hallmarks: the accumulation of amyloid β (Aβ) plaques, in which soluble Aβ oligomers are correlated with memory loss in early stages of AD [123, 124], and neurofibrillary (tau) tangles, where hyperphosphorylation of tau corresponds to memory loss and neurodegeneration [125-127]. Accumulated Aβ disrupts synaptic transmission and disturbs the excitatory and inhibitory balance, contributing to cognitive decline Major changes in both excitatory and inhibitory synaptic strength are associated with this disease, where high Aβ levels are shown to cause synaptic loss, disrupt synaptic transmission, and disturb the excitatory and inhibitory balance [128-131] and to not only decrease glutamatergic synaptic transmission and long-term potentiation (LTP)[132], but also to *increase* long-term depression (LTD) in mouse models of AD [133]. AD is also a hyperexcitability

disease associated with seizure activity and neuronal network dysfunction [134]. Based on the literature, there appears to be strong evidence suggesting that changes in STEP phosphorylation or protein levels may underlie the hyperexcitability seen in AD animal models and patients - notably, it is the Tyr phosphorylation of $STEP_{61}$ and surface density of glutamatergic NMDA and AMPA receptors that associates it with the postsynaptic density [34, 36, 37] and the specific regulation of these receptors contributes to Hebbian LTP. Extrasynaptic NMDAR stimulation also enacts calpain-mediated cleavage of $STEP_{61}$, which in turn selectively activates p38 and promotes cell death [28]. STEP levels are shown to be elevated in the prefrontal cortex of both human Alzheimer's Disease (AD) patients and in animal models of AD (Tg-2576 and J20) [36, 135]. Genetically reducing STEP activity in a triple transgenic AD mouse model by crossing $STEP^{-/-}$ mice with 3xTg-AD mice to produce 3xTg-AD/$STEP^{-/-}$ double mutants showed that a decrease in STEP levels reverses cognitive and cellular deficits observed in these mice, such as spatial reference memory, spatial working memory, and object recognition [35]. Genetically reducing STEP also reversed the loss of glutamate receptors from synaptosomal membranes – phosphorylated-ERK and phosphorylated-Fyn kinase levels increased, as well. Field potentials recorded within the CA1 region in hippocampal slices from 10-mo-old double mutant mice compared with 3xTg-AD mice revealed CA1-LTP were significantly enhanced [36]. Recent findings also show that STEP inhibition improves cognitive function in tandem with increasing synaptic connectivity *in vitro* as well as in the triple transgenic AD mouse model [136].

Amyloid-β (Aβ) oligomers are shown to cause synaptic dysfunction early in AD by enhancing mGluR-dependent LTD via $STEP_{61}$ [137]. Chemical induction of mGluR-LTD by a selective mGluR5 agonist Dihydroxyphenylglycine (DHPG) increases $STEP_{61}$ levels and induces dephosphorylation of AMPAR subunit GluA2 [34]. This mGluR-dependent enhancement of $STEP_{61}$ and LTD is blocked by exogenous application of Reelin [137], a neuromodulator that regulates synaptic plasticity and prevents Aβ toxicity via apolipoprotein E (ApoE) receptors [138]. By contrast, conditional deletion of Reelin increases DHPG-induced $STEP_{61}$ level and calcium-permeable GluA2-lacking AMPARs, and occludes the mGluR-LTD [137]. Since $STEP_{61}$ plays an important role in neurodegeneration [36, 96] and Reelin signaling is impaired by ApoE4 [138], a major risk factor of sporadic AD [139], it is tempting to speculate that downregulation of Reelin signaling by ApoE4 may in part contribute to upregulation of $STEP_{61}$ seen in AD.

Recently, another study was conducted to investigate the effects of a synthetic compound called Dl-3-n-butylphthalide (NBP), which was approved for the treatment of ischemic stroke in China [140]. By exploring the mechanism of NBP therapy in APP/presenilin 1 (PS1) transgenic mice and its involvement in the STEP/ERK/CREB signaling pathway, it was discovered that NBP treatment effectively ameliorated the spatial learning and memory impairment of the APP/PS1 transgenic mice while conducting experiments in the Morris water maze. NBP also reduced amyloid-induced activation of $STEP_{61}$ levels and increased pERK1/2 and pCREB levels in the cortex and hippocampus of APP/PS1 transgenic mice [140]. NBP may serve as an effective treatment for AD by acting through the STEP/ERK/CREB signaling pathway to alleviate cognitive impairment related to AD, reduce STEP levels, and increase its phosphorylated substrate levels.

A few notable hallmarks of neurodegeneration, specifically in patients with AD, are excitotoxicity and neuronal death – it is established that following pilocarpine-induced status epilepticus (SE), STEP-expressing somatostatin-immunoreactive interneurons in the hilus and CA1 region of the hippocampus experience excitotoxic cell death. These neurons were made less susceptible to excitotoxic insult from seizures by disrupting STEP function and ultimately allowing MAPK pathway activation, immediate early gene expression, and significant rescue from cell death [74]. In addition to these findings, it was later discovered that the STEP KO model of mice are more resistant to pilocarpine-induced seizures when compared to their wild-type littermates [64]. The results from Choi et al. suggested that STEP acts to increase neuronal sensitivity to SE-induced excitotoxicity by blocking neuroprotective responses initiated by the MAPK pathway. One of the main STEP substrates, p38 MAPK, is involved in regulating cell death pathways and NMDAR-mediated excitotoxicity.

Seizures, epileptiform activity, and hippocampal network hyperactivity have all been reported in humans in the mild cognitive impairment (MCI) and early stages of AD – for these patients, cognitive decline also began 5 to 7 years earlier in patients with epilepsy compared to patients without [37, 141]. One potential cause underlying hyperexcitability in AD could be that STEP – specifically $STEP_{61}$ – regulates unknown ionic currents critical for maintaining intrinsic neuronal excitability, as similarly observed in hippocampal pyramidal neurons treated with STEP inhibitor TC-2153, where intrinsic excitability was reduced [100]. The interactome of $STEP_{61}$ is vast and interacts with numerous ion channels, ion transporters and signaling proteins that are critical for

proper neuronal excitability and synaptic transmission [41] – specifically, there is a possibility that STEP interacts with and dephosphorylate ion channels such as hyperpolarization-induced cyclic nucleotide (HCN) channels, which produce an I_h current responsible for the control of neuronal burst firing [116]. HCN channel mislocalization has been shown to occur in CA1 pyramidal cells within a rodent model of TLE [142], where auxiliary subunit tetratricopeptide repeat–containing Rab8b-interacting protein (TRIP8b) regulates its subcellular localization and function [143]. Moreover, HCN channel trafficking and gating can be modulated by various other kinases, one of which is p38 MAPK [144]. Intriguingly, acute inhibitor TC-2153 is shown to specifically decrease I_h current in cultured hippocampal pyramidal neurons [3], whether TC-2153 is acting indirectly through STEP or directly modulating HCN channel function is unknown. One suggestion is that STEP has the ability to modulate HCN channels by either direct dephosphorylation of the channel or TRIP8b, or by way of one of its main substrates, such as p38 MAPK (Fig. 1.4).

Alternatively, neural network synchrony and brain oscillatory rhythms are governed by inhibitory GABAergic interneuron activity and that inhibitory interneuron dysfunction is linked to network abnormalities in AD [134]. Here, one likely cause underlying hyperexcitability in AD is that STEP – specifically, $STEP_{61}$ – is recruited and upregulated by Aβ [37] and this level increase may lead to heightened susceptibility to excitotoxicity in GABAergic hilar interneurons, perpetuating the progression of further cell death, decreased inhibition, and neurodegeneration.

1.16 STEP and its Role in Schizophrenia Associated with Hyperexcitability

Schizophrenia (SZ) is a heterogeneous disorder where patients exhibit positive symptoms (i.e. delusions, hallucinations), negative symptoms (i.e. anhedonia, avolition, social withdrawal), and cognitive dysfunction [145]. A proposed contributing factor to the etiology of SZ involves the disruption of glutamatergic signaling, specifically the hypofunction, of NMDARs [146], and it shown that brains of patients with SZ maintain abnormal glutamate receptor densities in the prefrontal cortex, thalamus, and temporal lobe, in addition to decreased receptor function [147, 148]. Interestingly, $STEP_{61}$ levels are significantly higher in the postmortem anterior cingulate cortex and dorsolateral prefrontal cortex of schizophrenia patients, as well as in mice treated with the psychotomimetics MK-801 and phencyclidine (PCP) [65]. This is intriguing, considering the main function of STEP is to dephosphorylate and either inactive or internalize its main substrates, particularly NMDARs and AMPARs. Higher STEP expression would thus lead to reduced

expression of surface glutamatergic receptors, which would likely disrupt glutamatergic signaling and function. STEP inhibition has also been shown to influence models of schizophrenia, such as reversing the behavioral and cognitive deficits in the Nrg1+/− knockout mouse model of schizophrenia [149]. In addition, STEP KO mice are less sensitive to both the locomotor and cognitive effects of acute and chronic administration of phenycyclidine (PCP) [65] . Lastly, it has been shown that chronic treatment using both typical and atypical antipsychotic medications in mice result in PKA-mediated phosphorylation of $STEP_{61}$, resulting in increased surface expression of GluN1/GluN2B receptors – in short, these treatments ultimately restore NMDAR density and proper glutamatergic function to these models [65]. SZ is shown to feature characteristics of a hyperexcitability disease, such as increased cortical excitability and aberrant hippocampal activity [150]. Neurodevelopmental models of SZ also show altered hippocampal excitability, synaptic transmission and synaptic plasticity [151]. Increased STEP expression may underlie the excitability dysfunction observed in SZ by disrupting the density of glutamatergic receptors at the postsynaptic membrane by internalizing NMDARs and AMPARs (while it is well-established that NMDAR antagonists induce psychotic-like symptoms in models of SZ, whereas the results for AMPAR disruption is more controversial [152]).

1.17 STEP and its Role in Fragile X Syndrome and Autism

Fragile X syndrome (FXS) is the leading cause of inherited intellectual disability [153] caused by an increase in the number of repeats of a short nucleotide sequence located in the fragile X mental retardation 1 gene (FMR1) on the X chromosome, which encodes the RNA-binding protein FMRP [154]. Clinical features of FXS include hyperactivity, hypersensitivity, learning disability, and hyperarousal to seizures [155]. In turn, Autism Spectrum Disorder (ASD) is also a form of hyperexcitability disorder in which there appears to be a reduction in synaptic pruning, resulting in higher synapse formation and an increase in dendritic spine number [156]. A particular trait in both FXS and ASD individuals is that they display less neural habituation, or even increased responses to repeated stimuli, resulting in hypersensitivity [157]. Many studies have investigated the role of STEP and its deletion or inhibition in models of FXS and ASD. Inhibition of STEP in a VPA-exposed rodent model of autism shows that behavior deficits such as reduced sociability, repetitive and abnormal anxiety phenotypes associated with ASD are rescued [158]. Previous literature also shows that acute pharmacological inhibition of STEP using TC-2153 induced the reduction of

behavioral hyperactivity, reversal of audiogenic seizures, decrease in dendritic spine density and mGluR-mediated exaggerated LTD in *Fmr1* KO mice [83]. The pharmacological inhibition of STEP has been shown to reduce mGluR-mediated exaggerated long-term depression (LTD) in *Fmr1* KO mice [62]. In cell-based secondary assays, global STEP inhibitor TC-2153 also increased tyrosine phosphorylation of GluA2 and GluN2B, resulting in the internalization of synaptic AMPARs and NMDARs [73]. Genetic STEP deletion also reduces audiogenic seizures in *Fmr1* KO mice and restores specific social and nonsocial anxiety-related behaviors [83]. As suggested by Chatterjee et al., it is possible that significantly upregulated STEP may be involved in the disruption of spine pruning through hyposignaling of the BDNF-TrkB signaling pathway [83], since BDNF plays a critical role in spine maturation and pruning [159].

1.18 Role of STEP in regulating GnRH-induced FSH secretion and PGE2 release from neurons

It was recently found that follicle-stimulating hormone (FSH) secretion in gonadotropes is regulated by PTPN5 by way of its role in binding GnRH to GnRH receptors [21]. Gs-protein kinase A (PKA) and Gq-phospholipases C (PLC) signaling pathways cooperatively regulate GnRH-induced FSH secretion – this work shows that Ca^{2+} influx activates Ca^{2+}-dependent phosphatase calcineurin, leading to the phosphorylation (and thus activation) of PTPN5, and that the intracellular release of Ca^{2+} is reduced by administration of TC-2153. This study concludes that by either blocking or knocking out PTPN5, FSH is reduced in the whole pituitary [21].

Interestingly, a separate investigation of the role of STEP as a key regulator of neuronal release of the proinflammatory prostanoid prostaglandin E2 (PGE2) was also recently conducted [160]. This study portrayed evidence that glutamate-mediated activation of NMDARs in STEP-deficient neurons led to a rapid, sustained increase in p38 MAPK phosphorylation in corticostriatal neuronal cultures at 12-14 days *in vitro*, which were exposed to excitotoxic insult. This sustained p38 MAPK phosphorylation, in the absence of STEP, enhanced activation of cytosolic phospholipase A2 (cPLA2), which is mediated by p38 MAPK and catalyzes the release of arachidonic acid (the initial substrate for PGE2 bionsynthesis) [161] and induced the increase of cyclooxygenase-2 (COX-2) expression, which is involved in the conversion of arachidonic acid to prostanoids [162]. Together, these results were found to significantly increase neuronal PGE2 release from STEP KO neurons within 2 h post-insult. Restoring STEP function to neurons using a STEP mimetic generated from

$STEP_{61}$ (TAT-STEP-myc peptide) was found to significantly decrease activation of the cPLA2/COX-2/PGE2 signaling cascade by attenuating glutamate-induced p38 MAPK activation, COX-2 expression, and PGE2 release in STEP KO cultures. Ultimately, these findings simultaneously identified a mechanism involved in the role of STEP in the release of PGE2 after excitotoxic insult and was the first study to highlight the immunomodulatory ability of a neuronal tyrosine phosphatase.

1.19 Summary

Mesial temporal lobe epilepsy (TLE) is a hyperexcitability disease, in which seizures often begin in the hippocampus and progressively worsen over time [89, 90] to cause hippocampal sclerosis, cognitive decline, and drug-resistant seizures [1]. The molecular players and mechanisms underlying hippocampal hyperactivity that drive the seizure generation in TLE is unknown. STEP may be a good candidate for mitigating seizures in hyperexcitability disease. High levels of $STEP_{61}$ are associated with Alzheimer's disease (AD) [36] and FXS [83]. Pharmacological inhibition of STEP with TC-2153 alleviates excitatory synaptic defects and memory loss observed in AD mouse model [73] and reverses behavioral and synaptic deficits in FXS mouse model [83]. The previous literature demonstrates that STEP dephosphorylates subunits of key glutamate receptors and internalizes them, thereby weakening excitatory synaptic strength [40]; however, the roles of $STEP_{61}$ on susceptibility to seizures that arise from the hippocampus and hippocampal network excitability are not clear. Experiments published by Briggs et al. investigating the effect of pilocarpine-induced seizure susceptibility of a STEP KO murine model shows a reduction in seizures [64]. It has also been found that seizures diminish in the Fmr1 KO murine model when STEP is acutely inhibited [83]. Here, we find many open questions that need to be addressed:

(1) What effect does the genetic ablation or pharmacological inhibition of STEP have on the susceptibility to acute seizures that arise from the hippocampus?

(2) What effect does the genetic ablation or pharmacological inhibition of STEP have on the hippocampal network activity?

(3) Does STEP contribute to neuronal intrinsic excitability and regulate ion channels implicated in controlling intrinsic membrane properties?

(4) Since brain injury (such as injury-causing SE or traumatic brain injury) induces the development of TLE, does STEP expression level change upon brain injury and does STEP play a role in the development of post-traumatic epilepsy in animal models?

To address these questions, my doctoral research aims to investigate and assess the effects of both pharmacologically and genetically removing STEP on seizure severity, as well as determining the role of acutely inhibiting STEP on hippocampal circuitry, intrinsic excitability, and intrinsic membrane properties. The burning questions we wanted to answer were 1) does application of a STEP inhibitor reduce the hyperexcitability observed within the hippocampus, as seen in patients who suffer from TLE and acute seizures, and 2) since TC-2153 reduces the excitability of cultured rat hippocampal pyramidal neurons, will In Chapter 2, I will present our submitted study that delves into the effects of kainic acid-induced seizures in a STEP KO murine model, as well as administering acute STEP inhibitor, TC-2153, in a kainic acid-induced seizure model. We further observe the striking effect of TC-2153 on hippocampal network excitability in acute slice and cultured pyramidal hippocampal neurons [3]. It is well-known that current antiseizure drugs (ASDs) do not work for everyone, especially patients with TLE [1]. Finding small, novel chemicals that can be utilized as ASDs are in critical need – the inhibition of STEP by TC-2153 appears to possess this potential. In Chapter 3, I will present my findings from my project investigating the effects of repeated, low-dose kainate injections on the development and progression of TLE in a STEP KO murine model.

Figures

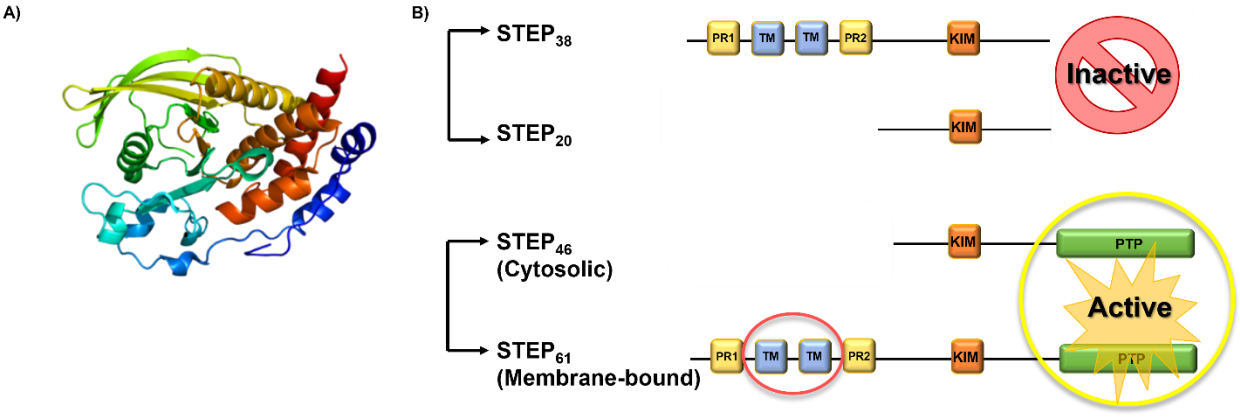

Figure 1.1. (A) Crystal structure of the PTPN5 gene that encodes STEP protein (PDB structure #2BIJ, *Homo sapien*), courtesy of the *Worldwide Protein Data Bank*). **(B)** The four main alternatively spliced isoforms of STEP. PR: Proline-rich region contributing to substrate specificity; TM: transmembrane domains that tether STEP to the plasma membrane of the endoplasmic reticulum and/or PSD; KIM: kinase-interacting motif; PTP: protein tyrosine phosphatase domain.

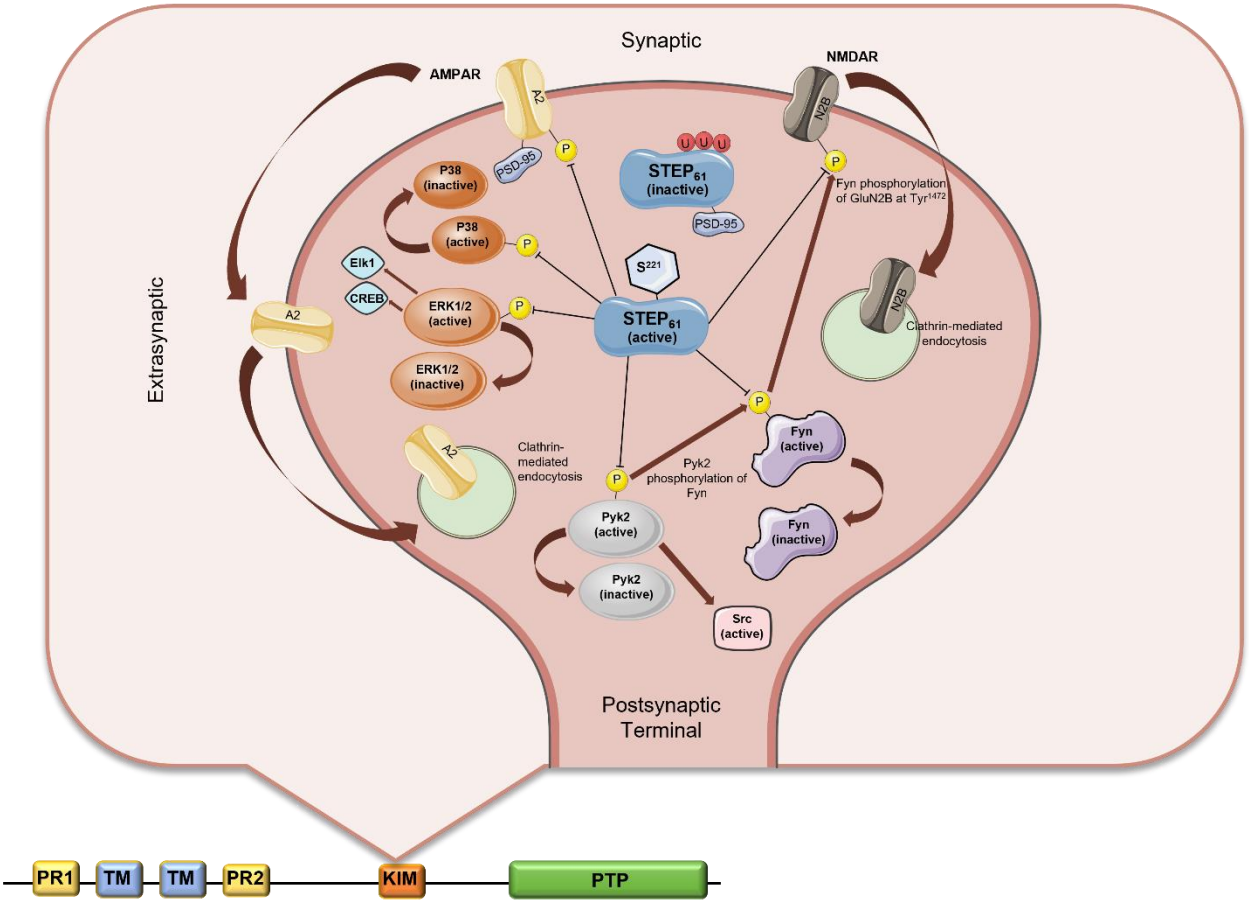

Figure 1.2. The outlined structure of special isoform $STEP_{61}$, its critical domains, and main substrates that inactivates/internalized. The PTP domain contains a catalytically active signature consensus sequence [I/V]HCxAGxxR[S/T]G at its C-terminus. Downstream from this catalytic sequence is the KIM domain, which is involved in binding to all of STEP's known substrates. At its N-terminus, STEP contains a 172 amino acid sequence that contains two hydrophobic domains (TM) that tether STEP to the endoplasmic reticulum or PSD of dendritic spines. STEP also contains two proline-rich regions (PR) that contribute toward its substrate binding and specificity – the first is required for binding to Fyn and the second is required for binding to Pyk2. $STEP_{61}$ dephosphorylates its main substrates at designated Tyr residues: ERK1/2 at Tyr^{187} or Tyr^{204}, respectively; p38 at Tyr^{182}; NMDARs at Tyr^{1472}; AMPARs at Tyr^{869}, Tyr^{873}, and Tyr^{876} (3Tyr); Fyn at Tyr^{420}; and Pyk2 at Tyr^{402}.

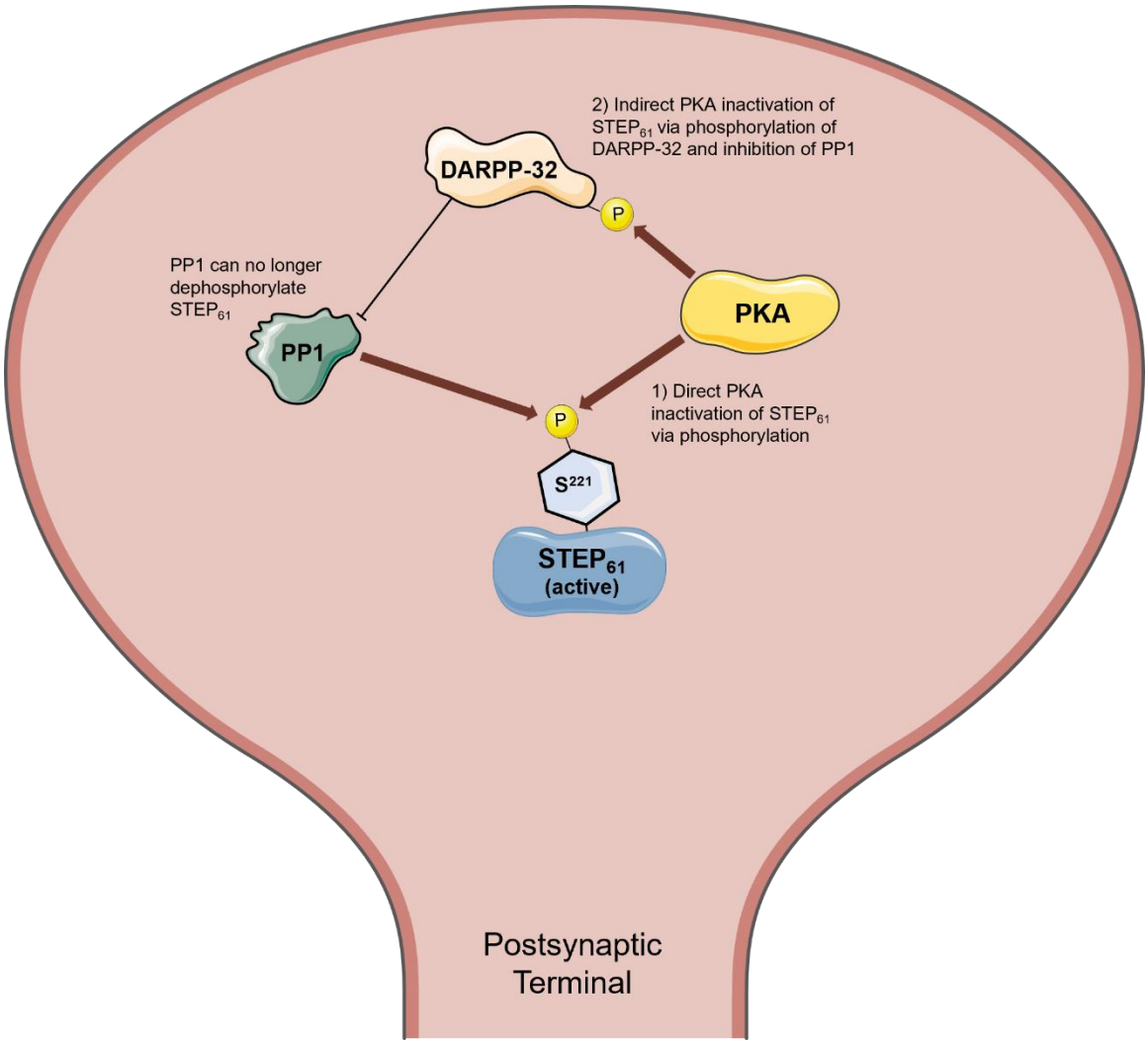

Figure 1.3. STEP regulation and function by PKA – this occurs via two separate ways: 1) Direct inactivation of $STEP_{61}$ by phosphorylation of regulatory Ser^{221}, thus preventing $STEP_{61}$ from binding to its main substrates; 2) Indirect inactivation of $STEP_{61}$ by phosphorylation of DARPP-32, which inhibits PP1. This ultimately prevents PP1 from dephosphorylating $STEP_{61}$ and reduces the overall level of active $STEP_{61}$.

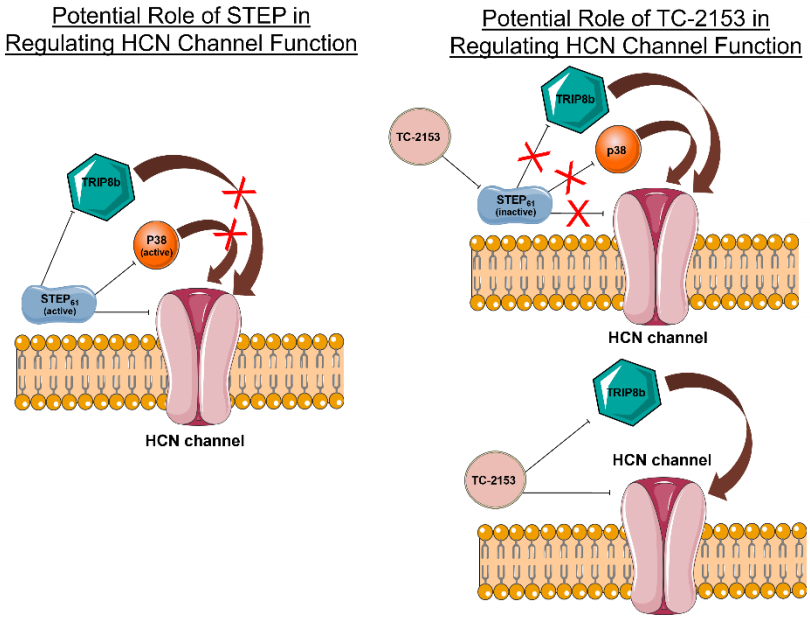

Figure 1.4. Novel potential mechanism of $STEP_{61}$'s role in the modulation and activity of HCN channels and/or auxiliary subunit TRIP8b, a protein responsible for HCN channel localization and function. Here, we propose that $STEP_{61}$ may be implicated in regulating HCN channels either directly or indirectly through proteins such as TRIP8b or p38. We also speculate acute STEP inhibitor may play a role by either directly or indirectly affecting the function of HCN channels or TRIP8b.

References

1. Spencer, S.S., *When should temporal-lobe epilepsy be treated surgically?* Lancet Neurol, 2002. **1**(6): p. 375-82.
2. Beck, H. and Y. Yaari, *Plasticity of intrinsic neuronal properties in CNS disorders.* Nat Rev Neurosci, 2008. **9**(5): p. 357-69.
3. Walters, J.M., et al., *Pharmacological inhibition of STriatal-Enriched protein tyrosine Phosphatase by TC-2153 reduces hippocampal excitability and seizure propensity.* Epilepsia, 2022.
4. Goebel-Goody, S.M., et al., *Therapeutic implications for striatal-enriched protein tyrosine phosphatase (STEP) in neuropsychiatric disorders.* Pharmacol Rev, 2012. **64**(1): p. 65-87.
5. Kamceva, M., et al., *Role of Striatal-Enriched Tyrosine Phosphatase in Neuronal Function.* Neural Plast, 2016. **2016**: p. 8136925.
6. Bult, A., et al., *STEP61: a member of a family of brain-enriched PTPs is localized to the endoplasmic reticulum.* J Neurosci, 1996. **16**(24): p. 7821-31.
7. Pulido, R., A. Zuniga, and A. Ullrich, *PTP-SL and STEP protein tyrosine phosphatases regulate the activation of the extracellular signal-regulated kinases ERK1 and ERK2 by association through a kinase interaction motif.* EMBO J, 1998. **17**(24): p. 7337-50.
8. Xu, J., et al., *Striatal-enriched protein tyrosine phosphatase regulates the PTPalpha/Fyn signaling pathway.* J Neurochem, 2015. **134**(4): p. 629-41.
9. Lombroso, P.J., et al., *A protein tyrosine phosphatase expressed within dopaminoceptive neurons of the basal ganglia and related structures.* J Neurosci, 1993. **13**(7): p. 3064-74.
10. Sharma, E., et al., *Identification of two alternatively spliced transcripts of STEP: a subfamily of brain-enriched protein tyrosine phosphatases.* Brain Res Mol Brain Res, 1995. **32**(1): p. 87-93.
11. Bult, A., et al., *STEP: a family of brain-enriched PTPs. Alternative splicing produces transmembrane, cytosolic and truncated isoforms.* Eur J Cell Biol, 1997. **72**(4): p. 337-44.
12. Boulanger, L.M., et al., *Cellular and molecular characterization of a brain-enriched protein tyrosine phosphatase.* J Neurosci, 1995. **15**(2): p. 1532-44.
13. Raghunathan, A., et al., *Transient compartmental expression of a family of protein tyrosine phosphatases in the developing striatum.* Brain Res Dev Brain Res, 1996. **91**(2): p. 190-9.
14. Lorber, B., et al., *Stimulated regeneration of the crushed adult rat optic nerve correlates with attenuated expression of the protein tyrosine phosphatases RPTPalpha, STEP, and LAR.* Mol Cell Neurosci, 2004. **27**(4): p. 404-16.
15. Oyama, T., et al., *Immunocytochemical localization of the striatal enriched protein tyrosine phosphatase in the rat striatum: a light and electron microscopic study with a complementary DNA-generated polyclonal antibody.* Neuroscience, 1995. **69**(3): p. 869-80.
16. Nguyen, T.H., J. Liu, and P.J. Lombroso, *Striatal enriched phosphatase 61 dephosphorylates Fyn at phosphotyrosine 420.* J Biol Chem, 2002. **277**(27): p. 24274-9.
17. Xu, J., et al., *Striatal-enriched protein tyrosine phosphatase in Alzheimer's disease.* Adv Pharmacol, 2012. **64**: p. 303-25.

18. Goebel-Goody, S.M., et al., *Phospho-regulation of synaptic and extrasynaptic N-methyl-d-aspartate receptors in adult hippocampal slices.* Neuroscience, 2009. **158**(4): p. 1446-59.
19. Hasegawa, S., et al., *Expression of neuron specific phosphatase, striatal enriched phosphatase (STEP) in reactive astrocytes after transient forebrain ischemia.* Glia, 2000. **29**(4): p. 316-29.
20. Okamura, A., et al., *Postnatal ontogeny of striatal-enriched protein tyrosine phosphatase (STEP) in rat striatum.* Exp Neurol, 1997. **145**(1): p. 228-34.
21. Wang, H., et al., *PTPN5 promotes follicle-stimulating hormone secretion through regulating intracellular calcium homeostasis.* FASEB J, 2021. **35**(8): p. e21756.
22. Paul, S., et al., *The Dopamine/D1 receptor mediates the phosphorylation and inactivation of the protein tyrosine phosphatase STEP via a PKA-dependent pathway.* J Neurosci, 2000. **20**(15): p. 5630-8.
23. Valjent, E., et al., *Regulation of a protein phosphatase cascade allows convergent dopamine and glutamate signals to activate ERK in the striatum.* Proc Natl Acad Sci U S A, 2005. **102**(2): p. 491-6.
24. Paul, S., et al., *NMDA-mediated activation of the tyrosine phosphatase STEP regulates the duration of ERK signaling.* Nat Neurosci, 2003. **6**(1): p. 34-42.
25. Paul, S. and J.A. Connor, *NR2B-NMDA receptor-mediated increases in intracellular Ca2+ concentration regulate the tyrosine phosphatase, STEP, and ERK MAP kinase signaling.* J Neurochem, 2010. **114**(4): p. 1107-18.
26. Davis, S., et al., *The MAPK/ERK cascade targets both Elk-1 and cAMP response element-binding protein to control long-term potentiation-dependent gene expression in the dentate gyrus in vivo.* J Neurosci, 2000. **20**(12): p. 4563-72.
27. Sweatt, J.D., *Mitogen-activated protein kinases in synaptic plasticity and memory.* Curr Opin Neurobiol, 2004. **14**(3): p. 311-7.
28. Xu, J., et al., *Extrasynaptic NMDA receptors couple preferentially to excitotoxicity via calpain-mediated cleavage of STEP.* J Neurosci, 2009. **29**(29): p. 9330-43.
29. Munoz, J.J., et al., *Differential interaction of the tyrosine phosphatases PTP-SL, STEP and HePTP with the mitogen-activated protein kinases ERK1/2 and p38alpha is determined by a kinase specificity sequence and influenced by reducing agents.* Biochem J, 2003. **372**(Pt 1): p. 193-201.
30. Kim, S.Y., et al., *Striatal-enriched protein tyrosine phosphatase regulates dopaminergic neuronal development via extracellular signal-regulated kinase signaling.* Exp Neurol, 2008. **214**(1): p. 69-77.
31. Poddar, R., et al., *NR2B-NMDA receptor mediated modulation of the tyrosine phosphatase STEP regulates glutamate induced neuronal cell death.* J Neurochem, 2010. **115**(6): p. 1350-62.
32. Cuadrado, A. and A.R. Nebreda, *Mechanisms and functions of p38 MAPK signalling.* Biochem J, 2010. **429**(3): p. 403-17.
33. Turrigiano, G., *Homeostatic synaptic plasticity: local and global mechanisms for stabilizing neuronal function.* Cold Spring Harb Perspect Biol, 2012. **4**(1): p. a005736.
34. Zhang, Y., et al., *The tyrosine phosphatase STEP mediates AMPA receptor endocytosis after metabotropic glutamate receptor stimulation.* J Neurosci, 2008. **28**(42): p. 10561-6.

35. Zhang, Y., et al., *Genetic reduction of striatal-enriched tyrosine phosphatase (STEP) reverses cognitive and cellular deficits in an Alzheimer's disease mouse model.* Proc Natl Acad Sci U S A, 2010. **107**(44): p. 19014-9.
36. Kurup, P., et al., *Abeta-mediated NMDA receptor endocytosis in Alzheimer's disease involves ubiquitination of the tyrosine phosphatase STEP61.* J Neurosci, 2010. **30**(17): p. 5948-57.
37. Snyder, E.M., et al., *Regulation of NMDA receptor trafficking by amyloid-beta.* Nat Neurosci, 2005. **8**(8): p. 1051-8.
38. Lavezzari, G., et al., *Differential binding of the AP-2 adaptor complex and PSD-95 to the C-terminus of the NMDA receptor subunit NR2B regulates surface expression.* Neuropharmacology, 2003. **45**(6): p. 729-37.
39. Nakazawa, T., et al., *Characterization of Fyn-mediated tyrosine phosphorylation sites on GluR epsilon 2 (NR2B) subunit of the N-methyl-D-aspartate receptor.* J Biol Chem, 2001. **276**(1): p. 693-9.
40. Jang, S.S., et al., *Regulation of STEP61 and tyrosine-phosphorylation of NMDA and AMPA receptors during homeostatic synaptic plasticity.* Mol Brain, 2015. **8**(1): p. 55.
41. Won, S., et al., *The STEP61 interactome reveals subunit-specific AMPA receptor binding and synaptic regulation.* Proc Natl Acad Sci U S A, 2019. **116**(16): p. 8028-8037.
42. Won, S., et al., *PSD-95 stabilizes NMDA receptors by inducing the degradation of STEP61.* Proc Natl Acad Sci U S A, 2016. **113**(32): p. E4736-44.
43. Pelkey, K.A., et al., *Tyrosine phosphatase STEP is a tonic brake on induction of long-term potentiation.* Neuron, 2002. **34**(1): p. 127-38.
44. Santos, S.D., et al., *Regulation of AMPA receptors and synaptic plasticity.* Neuroscience, 2009. **158**(1): p. 105-25.
45. Traynelis, S.F., et al., *Glutamate receptor ion channels: structure, regulation, and function.* Pharmacol Rev, 2010. **62**(3): p. 405-96.
46. Gladding, C.M., et al., *Tyrosine dephosphorylation regulates AMPAR internalisation in mGluR-LTD.* Mol Cell Neurosci, 2009. **40**(2): p. 267-79.
47. Chen, X., et al., *Enhancement of long-term depression by soluble amyloid beta protein in rat hippocampus is mediated by metabotropic glutamate receptor and involves activation of p38MAPK, STEP and caspase-3.* Neuroscience, 2013. **253**: p. 435-43.
48. Venkitaramani, D.V., et al., *Striatal-enriched protein tyrosine phosphatase (STEP) knockout mice have enhanced hippocampal memory.* Eur J Neurosci, 2011. **33**(12): p. 2288-98.
49. Ashby, M.C., et al., *Removal of AMPA receptors (AMPARs) from synapses is preceded by transient endocytosis of extrasynaptic AMPARs.* J Neurosci, 2004. **24**(22): p. 5172-6.
50. Lee, S.H., A. Simonetta, and M. Sheng, *Subunit rules governing the sorting of internalized AMPA receptors in hippocampal neurons.* Neuron, 2004. **43**(2): p. 221-36.
51. Tovar, K.R. and G.L. Westbrook, *The incorporation of NMDA receptors with a distinct subunit composition at nascent hippocampal synapses in vitro.* J Neurosci, 1999. **19**(10): p. 4180-8.
52. Roche, K.W., et al., *Molecular determinants of NMDA receptor internalization.* Nat Neurosci, 2001. **4**(8): p. 794-802.
53. Ivanov, A., et al., *Opposing role of synaptic and extrasynaptic NMDA receptors in regulation of the extracellular signal-regulated kinases (ERK) activity in cultured rat hippocampal neurons.* J Physiol, 2006. **572**(Pt 3): p. 789-98.

54. Semenova, M.M., et al., *Rho mediates calcium-dependent activation of p38alpha and subsequent excitotoxic cell death.* Nat Neurosci, 2007. **10**(4): p. 436-43.
55. Menegon, A., et al., *FAK+ and PYK2/CAKbeta, two related tyrosine kinases highly expressed in the central nervous system: similarities and differences in the expression pattern.* Eur J Neurosci, 1999. **11**(11): p. 3777-88.
56. Bartos, J.A., et al., *Postsynaptic clustering and activation of Pyk2 by PSD-95.* J Neurosci, 2010. **30**(2): p. 449-63.
57. Schlaepfer, D.D., C.R. Hauck, and D.J. Sieg, *Signaling through focal adhesion kinase.* Prog Biophys Mol Biol, 1999. **71**(3-4): p. 435-78.
58. Schauwienold, D., et al., *The transactivated epidermal growth factor receptor recruits Pyk2 to regulate Src kinase activity.* J Biol Chem, 2008. **283**(41): p. 27748-27756.
59. Venkitaramani, D.V., et al., *Knockout of striatal enriched protein tyrosine phosphatase in mice results in increased ERK1/2 phosphorylation.* Synapse, 2009. **63**(1): p. 69-81.
60. Kohl, S., et al., *Prepulse inhibition in psychiatric disorders--apart from schizophrenia.* J Psychiatr Res, 2013. **47**(4): p. 445-52.
61. Li, L., et al., *Top-down modulation of prepulse inhibition of the startle reflex in humans and rats.* Neurosci Biobehav Rev, 2009. **33**(8): p. 1157-67.
62. Goebel-Goody, S.M., et al., *Genetic manipulation of STEP reverses behavioral abnormalities in a fragile X syndrome mouse model.* Genes Brain Behav, 2012. **11**(5): p. 586-600.
63. Sukoff Rizzo, S.J., et al., *Behavioral characterization of striatal-enriched protein tyrosine phosphatase (STEP) knockout mice.* Genes Brain Behav, 2014. **13**(7): p. 643-52.
64. Briggs, S.W., et al., *STEP regulation of seizure thresholds in the hippocampus.* Epilepsia, 2011. **52**(3): p. 497-506.
65. Carty, N.C., et al., *The tyrosine phosphatase STEP: implications in schizophrenia and the molecular mechanism underlying antipsychotic medications.* Transl Psychiatry, 2012. **2**: p. e137.
66. Turski, L., et al., *Review: cholinergic mechanisms and epileptogenesis. The seizures induced by pilocarpine: a novel experimental model of intractable epilepsy.* Synapse, 1989. **3**(2): p. 154-71.
67. Amidfar, M., et al., *The role of CREB and BDNF in neurobiology and treatment of Alzheimer's disease.* Life Sci, 2020. **257**: p. 118020.
68. Song, M.S., et al., *In vitro validation of effects of BDNF-expressing mesenchymal stem cells on neurodegeneration in primary cultured neurons of APP/PS1 mice.* Neuroscience, 2015. **307**: p. 37-50.
69. Garzon, D.J. and M. Fahnestock, *Oligomeric amyloid decreases basal levels of brain-derived neurotrophic factor (BDNF) mRNA via specific downregulation of BDNF transcripts IV and V in differentiated human neuroblastoma cells.* J Neurosci, 2007. **27**(10): p. 2628-35.
70. Amidfar, M., Y.K. Kim, and O. Wiborg, *Effectiveness of memantine on depression-like behavior, memory deficits and brain mRNA levels of BDNF and TrkB in rats subjected to repeated unpredictable stress.* Pharmacol Rep, 2018. **70**(3): p. 600-606.
71. Xu, J., et al., *Down-regulation of BDNF in cell and animal models increases striatal-enriched protein tyrosine phosphatase 61 (STEP61) levels.* J Neurochem, 2016. **136**(2): p. 285-94.

72. Saavedra, A., et al., *BDNF Induces Striatal-Enriched Protein Tyrosine Phosphatase 61 Degradation Through the Proteasome.* Mol Neurobiol, 2016. **53**(6): p. 4261-4273.
73. Xu, J., et al., *Inhibitor of the tyrosine phosphatase STEP reverses cognitive deficits in a mouse model of Alzheimer's disease.* PLoS Biol, 2014. **12**(8): p. e1001923.
74. Choi, Y.S., et al., *Status epilepticus-induced somatostatinergic hilar interneuron degeneration is regulated by striatal enriched protein tyrosine phosphatase.* J Neurosci, 2007. **27**(11): p. 2999-3009.
75. Hicklin, T.R., et al., *Alcohol inhibition of the NMDA receptor function, long-term potentiation, and fear learning requires striatal-enriched protein tyrosine phosphatase.* Proc Natl Acad Sci U S A, 2011. **108**(16): p. 6650-5.
76. Wu, P.H., et al., *Functional adaptation of the N-methyl-D-aspartate receptor to inhibition by ethanol is modulated by striatal-enriched protein tyrosine phosphatase and p38 mitogen-activated protein kinase.* Mol Pharmacol, 2011. **80**(3): p. 529-37.
77. Saavedra, A., et al., *Striatal-enriched protein tyrosine phosphatase expression and activity in Huntington's disease: a STEP in the resistance to excitotoxicity.* J Neurosci, 2011. **31**(22): p. 8150-62.
78. Tashev, R., et al., *A substrate trapping mutant form of striatal-enriched protein tyrosine phosphatase prevents amphetamine-induced stereotypies and long-term potentiation in the striatum.* Biol Psychiatry, 2009. **65**(8): p. 637-45.
79. Braithwaite, S.P., et al., *Expression and function of striatal enriched protein tyrosine phosphatase is profoundly altered in cerebral ischemia.* Eur J Neurosci, 2008. **27**(9): p. 2444-52.
80. Yang, H.B., et al., *cAMP-dependent protein kinase activated Fyn in spinal dorsal horn to regulate NMDA receptor function during inflammatory pain.* J Neurochem, 2011. **116**(1): p. 93-104.
81. Azkona, G., et al., *Striatal-enriched protein tyrosine phosphatase modulates nociception: evidence from genetic deletion and pharmacological inhibition.* Pain, 2016. **157**(2): p. 377-386.
82. Lee, Z.F., et al., *Altered nociception in Alzheimer disease is associated with striatal-enriched protein tyrosine phosphatase signaling.* Pain, 2021. **162**(6): p. 1669-1680.
83. Chatterjee, M., et al., *STEP inhibition reverses behavioral, electrophysiologic, and synaptic abnormalities in Fmr1 KO mice.* Neuropharmacology, 2018. **128**: p. 43-53.
84. Davis, K.E., S. Fox, and J. Gigg, *Increased hippocampal excitability in the 3xTgAD mouse model for Alzheimer's disease in vivo.* PLoS One, 2014. **9**(3): p. e91203.
85. Yan, X.X., et al., *Chronic temporal lobe epilepsy is associated with enhanced Alzheimer-like neuropathology in 3xTg-AD mice.* PLoS One, 2012. **7**(11): p. e48782.
86. Tombini, M., et al., *Temporal Lobe Epilepsy and Alzheimer's Disease: From Preclinical to Clinical Evidence of a Strong Association.* J Alzheimers Dis Rep, 2021. **5**(1): p. 243-261.
87. Davidson, Y.S., et al., *TDP-43 pathological changes in early onset familial and sporadic Alzheimer's disease, late onset Alzheimer's disease and Down's syndrome: association with age, hippocampal sclerosis and clinical phenotype.* Acta Neuropathol, 2011. **122**(6): p. 703-13.
88. Tai, X.Y., et al., *Hyperphosphorylated tau in patients with refractory epilepsy correlates with cognitive decline: a study of temporal lobe resections.* Brain, 2016. **139**(Pt 9): p. 2441-55.

89. Barr, W.B., *Do Patients With Temporal Lobe Epilepsy and Cognitive Decline Have Alzheimer's Disease or Chronic Traumatic Encephalopathy (CTE)?* Epilepsy Curr, 2017. **17**(2): p. 96-98.
90. Holler, Y. and E. Trinka, *What do temporal lobe epilepsy and progressive mild cognitive impairment have in common?* Front Syst Neurosci, 2014. **8**: p. 58.
91. Sharma, S., et al., *Status Epilepticus: Behavioral and Electroencephalography Seizure Correlates in Kainate Experimental Models.* Front Neurol, 2018. **9**: p. 7.
92. Mathern, G.W., et al., *The pathogenic and progressive features of chronic human hippocampal epilepsy.* Epilepsy Res, 1996. **26**(1): p. 151-61.
93. Carvajal, F.J. and W. Cerpa, *Regulation of Phosphorylated State of NMDA Receptor by STEP61 Phosphatase after Mild-Traumatic Brain Injury: Role of Oxidative Stress.* Antioxidants (Basel), 2021. **10**(10).
94. Ding, K., P.K. Gupta, and R. Diaz-Arrastia, *Epilepsy after Traumatic Brain Injury*, in *Translational Research in Traumatic Brain Injury*, D. Laskowitz and G. Grant, Editors. 2016: Boca Raton (FL).
95. Sloviter, R.S., *Decreased hippocampal inhibition and a selective loss of interneurons in experimental epilepsy.* Science, 1987. **235**(4784): p. 73-6.
96. Kurup, P., et al., *The role of STEP in Alzheimer's disease.* Channels (Austin), 2010. **4**(5): p. 347-50.
97. Konstantinova, L.S., O.A. Rakitin, and C.W. Rees, *Pentathiepins.* Chem Rev, 2004. **104**(5): p. 2617-30.
98. Kulikov, A.V., et al., *[Effect of new potential psychotropic drug, 8-(trifluoromethyl)-1,2,3,4,5-benzopentathiepin-6-amine hydrochloride, on the expression of serotonin-related genes in mouse brain].* Mol Biol (Mosk), 2011. **45**(2): p. 282-8.
99. Khomenko, M.T., et al., *8-(Trifluoromethyl)-1,2,3,4,5-benzopentathiepin-6-amine: Novel Aminobenzopentathiepine having In Vivo Anticonvulsant and Anxiolytic Activities.* Letters in Drug Design & Discovery, 2009. **6**(6): p. 464-467.
100. Walters, J.M., et al., *Pharmacological inhibition of STriatal-Enriched protein tyrosine Phosphatase by TC-2153 reduces hippocampal excitability and seizure propensity.* Epilepsia, 2022. **63**(5): p. 1211-1224.
101. Bell, M.R., *Comparing Postnatal Development of Gonadal Hormones and Associated Social Behaviors in Rats, Mice, and Humans.* Endocrinology, 2018. **159**(7): p. 2596-2613.
102. Sisk, C.L. and J.L. Zehr, *Pubertal hormones organize the adolescent brain and behavior.* Front Neuroendocrinol, 2005. **26**(3-4): p. 163-74.
103. Levesque, M. and M. Avoli, *The kainic acid model of temporal lobe epilepsy.* Neurosci Biobehav Rev, 2013. **37**(10 Pt 2): p. 2887-99.
104. Arshad, M.N. and J.R. Naegele, *Induction of Temporal Lobe Epilepsy in Mice with Pilocarpine.* Bio Protoc, 2020. **10**(4): p. e3533.
105. Reddy, D.S., et al., *Extrasynaptic gamma-aminobutyric acid type A receptor-mediated sex differences in the antiseizure activity of neurosteroids in status epilepticus and complex partial seizures.* Epilepsia, 2019. **60**(4): p. 730-743.
106. Backstrom, T., *Epileptic seizures in women related to plasma estrogen and progesterone during the menstrual cycle.* Acta Neurol Scand, 1976. **54**(4): p. 321-47.
107. Woolley, C.S., *Estradiol facilitates kainic acid-induced, but not flurothyl-induced, behavioral seizure activity in adult female rats.* Epilepsia, 2000. **41**(5): p. 510-5.

108. Mejias-Aponte, C.A., C.A. Jimenez-Rivera, and A.C. Segarra, *Sex differences in models of temporal lobe epilepsy: role of testosterone.* Brain Res, 2002. **944**(1-2): p. 210-8.
109. Reddy, D.S., et al., *Anticonvulsant activity of progesterone and neurosteroids in progesterone receptor knockout mice.* J Pharmacol Exp Ther, 2004. **310**(1): p. 230-9.
110. Christian, C.A., et al., *Sex Differences in the Epilepsies and Associated Comorbidities: Implications for Use and Development of Pharmacotherapies.* Pharmacol Rev, 2020. **72**(4): p. 767-800.
111. Woolley, C.S., *Estrogen-mediated structural and functional synaptic plasticity in the female rat hippocampus.* Horm Behav, 1998. **34**(2): p. 140-8.
112. Storm, J.F., *Potassium currents in hippocampal pyramidal cells.* Prog Brain Res, 1990. **83**: p. 161-87.
113. Bean, B.P., *The action potential in mammalian central neurons.* Nat Rev Neurosci, 2007. **8**(6): p. 451-65.
114. Brown, D.A. and G.M. Passmore, *Neural KCNQ (Kv7) channels.* Br J Pharmacol, 2009. **156**(8): p. 1185-95.
115. Berkefeld, H., B. Fakler, and U. Schulte, *Ca2+-activated K+ channels: from protein complexes to function.* Physiol Rev, 2010. **90**(4): p. 1437-59.
116. Biel, M., et al., *Hyperpolarization-activated cation channels: from genes to function.* Physiol Rev, 2009. **89**(3): p. 847-85.
117. Magee, J.C., *Dendritic lh normalizes temporal summation in hippocampal CA1 neurons.* Nat Neurosci, 1999. **2**(6): p. 508-14.
118. Poolos, N.P., M. Migliore, and D. Johnston, *Pharmacological upregulation of h-channels reduces the excitability of pyramidal neuron dendrites.* Nat Neurosci, 2002. **5**(8): p. 767-74.
119. George, M.S., L.F. Abbott, and S.A. Siegelbaum, *HCN hyperpolarization-activated cation channels inhibit EPSPs by interactions with M-type K(+) channels.* Nat Neurosci, 2009. **12**(5): p. 577-84.
120. Gasparini, S. and D. DiFrancesco, *Action of the hyperpolarization-activated current (Ih) blocker ZD 7288 in hippocampal CA1 neurons.* Pflugers Arch, 1997. **435**(1): p. 99-106.
121. Huang, J., et al., *Novel mechanism for suppression of hyperpolarization-activated cyclic nucleotide-gated pacemaker channels by receptor-like tyrosine phosphatase-alpha.* J Biol Chem, 2008. **283**(44): p. 29912-9.
122. Association, A.s., *2021 Alzheimer's disease facts and figures.* Alzheimer's & Dementia, 2021. **17**(3): p. 327-406.
123. Haass, C. and D.J. Selkoe, *Soluble protein oligomers in neurodegeneration: lessons from the Alzheimer's amyloid beta-peptide.* Nat Rev Mol Cell Biol, 2007. **8**(2): p. 101-12.
124. Gong, Y., et al., *Alzheimer's disease-affected brain: presence of oligomeric A beta ligands (ADDLs) suggests a molecular basis for reversible memory loss.* Proc Natl Acad Sci U S A, 2003. **100**(18): p. 10417-22.
125. Alonso, A.C., I. Grundke-Iqbal, and K. Iqbal, *Alzheimer's disease hyperphosphorylated tau sequesters normal tau into tangles of filaments and disassembles microtubules.* Nat Med, 1996. **2**(7): p. 783-7.
126. Kopke, E., et al., *Microtubule-associated protein tau. Abnormal phosphorylation of a non-paired helical filament pool in Alzheimer disease.* J Biol Chem, 1993. **268**(32): p. 24374-84.

127. Glenner, G.G. and C.W. Wong, *Alzheimer's disease: initial report of the purification and characterization of a novel cerebrovascular amyloid protein.* Biochem Biophys Res Commun, 1984. **120**(3): p. 885-90.
128. Mucke, L., et al., *High-level neuronal expression of abeta 1-42 in wild-type human amyloid protein precursor transgenic mice: synaptotoxicity without plaque formation.* J Neurosci, 2000. **20**(11): p. 4050-8.
129. Kashyap, G., et al., *Synapse loss and progress of Alzheimer's disease -A network model.* Sci Rep, 2019. **9**(1): p. 6555.
130. Palop, J.J. and L. Mucke, *Network abnormalities and interneuron dysfunction in Alzheimer disease.* Nat Rev Neurosci, 2016. **17**(12): p. 777-792.
131. Ren, S.Q., et al., *Amyloid beta causes excitation/inhibition imbalance through dopamine receptor 1-dependent disruption of fast-spiking GABAergic input in anterior cingulate cortex.* Sci Rep, 2018. **8**(1): p. 302.
132. Hsia, A.Y., et al., *Plaque-independent disruption of neural circuits in Alzheimer's disease mouse models.* Proc Natl Acad Sci U S A, 1999. **96**(6): p. 3228-33.
133. Kim, J.H., et al., *Use-dependent effects of amyloidogenic fragments of (beta)-amyloid precursor protein on synaptic plasticity in rat hippocampus in vivo.* J Neurosci, 2001. **21**(4): p. 1327-33.
134. Kazim, S.F., et al., *Neuronal Network Excitability in Alzheimer's Disease: The Puzzle of Similar versus Divergent Roles of Amyloid beta and Tau.* eNeuro, 2021. **8**(2).
135. Chin, J., et al., *Fyn kinase induces synaptic and cognitive impairments in a transgenic mouse model of Alzheimer's disease.* J Neurosci, 2005. **25**(42): p. 9694-703.
136. Chatterjee, M., et al., *STEP inhibition prevents Abeta-mediated damage in dendritic complexity and spine density in Alzheimer's disease.* Exp Brain Res, 2021. **239**(3): p. 881-890.
137. Durakoglugil, M.S., et al., *Reelin Regulates Neuronal Excitability through Striatal-Enriched Protein Tyrosine Phosphatase (STEP61) and Calcium Permeable AMPARs in an NMDAR-Dependent Manner.* J Neurosci, 2021. **41**(35): p. 7340-7349.
138. Durakoglugil, M.S., et al., *Reelin signaling antagonizes beta-amyloid at the synapse.* Proc Natl Acad Sci U S A, 2009. **106**(37): p. 15938-43.
139. Drzezga, A., et al., *Effect of APOE genotype on amyloid plaque load and gray matter volume in Alzheimer disease.* Neurology, 2009. **72**(17): p. 1487-94.
140. Zhao, Y., et al., *Dl-3-n-butylphthalide alleviates cognitive impairment in amyloid precursor protein/presenilin 1 transgenic mice by regulating the striatal-enriched protein tyrosine phosphatase/ERK/cAMP-response element-binding protein signaling pathway.* Exp Ther Med, 2022. **23**(5): p. 319.
141. Vossel, K.A., et al., *Seizures and epileptiform activity in the early stages of Alzheimer disease.* JAMA Neurol, 2013. **70**(9): p. 1158-66.
142. Shin, M., et al., *Mislocalization of h channel subunits underlies h channelopathy in temporal lobe epilepsy.* Neurobiol Dis, 2008. **32**(1): p. 26-36.
143. Han, Y., et al., *The structure and function of TRIP8b, an auxiliary subunit of hyperpolarization-activated cyclic-nucleotide gated channels.* Channels (Austin), 2020. **14**(1): p. 110-122.
144. Poolos, N.P., J.B. Bullis, and M.K. Roth, *Modulation of h-channels in hippocampal pyramidal neurons by p38 mitogen-activated protein kinase.* J Neurosci, 2006. **26**(30): p. 7995-8003.

145. Winship, I.R., et al., *An Overview of Animal Models Related to Schizophrenia.* Can J Psychiatry, 2019. **64**(1): p. 5-17.
146. Goff, D.C. and J.T. Coyle, *The emerging role of glutamate in the pathophysiology and treatment of schizophrenia.* Am J Psychiatry, 2001. **158**(9): p. 1367-77.
147. Beneyto, M., et al., *Abnormal glutamate receptor expression in the medial temporal lobe in schizophrenia and mood disorders.* Neuropsychopharmacology, 2007. **32**(9): p. 1888-902.
148. Meador-Woodruff, J.H., et al., *Molecular abnormalities of the glutamate synapse in the thalamus in schizophrenia.* Ann N Y Acad Sci, 2003. **1003**: p. 75-93.
149. Xu, J., et al., *Inhibition of STEP61 ameliorates deficits in mouse and hiPSC-based schizophrenia models.* Mol Psychiatry, 2018. **23**(2): p. 271-281.
150. Lodge, D.J. and A.A. Grace, *Aberrant hippocampal activity underlies the dopamine dysregulation in an animal model of schizophrenia.* J Neurosci, 2007. **27**(42): p. 11424-30.
151. Sanderson, T.M., *Molecular mechanisms involved in depotentiation and their relevance to schizophrenia.* Chonnam Med J, 2012. **48**(1): p. 1-6.
152. Tendilla-Beltran, H., et al., *The prefrontal cortex as a target for atypical antipsychotics in schizophrenia, lessons of neurodevelopmental animal models.* Prog Neurobiol, 2021. **199**: p. 101967.
153. Bagni, C., et al., *Fragile X syndrome: causes, diagnosis, mechanisms, and therapeutics.* J Clin Invest, 2012. **122**(12): p. 4314-22.
154. Jayaseelan, S. and S.A. Tenenbaum, *Neurodevelopmental disorders: Signalling pathways of fragile X syndrome.* Nature, 2012. **492**(7429): p. 359-60.
155. Contractor, A., V.A. Klyachko, and C. Portera-Cailliau, *Altered Neuronal and Circuit Excitability in Fragile X Syndrome.* Neuron, 2015. **87**(4): p. 699-715.
156. Penzes, P., et al., *Dendritic spine pathology in neuropsychiatric disorders.* Nat Neurosci, 2011. **14**(3): p. 285-93.
157. Takarae, Y. and J. Sweeney, *Neural Hyperexcitability in Autism Spectrum Disorders.* Brain Sci, 2017. **7**(10).
158. Chatterjee, M., et al., *Inhibition of striatal-enriched protein tyrosine phosphatase (STEP) activity reverses behavioral deficits in a rodent model of autism.* Behav Brain Res, 2020. **391**: p. 112713.
159. Kaneko, M., et al., *Dendritic BDNF synthesis is required for late-phase spine maturation and recovery of cortical responses following sensory deprivation.* J Neurosci, 2012. **32**(14): p. 4790-802.
160. Rajagopal, S., R. Poddar, and S. Paul, *Tyrosine phosphatase STEP is a key regulator of glutamate-induced prostaglandin E2 release from neurons.* J Biol Chem, 2021. **297**(2): p. 100944.
161. Clark, J.D., et al., *A novel arachidonic acid-selective cytosolic PLA2 contains a Ca(2+)-dependent translocation domain with homology to PKC and GAP.* Cell, 1991. **65**(6): p. 1043-5

CHAPTER 2: PHARMACOLOGICAL INHIBITION OF STEP AND ITS REDUCTION OF HIPPOCAMPAL EXCITABILITY AND SEIZURES[1]

2.1 Summary

***Objective*:** STriatal-Enriched protein tyrosine Phosphatase (STEP) is a brain-specific tyrosine phosphatase. Membrane-bound $STEP_{61}$ is the only isoform expressed in hippocampus and cortex. Genetic deletion of STEP enhances excitatory synaptic currents and long-term potentiation in the hippocampus. However, whether $STEP_{61}$ affects seizure susceptibility is unclear. Here we investigated the effects of STEP inhibitor TC-2153 on seizure propensity in a murine model displaying kainic acid (KA)-induced *status epilepticus* and its effect on hippocampal excitability.

***Methods*:** Adult male and female C57BL/6J mice received intraperitoneal injection of either vehicle (2.8% DMSO in saline) or TC-2153 (10 mg/kg) and then either saline or KA (30 mg/kg) 3 hours later before being monitored for behavioral seizures. A subset of female mice was ovariectomized (OVX). Acute hippocampal slices from GCaMP6s mice were treated with either DMSO or TC-2153 (10 μM) for 1 hour, and then incubated in ACSF and potassium chloride (15 mM) for 2 min prior to live calcium imaging. Pyramidal neurons in dissociated rat hippocampal culture (DIV 8-10) were pre-treated with DMSO or TC-2153 (10 uM) for 1 hour before whole-cell patch clamp recording.

[1] Title: Pharmacological inhibition of STriatal-Enriched protein tyrosine Phosphatase by TC-2153 reduces hippocampal excitability and seizure propensity.

Authors: Jennifer M. Walters[1,2,#], Eung Chang Kim[2,#], Jiaren Zhang[2], Han Gil Jeong[2], Archit Bajaj[2], Brian Baculis[1,2], Gregory Tracy[2], Baher Ibrahim[1,2,3], Catherine A. Christian-Hinman[1,2,3], Daniel A. Llano[1,2,3], Graham R. Huesmann[1,2,3,4,5], Hee Jung Chung[1,2,3*]

# These authors contributed equally.

Affiliations:
[1] Neuroscience Program, University of Illinois at Urbana-Champaign, Urbana, IL, USA
[2] Dept. of Molecular and Integrative Physiology, University of Illinois at Urbana-Champaign, Urbana, IL, USA
[3] Beckman Institute, University of Illinois at Urbana-Champaign, Urbana, IL, USA
[4] Department of Neurology, Carle Foundation Hospital, Urbana, IL, USA
[5] Carle Illinois College of Medicine, University of Illinois at Urbana-Champaign, Urbana, IL, USA

***Results*:** TC-2153 treatment significantly reduced KA-induced seizure severity, with greater trend seen in females. OVX abolished this TC-2153-induced decrease in seizure severity in females. TC-2153 application significantly decreased overall excitability of acute hippocampal slices from both sexes. Surprisingly, TC-2153 treatment hyperpolarized resting membrane potential and decreased firing rate, sag voltage, and hyperpolarization-induced current (I_h) of cultured hippocampal pyramidal neurons.

***Significance*:** This study is the first to demonstrate that pharmacological inhibition of STEP with TC-2153 decreases seizure severity and hippocampal activity in both sexes, and dampens hippocampal neuronal excitability and I_h. We propose that anti-seizure effects of TC-2153 are mediated by its unexpected action on suppressing neuronal intrinsic excitability.

KEY POINTS

- Administration of TC-2153 significantly reduces seizure severity in both males and females.
- Ovariectomy abolishes the TC-2153-induced decrease in seizure severity observed in females.
- TC-2153 treatment significantly decreases overall excitability of acute hippocampal slices prepared from both sexes.
- TC-2153 application decreases intrinsic excitability and hyperpolarization-induced currents of cultured hippocampal neurons.

2.2 Introduction

Temporal Lobe Epilepsy (TLE) is the most common form of focal-onset epilepsy in adults and accounts for 60% of epileptic patients [1]. In Mesial TLE, seizures often begin in the hippocampus and progressively worsen over time. Current anti-seizure drugs are ineffective for ~75% of the patients with advanced mesial TLE, leading to severe consequences including hippocampal sclerosis, high mortality rate, cognitive decline, depression, and temporal lobe resection [1]. Furthermore, dysregulation of intrinsic excitability and synaptic transmission has been widely thought to underlie hippocampal hyperactivity that drives the development of spontaneous

seizures in TLE [2, 3], underscoring a critical need to identify the underlying mechanisms and novel therapeutic targets.

STriatal Enriched protein tyrosine Phosphatase (STEP) is a brain-specific tyrosine (Tyr) phosphatase encoded by the *PTPN5* gene [4]. Among four STEP isoforms, cytosolic $STEP_{46}$ and membrane-bound $STEP_{61}$ are catalytically active and widely expressed in the brain except the cerebellum [4]. However, only $STEP_{61}$ is expressed in the hippocampus and neocortex [5] where it dephosphorylates N-Methyl-D-aspartic acid receptor (NMDAR) and α-amino-3-hydroxy-5-methyl-4-isoxazolepropionic acid receptor (AMPAR), the key glutamate receptors that mediate fast excitatory synaptic transmission. Specifically, $STEP_{61}$ dephosphorylates NMDAR subunit GluN2B at Tyr^{1472} and AMPAR subunit GluA2 at Tyr^{869}, Tyr^{873}, and Tyr^{876}, resulting in their internalization [6-10]. $STEP_{61}$ also dephosphorylates and inactivates protein kinases including extracellular signal-regulated kinase ½ (ERK1/2), p38, Fyn, and Pyk2 [4]. Reduction of STEP increases NMDAR and AMPAR surface expression and excitatory synaptic currents [11, 12], enhances long term potentiation [13], and prevents the internalization of GluA2-containing AMPARs during metabotropic glutamate receptor-dependent long term depression in the hippocampus [9]. Activity-dependent regulation of $STEP_{61}$ also contributes to homeostatic stabilization of excitatory synapses by regulating Tyr phosphorylation of GluN2B and GluA2 [10]. Thus, $STEP_{61}$ weakens excitatory synaptic strength.

Emerging evidence suggests that STEP may be a molecular target for seizure treatment. Deletion of STEP gene *PTPN5* results in resistance to pilocarpine-induced seizures [14] and diminishes audiogenic seizures in a fragile X syndrome (FXS) mouse model [15]. This reduction in seizure propensity is puzzling since loss of STEP would be expected to increase seizure susceptibility by potentiating excitatory synaptic strength. It is possible that genetic deletion of STEP may have compensatory effects on other related genes and/or pathways, complicating delineation of the role of STEP in seizure susceptibility. Therefore, here we tested the hypothesis that acute pharmacological inhibition of STEP increases seizure propensity.

TC-2153 (8-(trifluoro-methyl)-1,2,3,4,5-benzopentathiepin-6-amine-hydrochloride) is a selective STEP inhibitor, which forms irreversible covalent bonds with the cysteine residues near a signature catalytic domain in $STEP_{46}$ and $STEP_{61}$ [16]. Despite the low IC50 (24.6 nM), a higher concentration of TC-2153 is required to increase Tyr phosphorylation of $STEP_{61}$ substrates in

primary cortical neuronal culture (1-10 μM) and the cortex *in vivo* (10 mg/kg) and reverse cognitive deficits in a 3xTg mouse model of Alzheimer's Disease (AD) [16] which display hippocampal hyperactivity and spontaneous seizures [17, 18]. With a low level of acute toxicity (LD 50 > 1000 mg/kg) [19], TC-2153 can alleviate audiogenic seizures in FXS mouse model [15] and block pentylenetetrazole-induced convulsions [19] although the sex-dependence of anti-seizure effects of TC-2153 and the underlying mechanism were not described.

In this study, we discovered that TC-2153 dampens hippocampal activity and exerts anti-convulsant activity in both C57BL/6J male and female mice against a single systemic injection of kainic acid (KA), which induces status epilepticus (SE) arising from the hippocampus [20]. Furthermore, TC-2153 decreases action potential (AP) firing rate, sag voltage, and hyperpolarization-induced current (I_h) in hippocampal neurons, providing novel evidence that pharmacological inhibition of STEP by TC-2153 downregulates intrinsic neuronal excitability in contrast to its well-known role in synaptic transmission.

2.3 Materials and Methods

Kainic acid-induced seizures

All animal procedures were approved by the Institutional Animal Care and Use Committee of the University of Illinois at Urbana Champaign and conformed to the ARRIVE Guidelines. Both male and female *Ptpn5* homozygous knock-out mice (*Ptpn5*$^{-/-}$) [8], wild-type mice (*Ptpn5*$^{+/+}$), C57BL/6J mice (Jax.org, Stock Number: 000664) were used for seizure studies at 6-12 weeks old. C57BL/6J females received ovariectomy surgeries at 9-10 weeks old as described [21] and were used in seizure studies at 7-10 days after surgery. Behavioral seizures were induced in mice by a single intraperitoneal (i.p.) injection of saline or KA, (30 mg/kg, Abcam) [20] and monitored using modified Racine scale for 2 hours (h) [22]. To test the effects of TC-2153, C57BL/6J mice received KA at 3 h post i.p. injections with either vehicle control (saline containing 2.8% DMSO) or TC-2153 (10 mg/kg in saline containing 2.8% DMSO, Sigma Aldrich). This treatment was previously demonstrated to increase Tyr-phosphorylation of STEP substrates in the cortex [16].

Immunoblot Analysis

At 3 h post injection with either vehicle control or TC-2153, the mouse hippocampi were biochemically fractionated to the supernatant and the membrane fractions (0.5 mg/mL) as described [23]. Primary dissociated hippocampal cultures were prepared from Sprague-Dawley rat embryos at embryonic day 18 and plated at 330 cells/mm^2 as described [10]. To maximally inhibit STEP, neurons at 9-10 *days in vitro* (DIV) were treated for 1 h with either vehicle control (0.14% DMSO) or TC-2153 (10 μM) [16]. Although the pharmacokinetics of TC-2153 is unknown, Tyr-phosphorylation of $STEP_{61}$ substrates were previously reported to increase in both neuron culture upon 10 μM TC-2153 application and forebrain tissues upon its i.p. injection at 10 mg/kg [16], suggesting that a 10 μM concentration used in *in vitro* studies is equivalent or close to its brain concentration achieved by *in vivo* delivery. Samples were immunoblotted for $STEP_{61}$ and its substrates. Densitometric quantification was performed with ImageJ Software (National Institutes of Health) [10, 23].

GCaMP6s imaging in acute hippocampal slices

Acute coronal hippocampal slices (200 μm) were prepared from Thy1-GCaMP6s mice (Jax.org, Stock Number: 024275) at 4-11 weeks old. Slices were incubated for 1 h at room temperature in basal artificial cerebrospinal fluid (ACSF) with either DMSO (0.14%) or TC-2153 (10 μM) which was previously shown to enhance hippocampal LTP [24] similar to STEP deletion [13]. Time lapse fluorescence images of GCaMP6s (size: 640 x 404 pixel) were acquired in ACSF for 1 minute (min) at 3.6 frame per second (sec) with 25 msec exposure time, and 3x3 binning under a Zeiss Axio Observer microscope. Slices were then incubated with potassium chloride (KCl, 15 mM) in ACSF for 2 min and imaged for another 1 min. Images from 10-60 sec after KCl exposure were analyzed for mean fluorescence intensity (F) in dentate gyrus (DG), CA1, and CA3 using ImageJ. $\Delta F/F = (F-F_{min})/F_{min}$ was computed as described [25], where ΔF indicates the difference between the initial intensity in ACSF and the intensity after KCl stimulation. $\Delta F/F$ was normalized to ACSF.

Electrophysiology

At 1 h post treatment with DMSO (0.14%) or TC-2153 (10 μM), whole-cell patch-clamp recordings of evoked AP firing, sag voltage, and rebound potential were performed at 30–32°C from cultured hippocampal pyramidal neurons held at -60 mV in external solution containing

CNQX (20 μM), DL-AP5 (100 μM) and bicuculline (20 μM) under current clamp mode using a Multiclamp 700B amplifier, Digidata1440A, and pClamp 10.6 software (Molecular Devices) [26]. Voltage clamp recording of I_h was performed with CNQX (20 μM), DL-AP5 (50 μM), bicuculline (10 μM), and TTX (0.5 μM) as described [27]. Clampfit 10.7 software (Molecular Devices) were used for recording analyses [27].

Statistical analysis

Data are reported as mean ± STDEV. Statistical analyses were performed using Origin Pro 9.5 (Origin Lab) to compare differences between means in 2 groups using the Student's two-tailed *t* test, and in groups of ≥3 using post-hoc Tukey test. For non-parametric data, the Mann-Whitney *U*-test was used. Sex difference was analyzed by two-way ANOVA with sex as one factor and treatment as the other. The priori value (p) < 0.05 was considered statistically significant.

Detailed description of each method is provided in Supplementary Information.

2.4 Results

Homozygous loss of STEP affects sensitivity to KA-induced seizure severity in age- and sex-dependent manner.

Since $STEP_{61}$ weakens excitatory synaptic strength [7-10, 13], we hypothesized that genetic deletion of *PTPN5* would increase susceptibility to acute seizures. To test this hypothesis, homozygous *PTPN5*$^{-/-}$ mice (STEP KO) and their wild-type *PTPN5*$^{+/+}$ littermates (STEP WT) were treated with KA (30 mg/kg, *i.p.*) [20], and behavioral seizures were scored every 10 min for the first 2 h using a modified Racine scale (Fig. 2.1) [22]. Initially, we tested 6 to 7 week old adolescent STEP WT and KO mice (P42-55) in reference to the age range that was originally investigated by Briggs et al., which combined both sexes for analysis and showed that STEP KO mice are resistant to pilocarpine-induced seizures [14]. Consistent with Briggs et al., STEP KO males at this age displayed a decrease in KA-induced seizure severity at nearly every time interval (Fig. 2.1B), resulting in a lower cumulative seizure score compared to WT males (Fig. 2.1C). A similar trend was observed for STEP KO females, but did not reach statistical significance (Fig. 2.1B-C, Table

S2.2). The percentage (%) of mice that reached Stage 5 (SE) and Stage 6 (death) were also decreased in KO males but not females compared to WT mice (Fig. 2.1D-E).

We next tested adult mice at 8 to 12 weeks of age (P56-P90) to avoid the adolescence period when puberty onset and maturation occurs and corticolimbic circuits are still developing [28, 29]. In contrast to 6 to 7 weeks old STEP KO males (Fig. 2.1B-D), 8 to12 weeks old STEP KO males showed similar seizure severity to WT males for the first 100 min following KA injection. However, their seizure scores at 110 and 120 min post-KA injection, % SE, and % Death were higher than WT males (Fig. 2.1F-I), consistent with our original hypothesis that STEP KO mice would show increased seizure susceptibility. In contrast, STEP KO females displayed a decreasing trend in seizure severity, the % SE, and % Death compared to WT females (Fig. 2.1F-I). Significant interaction between sex and treatment was noted (Interaction: $F_{(1, 53)}$=7.69, p=0.008, Table S2).

TC-2153 decreases KA-induced seizure severity in C57BL/6J mice.

To test if effects of acute pharmacological inhibition of STEP on seizure susceptibility are similar to genetic deletion of STEP, C57BL/6J mice at 8 to 12 weeks of age (P56-P90) were i.p. injected first with STEP inhibitor TC-2153 (10 mg/kg) or vehicle control and 3 h later with KA (30 mg/kg) to induce behavioral seizures (Fig. 2.2A). Such treatment with TC-2153 was previously shown to increase Tyr-phosphorylation of $STEP_{61}$ substrates in the cortex including GluN2B and ERK1/2 [16]. Upon TC-2153 injection, males displayed lower seizure scores at 50, 90, 110, and 120 min post-KA injection (Fig. 2.2B), decreasing cumulative seizure score, % SE, and % Death compared to vehicle injection (Fig. 2.2C-E). In females, TC-2153 application induced a larger decrease in seizure scores at nearly every time intervals, except 20-40 min (Fig. 2.2B) and reduced cumulative seizure score, % SE, and % Death compared to vehicle controls (Fig. 2.2C-E). However, no sex difference was observed for the effect of TC-2153 on cumulative seizure scores (Sex: $F_{(1, 48)}$=1.32, p=0.26, Table S2.2). Importantly, TC-2153 treatment reduced the number of mice that died by KA injection from 5 to 1 in both sexes (Fig. 2.2E). These data indicate that TC-2153 reduced KA-induced seizure severity in C57BL/6J mice.

This result was contrary to our original hypothesis that seizure susceptibility will increase by acute pharmacological inhibition of STEP. To confirm that TC-2153 was blocking STEP

activity, primary rat hippocampal neuronal culture was treated with either DMSO (vehicle control) or TC-2153 (10 μM) for 1 h. Immunoblot analysis of $STEP_{61}$ substrates revealed that TC-2153 application significantly increased the levels of Tyr^{1472}-phosphorylated GluN2B and Tyr^{204}/Tyr^{187}-phosphorylated ERK1/2 compared to DMSO, without affecting the expression of GluN2B, ERK1/2, and $STEP_{61}$ (Fig. S2.1A-B). Consistent with the previous reports in cultured cortical neurons [16], these results demonstrate that TC-2153 inhibits $STEP_{61}$ activity in cultured hippocampal neurons.

To confirm that TC-2153 inhibits $STEP_{61}$ in the hippocampus *in vivo*, the hippocampi of C57BL/6J mice were collected at 3 h post injection with either vehicle control or TC-2153 (10 mg/kg). Unlike previous reports [16], TC-2153 treatment did not alter hippocampal level of phosphorylated ERK1/2 in both sexes (Fig. S2.2). However, TC-2153 application significantly increased the hippocampal level of phosphorylated GluN2B in females but not males, indicative of $STEP_{61}$ inhibition in females (Fig. S2.2). It is interesting to note that the effect of TC-2153 on enhancing phosphorylated GluN2B in females but not males (Fig. S2.2) mirrors its greater trends on reducing KA-induced seizure severity in females (Fig. 2.2B-D).

Ovariectomy abolishes the TC-2153-induced seizure suppression in female C57BL/6J mice.

To investigate whether ovarian hormones were implicated in the TC-2153-induced reduction in seizure severity seen in females, female C57BL6/J mice received ovariectomy (OVX), which eliminates bulk circulation of ovarian-derived hormones from the system [30]. Under DMSO injection, OVX females reached SE more quickly than ovary-intact females following KA injection (Fig. S2.3). Remarkably, TC-2153 injection no longer decreased KA-induced seizure severity, cumulative seizure scores, and % Death in OVX mice compared to DMSO injection (Fig. 2.2B-C, E). Furthermore, similar numbers of OVX females reached SE regardless of treatment (vehicle: 6 out of 6 mice, TC-2153: 6 out of 7 mice) (Fig. 2.2D). These data indicate that OVX abolishes the TC-2153-induced suppression of seizure severity seen in intact females.

TC-2153 treatment reduces the excitability of acute hippocampal slices.

To investigate if TC-2153 affects hippocampal excitability, calcium imaging was performed on acute hippocampal slices prepared from mice containing genetically encoded calcium indicator GCaMP6s [25]. Acute slices were treated with either DMSO or TC-2153 (10 μM) in ACSF for 1 h prior to imaging of GCaMP6s (Fig. 2.3A-C). Under DMSO application, KCl-mediated depolarization significantly increased calcium signals in the somatic and dendritic layers in the CA1, CA3, and DG regions from both sexes (Fig. 2.3C-D, Table S2.3). In contrast, TC-2153 treatment significantly reduced the KCl-evoked calcium signals in every region (Fig. 2.3C-D, Table S2.3), indicating that TC-2153 decreases the excitability of the hippocampal slices.

TC-2153 treatment hyperpolarizes resting membrane potential and decreases intrinsic excitability in cultured hippocampal neurons.

The inhibitory action of TC-2153 on the excitability of the hippocampal slices was contrary to the well-known role of $STEP_{61}$ in weakening excitatory synaptic strength in the hippocampus. Therefore, we hypothesized that TC-2153 may regulate intrinsic excitability of hippocampal pyramidal cells. To test this, we performed whole-cell patch-clamp recording of cultured hippocampal neurons (DIV 8-10) after pre-treating with either DMSO or TC-2153 (10 μM) for 1 h (Fig. 2.4A-C). TC-2153 application hyperpolarized resting membrane potentials (RMP) and decreased the input resistance (R_{in}), but did not affect membrane capacitance of recorded neurons (Fig. 2.4D). Current clamp recording in the presence of synaptic transmission blockers revealed that TC-2153 application reduced instantaneous firing rates and the number of APs at 20 to 200 pA injections compared to DMSO or no treatment (Fig. 2.4A-C). TC-2153 treatment also increased average rheobase current, interspike interval (ISI), AP rise time, AP decay time, and AP half width, while decreasing fast after-hyperpolarization (fAHP) amplitude at 100 pA injection (Table 2.1). These data indicate that TC-2153 decreases hippocampal neuronal excitability.

TC-2153 treatment decreases sag voltage and I_h in cultured hippocampal neurons.

To test if TC-2153 regulates intrinsic membrane properties of hippocampal pyramidal neurons upon membrane hyperpolarization, we measured the amplitude of voltage sag and rebound potential. We found that TC-2153 treatment significantly reduced voltage sag by 75.2% and

rebound potentials by 51.6% at -200 to -40 pA current injections compared to DMSO or no treatment (Fig. 2.5A-C).

Hyperpolarization-activated cyclic nucleotide-gated ion (HCN) channels produce a slowly depolarizing non-selective inward cationic current called I_h, which mediates voltage sag and rebound potentials and regulates RMP and excitability of the hippocampal pyramidal neurons [31]. Among HCN1-4 subunits, HCN1 and HCN2 subunits are predominantly expressed in the hippocampal and cortical excitatory neurons [32]. To test if TC-2153 modulates I_h, we first confirmed that cultured hippocampal neurons expressed HCN1 and HCN2 subunits (Fig. S2.1C-D). Voltage-clamp recording upon membrane hyperpolarization revealed that TC-2153-treated neurons displayed smaller I_h density (pA/pF) at -70 mV to -120 mV compared to DMSO-treated and untreated neurons (Fig. 2.5D-E). The normalized conductance (G/Gmax) and $V_{1/2}$ calculated from G/Gmax showed a depolarizing shift in voltage dependence (Fig. 2.5F, Table S2.4). Consistent with decreased sag voltage and rebound potential (Fig. 2.5A-C), these data indicate that TC-2153 down-regulates I_h.

2.5 Discussion

The role of $STEP_{61}$ in weakening excitatory synaptic strength in the hippocampus and cortex has been well-established [7-10, 13], but its effect on seizure susceptibility and regulation of hippocampal excitability remains elusive. In this study, we provide evidence that acute pharmacological inhibition of STEP with TC-2153 decreases KA-induced seizure severity and hippocampal excitability. Our study has also revealed a previously unknown actions of TC-2153 in modulating intrinsic membrane properties.

Genetic ablation of STEP exerts age- and sex-dependent effects on seizure severity

Since $STEP_{61}$ weakens excitatory synaptic strength in the hippocampus, seizure susceptibility should increase in STEP KO mice which deletes all STEP isoforms [8]. However, Briggs et al. combined both sexes for analyses and showed that STEP KO mice at 6-8 weeks of age are resistant to pilocarpine-induced seizures [14]. When we separated the sexes in our analysis for KA-induced seizure severity, there was a decrease in STEP KO males at 6-7 weeks of age but

an increase at 8-12 weeks of age (Fig. 2.1). STEP KO females at both age groups showed a decreasing trend in seizure severity (Fig. 2.1). Our study thus demonstrates that genetic ablation of STEP, especially catalytic $STEP_{46}$ and $STEP_{61}$, most likely affects seizure severity in an age- and sex-dependent manner.

In rodents at 6 to 8 weeks of age, sexual maturation occurs in association with significant changes in sex hormone-dependent synapse formation and circuit maturation in the brain, particularly in the hippocampus and cortex [28, 29]. The 8th week of age marks the end of the puberty and adolescence period [28]. These critical changes in hippocampal circuitry and synapse formation due to sex hormone shifts may influence sensitivity to pilocarpine and KA which have different mechanisms for inducing limbic seizures [20, 33] and may explain the age-dependent switch in seizure susceptibility of STEP KO mice.

Anti-seizure effect of the STEP inhibitor TC-2153.

TC-2153 inhibits two catalytically active STEP isoforms, $STEP_{46}$ and $STEP_{61}$ [4]. Both isoforms are expressed in the striatum and amygdala [5] although only $STEP_{61}$ is expressed in the hippocampus and neocortex [5]. In both male and female mice, TC-2153 treatment decreased hippocampal excitability (Fig. 2.3) and the severity of KA-induced seizures (Fig. 2.2) that arise mostly from the hippocampus where KA subtype glutamate receptors are highly expressed especially in the CA3 region compared to other brain regions including amygdala, striatum, and cortex [20]. Therefore, the majority of anti-seizure effect of TC-2153 is likely mediated by $STEP_{61}$ inhibition in the hippocampus, although we cannot exclude the possible contributions of inhibiting both $STEP_{46}$ and $STEP_{61}$ in other brain regions. While our studies with TC-2153 pretreatment demonstrate its proof-of-concept anticonvulsant efficacy, investigating its pharmacokinetics and anti-seizure effects during SE and TLE will be critical to assess its clinically relevant efficacy.

Compared to males, females displayed a greater trend in anti-seizure effect of TC-2153, which was abolished by OVX (Fig. 2.2). Greater anti-seizure potency in females than males has also been reported for neurosteroids in various acute seizure models [34]. The possible involvement of ovarian-derived hormones [30] is interesting because prevalence, frequency, and semiology of focal seizures and TLE have been reported to differ by sex in both clinical patient populations and

preclinical animal models due to their neurobiological actions [35]. Estrogen exacerbates seizures in women with epilepsy [36] and both estrogen and testosterone increase seizure susceptibility in rodent KA models [37,38]. In contrast, seizure frequency in mice and women with epilepsy is reduced by high progesterone level [36,39].

It is interesting that anti-seizure effect of TC-2153 was lost in OVX females, whereas the effect was present in males (Fig. 2.2). TC-2153 application also reduced the excitability of hippocampal slices from both male and female mice (Fig. 2.3) even after circulating gonadal hormones had washed away while acclimating the slices in ACSF [40], suggesting that gonadal hormone cannot fully explain the subtle sex difference in the response to TC-2153. Considering that women display higher drug concentration in blood and longer duration for drug metabolism and clearance than men [35], a greater trend in anti-seizure effect in females may arise from higher brain concentration of TC-2153 in females than males. Alternatively, the enhanced seizure severity in OVX females compared to naïve females (Fig. S2.3) may also contribute to the diminished efficacy of TC-2153 in OVX females. Future studies shall evaluate ADME properties of TC-2153 in both sexes and use gonadectomy in combination with hormone replacement to confirm whether TC-2153 decreases KA-induced seizure severity by altered pharmacokinetics of TC-2153 or suppressing proconvulsant actions of estrogen or testosterone, and/or potentiating anti-convulsant actions of progesterone.

Decrease in hippocampal intrinsic excitability as a mechanism for anti-seizure effect of TC-2153.

Our study demonstrates novel actions of STEP inhibitor TC-2153 (Fig. 2.4-5). TC-2153 application markedly decreases intrinsic excitability of cultured hippocampal pyramidal neurons (Fig. 2.4). Considering that $STEP_{61}$ interacts with a variety of proteins including ion channels, ion transporters, and signaling proteins important for neuronal excitability and synaptic transmission [12], our findings suggest a compelling possibility that $STEP_{61}$ may regulate ionic currents critical for intrinsic neuronal excitability and AP waveform, in contrast to its well-known role in weakening synaptic transmission.

Indeed, hyperpolarized RMP and decreased R_{in} in TC-2153-treated hippocampal neurons (Fig. 2.4D) suggest the opening of potassium channels. Among major potassium currents in hippocampal pyramidal neurons [41], fast activating and inactivating I_A and fast activating and slowly inactivating I_D delay the onset of firing and contribute to AP repolarization and firing rate [41, 42]. Slowly activating and inactivating I_K mediates AP repolarization [42], whereas slowly activating and non-inactivating I_M hyperpolarizes RMP and suppresses repetitive firing of APs without affecting their latency [43]. Calcium-activated I_C contributes to fAHP and regulates AP repolarization, firing rate, and half-width [44]. The effects of TC-2153 on ISI, AP rise and decay times, AP half width, and fAHP amplitude (Table 2.1) suggest that one or more of these potassium currents may be regulated by TC-2153 to control intrinsic excitability and AP waveform.

I_h as a novel target of TC-2153.

We discover that TC-2153 treatment decreases I_h which contributes to sag voltage and rebound potential evoked by membrane hyperpolarization (Fig. 2.5). The role of I_h in hippocampal neuronal excitability is complex, as I_h exerts both excitatory and inhibitory effects on the ability of an excitatory postsynaptic potential (EPSP) to trigger an AP [31]. In hippocampal CA1 pyramidal neurons, HCN1 and HCN2 are preferentially enriched in the distal dendrites [31], where I_h decreases EPSP summation [45], but dendritic excitability can be enhanced or reduced by I_h [46, 47]. I_h can also increase AP firing rate by depolarizing RMP and decreasing R_{in} [48]. Therefore, TC-2153-induced I_h reduction (Fig. 2.5) may contribute to hyperpolarized RMP and decreased excitability seen in TC-2153-treated neurons (Fig. 2.4).

How TC-2153 decreases I_h is unknown. Activation kinetic of HCN2 channel is regulated by Src phosphorylation of its Tyr^{476}, whereas the receptor-like protein-tyrosine phosphatase-alpha can dephosphorylate HCN2 and decrease its surface and current expression [49], raising a possibility that $STEP_{61}$ may dephosphorylate HCN2, and its inhibition by TC-2153 may modify HCN2 channel function or expression. Alternatively, TC-2153 may directly bind to and decrease current expression of HCN1 and/or HCN2 channels. The mechanism underlying inhibitory actions of TC-2153 on I_h warrants future studies.

Therapeutic potential of TC-2153.

High levels of $STEP_{61}$ are associated with Alzheimer's disease (AD) [7] and FXS [15]. Pharmacological inhibition of STEP with TC-2153 alleviates excitatory synaptic defects and memory loss observed in AD mouse model [16] and reverses behavioral and synaptic deficits in FXS mouse model [15]. In addition to these therapeutic potentials, our present study demonstrates that TC-2153 reduces seizure severity in both male and female mice and the activity of their hippocampi (Fig. 2.1-2.3) and dampens intrinsic excitability and I_h of hippocampal neurons (Fig. 2.4-2.5). Clinical challenges exist in the use of anti-seizure drugs that are ineffective or can differ by sex [1,50], urging a need for new therapeutic targets. Our study presents TC-2153 as an attractive therapeutic candidate for epilepsy with novel mechanistic actions.

2.6 Acknowledgments

This research was supported by the National Institutes of Health under awards R01 NS083402, R01 NS097610, and R01 NS100019 (to H.J.C.), R01 NS105825 and R03 NS103029 (to C.A.C.-H.), R21 EB029076 (to G.R.H.), and R01 DC013073 and R01 DC016599 (to D.A.L.), University of Illinois Campus Research Board RB21053 (to H.J.C.), and Carle Illinois Collaborative Research Seed Grant 083630 (to H.J.C. and G.R.H).

CONFLICT OF INTEREST

None of the authors have any conflict of interest to disclose.

ETHICAL PUBLICATION STATEMENT

We confirm that we have read the Journal's position on issues involved in ethical publication and affirm that this report is consistent with those guidelines.

Main Figures and Legends

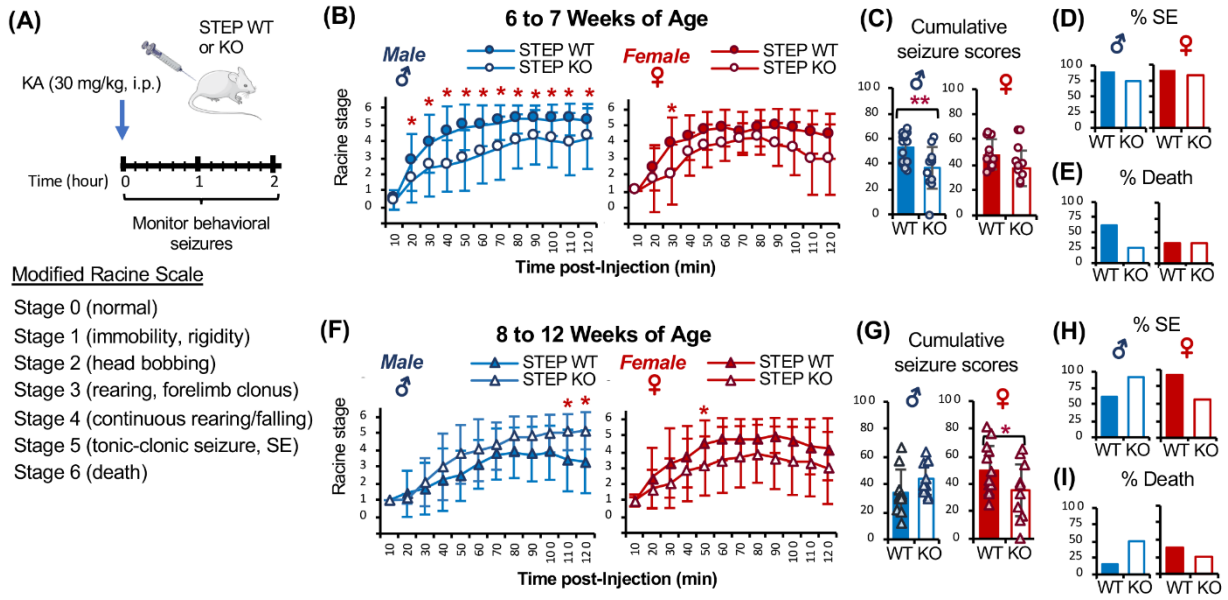

Figure 2.1. Homozygous loss of STEP affects sensitivity to KA-induced seizures in age- and sex-dependent manner. (A) Experimental schematic of kainic acid (KA)-induced seizures in STEP knockout (KO) and wild-type (WT) mice. A modified Racine scale was used to score behavioral seizures. **(B-D)** KA-induced seizures in STEP WT and KO mice at age 6 to 7 weeks (P42-P55). **(B)** STEP KO males at age 6-7 weeks (n=12) show a significant decrease in seizure scores at 20-110 min after KA injection compared to WT males (n=21). STEP KO females at age 6-7 weeks (n=12) show a significant decrease in seizure scores at 30 min post KA injection compared to WT females (n=12). Mann-Whitney *U*-test results are shown (*p<0.05). **(C)** Cumulative seizure scores. Two-tailed Student *t*-test results are shown (*p<0.05). **(D-E)** Percentage (%) of mice that achieved Stage 5 (D) and Stage 6 (E). **(F-I)** KA induced seizures in STEP WT and KO mice at age 8 to 12 weeks (P56-P90). **(F)** STEP KO males at age 8-12 weeks (n=12) show a significant increase in seizure scores at 110 and 120 min compared to WT males (n=13). STEP KO females at age 8-12 weeks (n=16) show a decreased trend in seizure propensity compared to WT females (n=13), but this trend was not statistically significant. Mann-Whitney *U*-test results are shown (*p<0.05). **(G)** Cumulative seizure scores. Two-tailed Student *t*-test results are shown (*p<0.05). **(H-I)** Percentage (%) of mice that achieved Stage 5 (D) and Stage 6 (E). Data shown represent the mean ± STDEV (*p<0.05).

Figure 2.1 animal experiments were performed and data was collected by Jennifer Walters and Archit Bajaj; data was analyzed by Jennifer Walters.

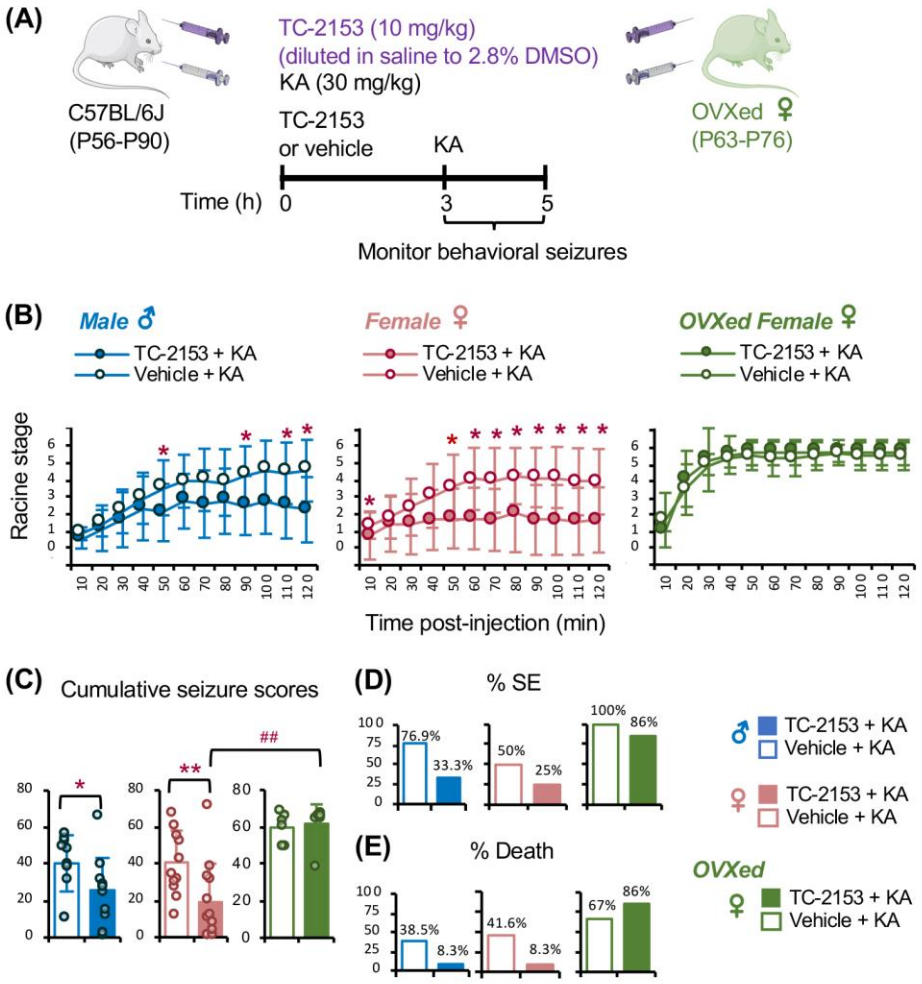

Figure 2.2. TC-2153 treatment decreases KA-induced seizure severity in adult C57BL/6J mice compared to vehicle control with greater effects seen in females. (A) Experimental schematic of kainic acid (KA)-induced seizure severity in both male and female C57BL/6J mice at 8-12 weeks (P56-P90) and ovariectomized (OVX) C57BL/6J females at 9-10 weeks (P63-P76) at 3 h post i.p. injection with STEP inhibitor TC-2153 (10 mg/kg in saline containing 2.8% DMSO) or vehicle control (saline containing 2.8% DMSO). Behavioral seizures were monitored using modified Racine scale. **(B)** TC-2153 treatment in male mice (n=12) decreases severity of KA-induced seizures at 90-120 min post injection compared to vehicle treatment (n=13). TC-2153 injection in female mice (n=12) significantly decreases KA-induced seizure severity at nearly every time point compared to vehicle treatment (n=12), whereas KA-induced seizures were similar between vehicle-injected OVX females (n=6) and TC-2153-injected OVX females (n=7) for the first 2 h. Mann-Whitney *U*-test results are shown (*p<0.05). **(C)** Cumulative seizure scores. Two-tailed Student *t*-test results are shown (*p<0.05). **(D-E)** Percentage (%) of mice that achieved

Figure 2.2 (cont.) Stage 5 (D) and Stage 6 (E). Data shown as mean ± STDEV. Table S2.1 shows two-way ANOVA test results with sex as one factor and treatment as the other.

Figure 2.2 ovariectomies were performed by Dr. Catherine Christian-Hinman; animal experiments were performed by Jennifer Walters; data was analyzed by Jennifer Walters.

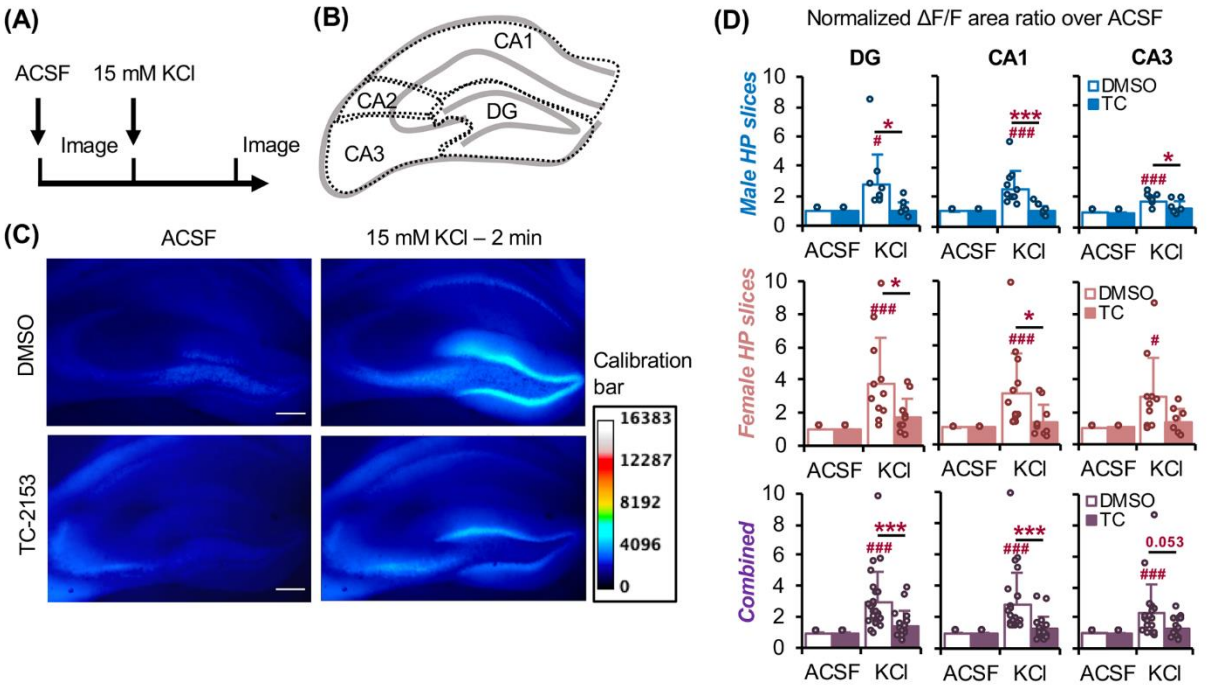

Figure 2.3. TC-2153 treatment reduces the excitability of acute hippocampal slices. (A) Experimental schematic of calcium imaging on coronal acute hippocampal slices prepared from Thy1-GCaMP6s mice at P28-90. The slices were incubated with DMSO (0.14%) or TC-2153 (10 μM) for 1 h, and subjected to GCaMP6s imaging first in ACSF and then after 2 min of 15 mM KCl application. **(B)** Manual tracing of hippocampal CA1, CA3, and DG regions for analysis. **(C)** Representative GCaMP6s fluorescence images of slices. Raw pixel intensity is shown. **(D)** Quantification of GCaMP6s fluorescence (ΔF/F) in DG, CA1, and CA3 regions normalized to ACSF. The total number of slices imaged: DMSO-treated slices (n=23 including 10 from 4 males, 13 from 5 females); TC-2153-treated slices (n=16 including 7 from 4 males and 9 from 5 females). Compared to DMSO treatment, TC-2153 treatment reduces GCaMP6s signals in DG, CA1, and CA3 regions of hippocampal slices prepared from both males and females. The total number of analyzed slices from males: DG (10 DMSO, 7 TC-2153), CA1 (10 DMSO, 7 TC-2153), and CA3 (8 DMSO, 6 TC-2153). The total number of analyzed slices from females: DG (11 DMSO, 9 TC-2153), CA1 (11 DMSO, 9 TC-2153), CA3 (8 DMSO, 7 TC-2153). Data shown as mean ± STDEV. Post-hoc Tukey test results are shown for ACSF vs. KCl ($^{\#}p<0.05$, $^{\#\#\#}p<0.005$) and for DMSO+KCl vs. TC+KCl (*p<0.05, ***p < 0.005). Table S2.2 shows two-way ANOVA test results with sex as one factor and treatment as the other.

Figure 2.3 data was collected and imaged by Jiaren Zhang, Eung Chang Kim, and Jennifer Walters; data was analyzed by Jennifer Walters.

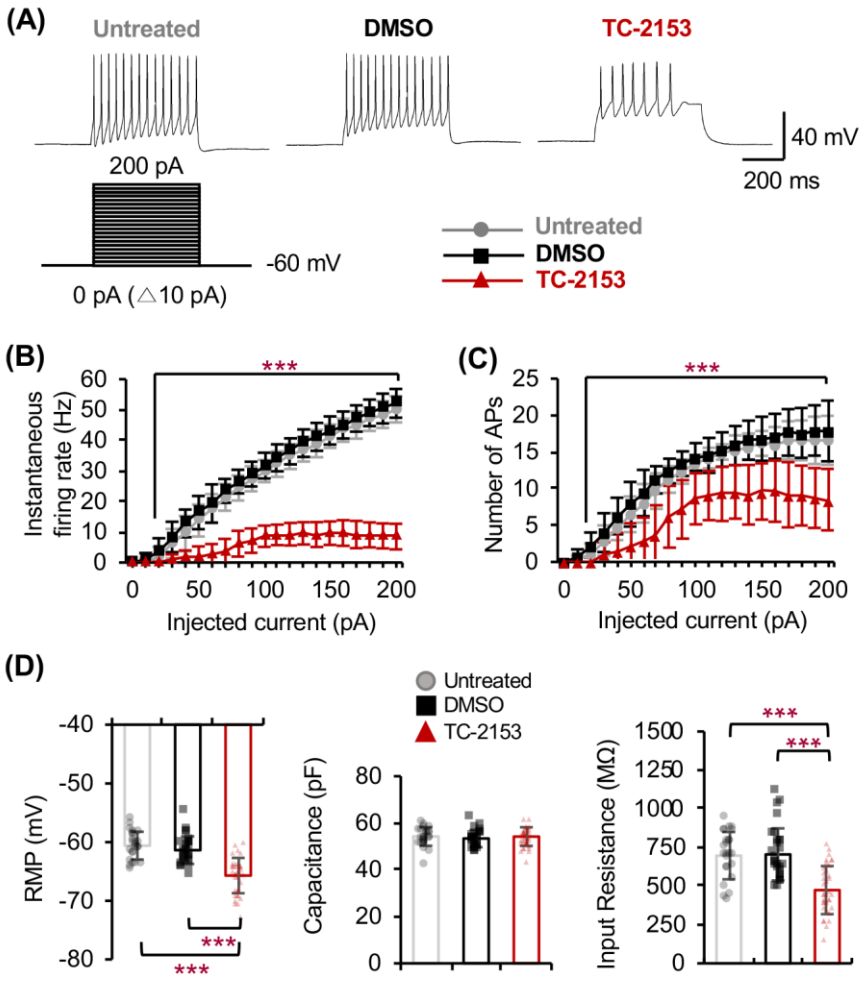

Figure 2.4. TC-2153 hyperpolarizes RMP and reduces AP firing and input resistance in cultured hippocampal neurons. Whole-cell current-clamp recording of hippocampal pyramidal neurons in dissociated culture (DIV 8–10) was performed in current clamp mode after 1 h treatment with TC-2153 (10 μM) or DMSO (0.14%). **(A-C)** TC-2153 reduces AP firing in cultured hippocampal neurons. Spike trains were evoked in pyramidal neurons in the presence of synaptic transmission blockers by delivering constant somatic current pulses of 500 ms duration in the range 0–200 pA with a step interval of 10 s at a holding potential of −60 mV. **(A)** Representative traces of APs at 100 pA injection. **(B)** Average instantaneous AP firing rate. **(C)** Average number of APs. The number of recorded neurons: untreated (gray circle, n=12), DMSO (black square, n=15), or TC-2153 (red triangle, n=18). **(D)** TC-2153 reduces hyperpolarizes RMP and decreases input resistance in cultured hippocampal neurons. Average resting membrane potential, capacitance, and input resistance in the recorded neurons: untreated (n=24), DMSO (n=28), or TC-2153 (n=36). Data shown as mean ± STDEV. Post-hoc Tukey test results are shown for TC-2153 vs. untreated or DMSO (***$p < 0.005$).

Figure 2.4 data was recorded by Eung Chang Kim; analyzed by Eung Chang Kim and Jennifer Walters.

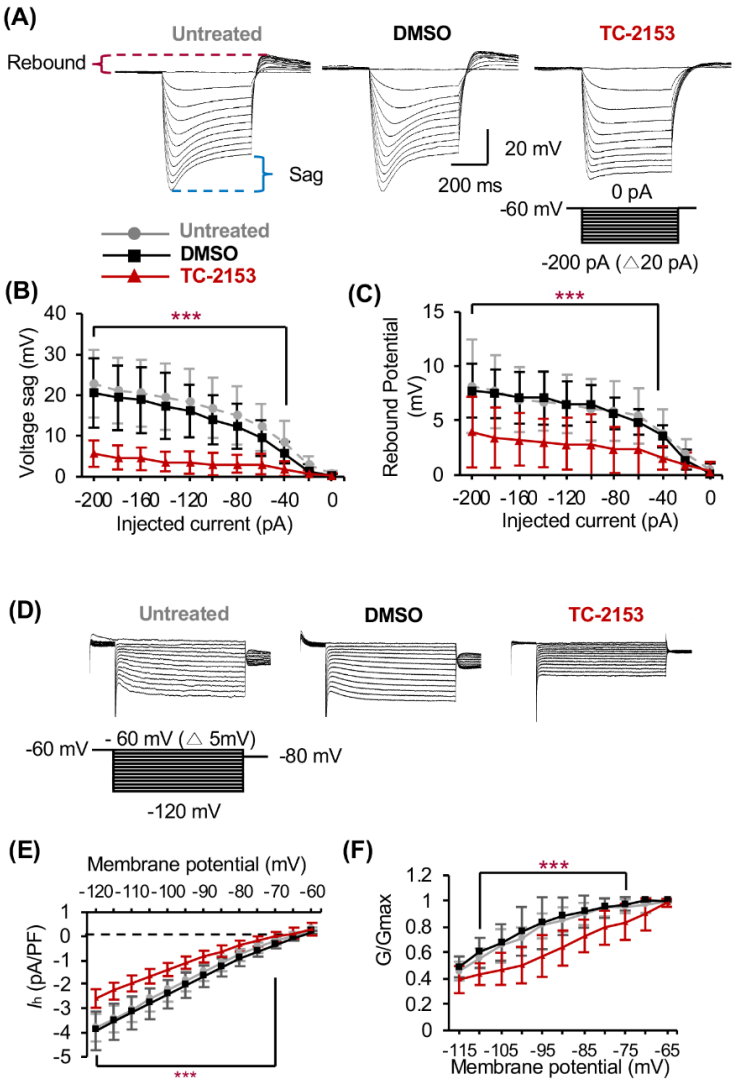

Figure 2.5. TC-2153 treatment reduces I_h in cultured hippocampal neurons. Whole-cell current clamp recording of cultured hippocampal neurons (DIV 8–10) was performed after 1 h treatment with TC 2153 (10 μM) or DMSO (0.14%). **(A-C)** TC-2153 reduces voltage sag and rebound voltage in cultured hippocampal neurons. **(A)** Representative responses to hyperpolarizing current steps from -200 to 0 pA in 20 pA increments in current clamp mode. The amount of voltage sag (blue lines) and rebound potential (red lines) was determined as difference between the maximum and steady-state voltage during the hyperpolarizing current injection. **(B)** Average sag voltage**. (C)** Average rebound voltage. The number of recorded neurons: untreated (gray circle, n=12), DMSO (black square, n=13), or TC-2153 (red triangle, n=18). **(D-F)** In voltage clamp mode, I_h was evoked by applying voltage steps from the holding potential of -60 mV to -120 mV in 5 mV decrements. **(D)** Representative traces of I_h. **(E)** I_h density at all voltage steps. **(F)** Normalized conductance (G/G_{max}) at all voltage steps. The number of recorded neurons: untreated (n=9), DMSO (n=12), TC-2153 (n=15). Data shown as mean ± STDEV. Post-hoc Tukey test results are shown for TC-2153 vs. untreated or DMSO (***$p < 0.005$).

Figure 2.5 data was recorded by Eung Chang Kim; analyzed by Eung Chang Kim and Jennifer Walters.

Main References

1. Spencer, S.S., *When should temporal-lobe epilepsy be treated surgically?* Lancet Neurol, 2002. **1**(6): p. 375-82.
2. Goldberg, E.M. and D.A. Coulter, *Mechanisms of epileptogenesis: a convergence on neural circuit dysfunction.* Nat Rev Neurosci, 2013. **14**(5): p. 337-49.
3. Beck, H. and Y. Yaari, *Plasticity of intrinsic neuronal properties in CNS disorders.* Nat Rev Neurosci, 2008. **9**(5): p. 357-69.
4. Goebel-Goody, S.M., et al., *Therapeutic implications for striatal-enriched protein tyrosine phosphatase (STEP) in neuropsychiatric disorders.* Pharmacol Rev, 2012. **64**(1): p. 65-87.
5. Boulanger, L.M., et al., *Cellular and molecular characterization of a brain-enriched protein tyrosine phosphatase.* J Neurosci, 1995. **15**(2): p. 1532-44.
6. Nakazawa, T., et al., *Characterization of Fyn-mediated tyrosine phosphorylation sites on GluR epsilon 2 (NR2B) subunit of the N-methyl-D-aspartate receptor.* J Biol Chem, 2001. **276**(1): p. 693-9.
7. Kurup, P., et al., *Abeta-mediated NMDA receptor endocytosis in Alzheimer's disease involves ubiquitination of the tyrosine phosphatase STEP61.* J Neurosci, 2010. **30**(17): p. 5948-57.
8. Zhang, Y., et al., *Genetic reduction of striatal-enriched tyrosine phosphatase (STEP) reverses cognitive and cellular deficits in an Alzheimer's disease mouse model.* Proc Natl Acad Sci U S A, 2010. **107**(44): p. 19014-9.
9. Zhang, Y., et al., *The tyrosine phosphatase STEP mediates AMPA receptor endocytosis after metabotropic glutamate receptor stimulation.* J Neurosci, 2008. **28**(42): p. 10561-6.
10. Jang, S.S., et al., *Regulation of STEP61 and tyrosine-phosphorylation of NMDA and AMPA receptors during homeostatic synaptic plasticity.* Mol Brain, 2015. **8**(1): p. 55.
11. Won, S., et al., *PSD-95 stabilizes NMDA receptors by inducing the degradation of STEP61.* Proc Natl Acad Sci U S A, 2016. **113**(32): p. E4736-44.
12. Won, S., et al., *The STEP61 interactome reveals subunit-specific AMPA receptor binding and synaptic regulation.* Proc Natl Acad Sci U S A, 2019. **116**(16): p. 8028-8037.
13. Pelkey, K.A., et al., *Tyrosine phosphatase STEP is a tonic brake on induction of long-term potentiation.* Neuron, 2002. **34**(1): p. 127-38.
14. Briggs, S.W., et al., *STEP regulation of seizure thresholds in the hippocampus.* Epilepsia, 2011. **52**(3): p. 497-506.
15. Chatterjee, M., et al., *STEP inhibition reverses behavioral, electrophysiologic, and synaptic abnormalities in Fmr1 KO mice.* Neuropharmacology, 2018. **128**: p. 43-53.
16. Xu, J., et al., *Inhibitor of the tyrosine phosphatase STEP reverses cognitive deficits in a mouse model of Alzheimer's disease.* PLoS Biol, 2014. **12**(8): p. e1001923.
17. Davis, K.E., S. Fox, and J. Gigg, *Increased hippocampal excitability in the 3xTgAD mouse model for Alzheimer's disease in vivo.* PLoS One, 2014. **9**(3): p. e91203.
18. Yan, X.X., et al., *Chronic temporal lobe epilepsy is associated with enhanced Alzheimer-like neuropathology in 3xTg-AD mice.* PLoS One, 2012. **7**(11): p. e48782.
19. Khomenko, T.M., et al., *8-(Trifluoromethyl)-1,2,3,4,5-benzopentathiepin-6-amine: Novel Aminobenzopentathiepine having In Vivo Anticonvulsant and Anxiolytic Activities.* Letters in Drug Design & Discovery 2009. **6**(6): p. 464-467.
20. Levesque, M. and M. Avoli, *The kainic acid model of temporal lobe epilepsy.* Neurosci Biobehav Rev, 2013. **37**(10 Pt 2): p. 2887-99.

21. Ujjainwala, A.L., et al., *Genetic loss of diazepam binding inhibitor in mice impairs social interest.* Genes Brain Behav, 2018. **17**(5): p. e12442.
22. Racine, R.J., J.G. Gartner, and W.M. Burnham, *Epileptiform activity and neural plasticity in limbic structures.* Brain Res, 1972. **47**(1): p. 262-8.
23. Jang, S.S., et al., *Seizure-Induced Regulations of Amyloid-beta, STEP61, and STEP61 Substrates Involved in Hippocampal Synaptic Plasticity.* Neural Plast, 2016. **2016**: p. 2123748.
24. Saavedra, A., et al., *Proteolytic Degradation of Hippocampal STEP61 in LTP and Learning.* Mol Neurobiol, 2019. **56**(2): p. 1475-1487.
25. Dana, H., et al., *Thy1-GCaMP6 transgenic mice for neuronal population imaging in vivo.* PLoS One, 2014. **9**(9): p. e108697.
26. Ratkai, A., et al., *Homeostatic plasticity and burst activity are mediated by hyperpolarization-activated cation currents and T-type calcium channels in neuronal cultures.* Sci Rep, 2021. **11**(1): p. 3236.
27. Bonin, R.P., et al., *Hyperpolarization-activated current (In) is reduced in hippocampal neurons from Gabra5-/- mice.* PLoS One, 2013. **8**(3): p. e58679.
28. Bell, M.R., *Comparing Postnatal Development of Gonadal Hormones and Associated Social Behaviors in Rats, Mice, and Humans.* Endocrinology, 2018. **159**(7): p. 2596-2613.
29. Sisk, C.L. and J.L. Zehr, *Pubertal hormones organize the adolescent brain and behavior.* Front Neuroendocrinol, 2005. **26**(3-4): p. 163-74.
30. Koebele, S.V. and H.A. Bimonte-Nelson, *Modeling menopause: The utility of rodents in translational behavioral endocrinology research.* Maturitas, 2016. **87**: p. 5-17.
31. Biel, M., et al., *Hyperpolarization-activated cation channels: from genes to function.* Physiol Rev, 2009. **89**(3): p. 847-85.
32. Moosmang, S., et al., *Differential distribution of four hyperpolarization-activated cation channels in mouse brain.* Biol Chem, 1999. **380**(7-8): p. 975-80.
33. Arshad, M.N. and J.R. Naegele, *Induction of Temporal Lobe Epilepsy in Mice with Pilocarpine.* Bio Protoc, 2020. **10**(4): p. e3533.
34. Reddy, D.S., et al., *Extrasynaptic gamma-aminobutyric acid type A receptor-mediated sex differences in the antiseizure activity of neurosteroids in status epilepticus and complex partial seizures.* Epilepsia, 2019. **60**(4): p. 730-743.
35. Christian, C.A., et al., *Sex Differences in the Epilepsies and Associated Comorbidities: Implications for Use and Development of Pharmacotherapies.* Pharmacol Rev, 2020. **72**(4): p. 767-800.
36. Backstrom, T., *Epileptic seizures in women related to plasma estrogen and progesterone during the menstrual cycle.* Acta Neurol Scand, 1976. **54**(4): p. 321-47.
37. Woolley, C.S., *Estradiol facilitates kainic acid-induced, but not flurothyl-induced, behavioral seizure activity in adult female rats.* Epilepsia, 2000. **41**(5): p. 510-5.
38. Mejias-Aponte, C.A., C.A. Jimenez-Rivera, and A.C. Segarra, *Sex differences in models of temporal lobe epilepsy: role of testosterone.* Brain Res, 2002. **944**(1-2): p. 210-8.
39. Reddy, D.S., et al., *Anticonvulsant activity of progesterone and neurosteroids in progesterone receptor knockout mice.* J Pharmacol Exp Ther, 2004. **310**(1): p. 230-9.
40. Woolley, C.S., *Estrogen-mediated structural and functional synaptic plasticity in the female rat hippocampus.* Horm Behav, 1998. **34**(2): p. 140-8.

41. Storm, J.F., *Potassium currents in hippocampal pyramidal cells.* Prog Brain Res, 1990. **83**: p. 161-87.
42. Bean, B.P., *The action potential in mammalian central neurons.* Nat Rev Neurosci, 2007. **8**(6): p. 451-65.
43. Brown, D.A. and G.M. Passmore, *Neural KCNQ (Kv7) channels.* Br J Pharmacol, 2009. **156**(8): p. 1185-95.
44. Berkefeld, H., B. Fakler, and U. Schulte, *Ca2+-activated K+ channels: from protein complexes to function.* Physiol Rev, 2010. **90**(4): p. 1437-59.
45. Magee, J.C., *Dendritic lh normalizes temporal summation in hippocampal CA1 neurons.* Nat Neurosci, 1999. **2**(6): p. 508-14.
46. Poolos, N.P., M. Migliore, and D. Johnston, *Pharmacological upregulation of h-channels reduces the excitability of pyramidal neuron dendrites.* Nat Neurosci, 2002. **5**(8): p. 767-74.
47. George, M.S., L.F. Abbott, and S.A. Siegelbaum, *HCN hyperpolarization-activated cation channels inhibit EPSPs by interactions with M-type K(+) channels.* Nat Neurosci, 2009. **12**(5): p. 577-84.
48. Gasparini, S. and D. DiFrancesco, *Action of the hyperpolarization-activated current (Ih) blocker ZD 7288 in hippocampal CA1 neurons.* Pflugers Arch, 1997. **435**(1): p. 99-106.
49. Huang, J., et al., *Novel mechanism for suppression of hyperpolarization-activated cyclic nucleotide-gated pacemaker channels by receptor-like tyrosine phosphatase-alpha.* J Biol Chem, 2008. **283**(44): p. 29912-9.
50. Perucca, E., D. Battino, and T. Tomson, *Gender issues in antiepileptic drug treatment.* Neurobiol Dis, 2014. **72 Pt B**: p. 217-23.

Supplementary Figures and Legends

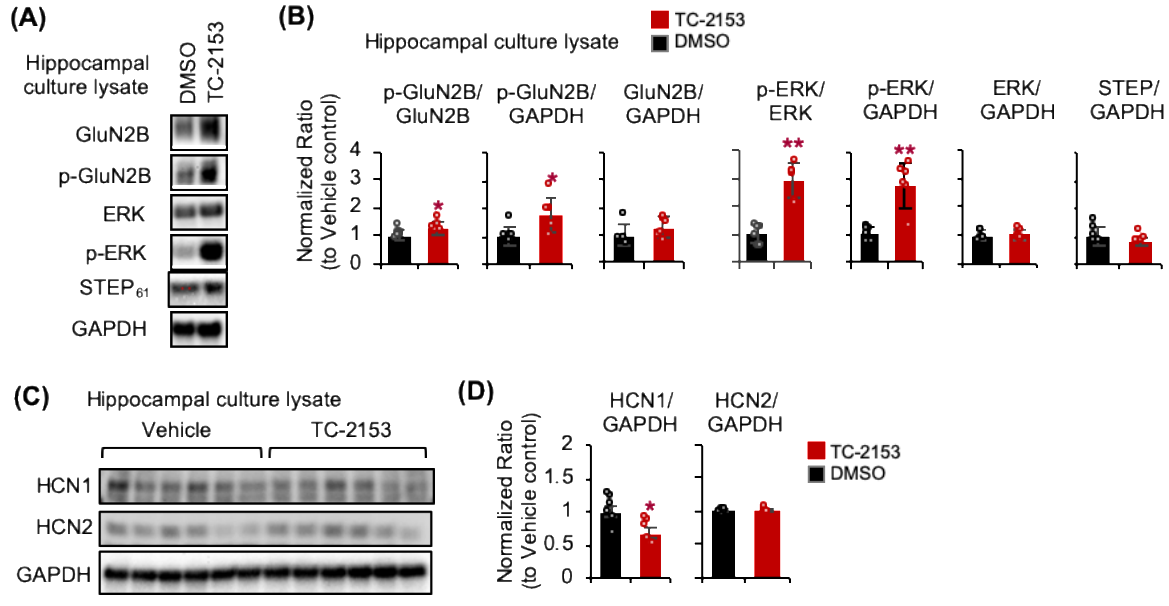

Supplementary Figure 2.1. TC-2153 application increases Tyr-phosphorylation of STEP$_{61}$ substrates in hippocampal neuronal culture. Dissociated rat primary hippocampal neuronal culture that were treated for 1 h with either DMSO as a vehicle control, or TC-2153 (10 μM) at DIV (days in vitro) 9-10. **(A-B)** Immunoblot analysis of STEP$_{61}$, Tyr^{1472}-phosphorylated GluN2B (p-GluN2B), total GluN2B (GluN2B), Tyr$^{202/204}$-phosphorylated ERK1/2 (p-ERK), total ERK1/2 (ERK), and GAPDH. **(A)** Representative immunoblots. **(B)** Quantification of immunoblots. The ratios of the phosphorylated or total protein band intensity over the GAPDH band intensity were calculated and normalized to vehicle control. TC-2153 treatment significantly increases the level of Tyr^{1472}-phosphorylated GluN2B and Tyr$^{204/187}$-phosphorylated ERK1/2 compared to DMSO treatment. **(C-D)** Immunoblot analysis of HCN1, HCN2, and GAPDH. **(C)** Representative immunoblots. **(D)** Quantification of immunoblots. TC-2153 treatment significantly decreases the level of HCN1 but not HCN2 compared to DMSO treatment. Data shown as mean ± STDEV for 6 dishes per treatment group. Student *t*-test results are shown (*p<0.05, **p<0.01).

Supplemental figure 2.1 data was collected by Brian C. Baculis and Archit Bajaj; analyzed by Brian C. Baculis.

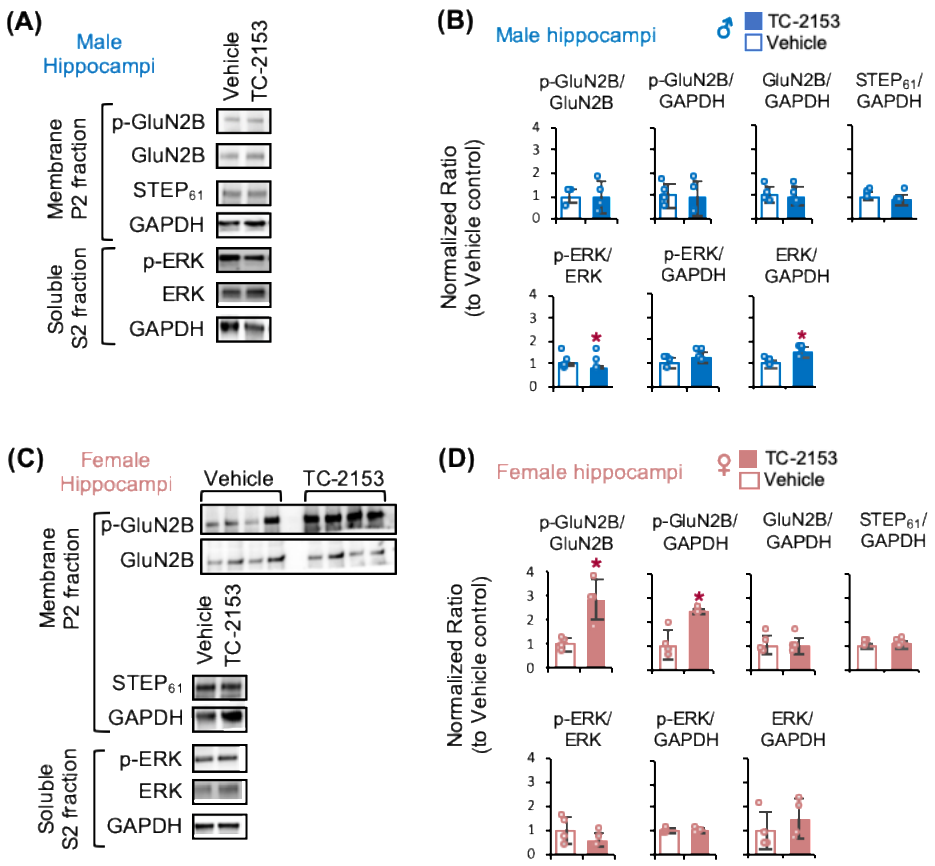

Supplementary Figure 2.2. The effect of TC-2153 injection on Tyr-phosphorylation of STEP$_{61}$ substrates in mouse hippocampi *in vivo*. Immunoblot analysis of hippocampal tissues of C57BL6/J mice (8-12 weeks old) at 3 h post injection with TC-2153 (10 mg/kg) or vehicle control. Hippocampal tissues were fractionated into membrane (P2) and soluble (S2) lysate fractions, which were then subjected to immunoblot analysis for STEP$_{61}$, Tyr^{1472}-phosphorylated GluN2B (p-GluN2B), total GluN2B (GluN2B), Tyr$^{202/204}$-phosphorylated ERK1/2 (p-ERK), total ERK1/2 (ERK), and GAPDH. **(A, C)** Representative immunoblots of male hippocampi (A) and female hippocampi (C) fractions. **(B, D)** Quantification of immunoblots of male hippocampi (B) and female hippocampi (D). TC-2153 injection significantly increases the hippocampal level of Tyr^{1472} -phosphorylated GluN2B in females but not male. Data shown as mean ± STDEV for 4 mice per treatment group per sex. Student *t*-test results are shown (*p<0.05, **p<0.01).

Supplemental figure 2.2 data was collected and analyzed by Jennifer Walters.

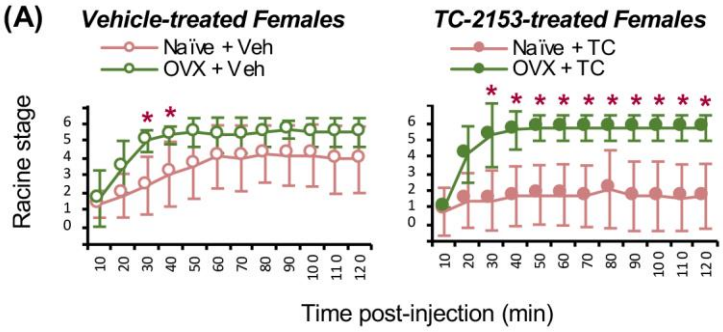

Supplemental Figure 2.3. TC-2153 injection decreases seizure severity in ovary-intact but not ovariectomized female mice. The data points of ovary-intact females (naïve) and ovariectomized (OVX) females from Figure 2B were replotted to compare the effects of OVX. Under DMSO vehicle treatment, OVX females (n=6) reached SE more quickly than ovary-intact females following KA injection (n=12). Under TC-2153 injection, OVX females (n=7) displayed higher seizure scores compared to ovary-intact females (n=12). Data shown represent the mean ± STDEV. Mann-Whitney U-test results are shown (*$p<0.05$).

Supplemental figure 2.3 data was collected and analyzed by Jennifer Walters; ovariectomies were performed by Dr. Catherine Christian-Hinman; animal experiments were performed by Jennifer Walters.

Supplementary Tables

Supplementary Table 2.1. Two-way ANOVA statistical analysis for Figure 1C, G

Behavior Test	Result	ANOVA table	F(DFn, DFd)	p value
KA-induced seizure of WT and STEP KO Mice (P42-P55)	Cumulative Seizure Score	Sex	F(1, 56) = 0.087	p = 0.769
		Genotype	F(1, 56) = 9.245	p = 0.004
		Interaction	F(1, 56) = 1.854	p = 0.179
KA-induced seizure of WT and STEP KO Mice (P56-P90)	Cumulative Seizure Score	Sex	F(1, 53) = 0.61	p = 0.438
		Genotype	F(1, 53) = 0.22	p = 0.644
		Interaction	F(1, 53) = 7.69	p = 0.008

Supplementary Table 2.2. Two-way ANOVA statistical analysis for Figure 2C

Experiment	Result	ANOVA table	F(DFn, DFd)	p value
KA-induced seizure of Mice Treated with TC-2153 or Vehicle	Cumulative Seizure Score	Sex	F(1, 48) = 1.32	p = 0.258
		Treatment	F(1, 48) = 15.94	p = 0.0003
		Interaction	F(1,48) = 2.08	p = 0.158

Supplementary Table 2.3. Two-way ANOVA statistical analysis for Figure 3

Experiment	Result	ANOVA table	F(DFn, DFd)	p value
GCaMP imaging analysis of DMSO and TC-2153 treated HP acute slice	Area Ratio over ACSF in *Dentate Gyrus (DG)*	Sex	F(1, 36) = 1.75	p = 0.195
		Treatment	F(1, 36) = 8.17	p = 0.007
		Interaction	F(1, 36) = 0.15	p = 0.699
	Area Ratio over ACSF in *CA1*	Sex	F(1, 38) = 0.79	p = 0.380
		Genotype	F(1, 38) = 8.79	p = 0.005
		Interaction	F(1, 38) = 0.05	p = 0.830
	Area Ratio over ACSF in *CA3*	Sex	F(1, 30) = 1.54	p = 0.226
		Genotype	F(1, 30) = 3.66	p = 0.066
		Interaction	F(1, 30) = 1.05	p = 0.314

Supplementary Table 2.4. Passive and I_h properties of cultured hippocampal pyramidal neurons treated with DMSO or TC-2153 in Figure 5D-E.

	n	V_m (mV)	C_m (pF)	G/G_{max} $V_{1/2}$ (mV)	G/G_{max} *k* (mV/efold)
Untreated	9	-61.8 ± 1.54	65.2 ± 5.33	-106.1 ± 11.14	4.4 ± 1.88
DMSO	12	-62.0 ± 1.68	65.4 ± 6.28	-105.9 ± 4.75	4.3 ± 1.63
TC-2153	15	-67.0 ± 2.23*^	62.4 ± 7.25	-97.2 ± 11.96*^	8.8 ± 3.33*^

n, number; Vm, resting membrane potential; Cm, whole cell membrane capacitance; $V_{1/2}$, half-activation potential; k, the slope factor. $V_{1/2}$ and k are calculated from normalized conductance G/Gmax. Data shown represents the mean ± STDEV. Post-hoc Tukey test results are shown for TC-2153 vs. untreated (*p<0.05) and TC-2153 vs. DMSO (^p<0.05).

Supplementary Methods

Experimental animals

All experiments involving the use of animal procedures were approved by and in compliance with the Institutional Animal Care and Use Committee of the University of Illinois at Urbana Champaign and the ARRIVE Guidelines [1]. All efforts were made to follow the principle of 3Rs (Replace, Reduce, Refine) and minimize both the suffering and unnecessary use of animals. All mice were housed in a standard humidity- and temperature-controlled environment on a on a normal 14:10 light:dark cycle under the permanent supervision of professional technicians of the Division of Animal Research at the University of Illinois. Food and water were provided ad libitum. At weaning, littermates of the same sex were group housed up to 5 mice per cage. Animals were euthanized by CO2 asphyxiation.

The *Ptpn5* gene knock-out mice on C57BL/6NCrl background (STEP KO) have been previously described [2] and obtained from Dr. Paul Lombroso (Yale University). Upon arrival at our laboratory, these mice were backcrossed at least 5 generations to C57BL/6J background (Jax.org, Stock Number: 000664) before performing seizure studies. Breeding pairs to generate experimental mice consisted of *Ptpn5*$^{+/-}$ and *Ptpn5*$^{+/-}$ mice, which yielded *Ptpn5*$^{+/+}$, *Ptpn5*$^{+/-}$, and *Ptpn5*$^{-/-}$. Another breeding pairs consisted of *Ptpn5*$^{+/-}$ and C57BL/6J mice, which yielded STEP$^{+/+}$ and STEP$^{+/-}$.

At weaning, genotyping of these mice was determined by Polymerase Chain Reaction (PCR) on their tail genomic DNA. The primers used in genotyping were the wild-type forward primer (5′-CCC-TAC-TCT-CAT-TCC-TCC-CTT-CCC-3′), the reverse primer common to both target and endogenous genes (5′-GGC-AGC-AGA-TGC-TGG-TGG-C-3′) and the Neo forward primer specific for the target gene only (5′-GGG-GAA-CTT-CCT-GAC-TAG-GG-3′).

Kainic acid (KA)-induced seizures

To induce seizures, both male and female mice were subjected to a single intraperitoneal (i.p.) injection of KA (Abcam, 30 mg/kg) as described [3]. For STEP WT (*Ptpn5*$^{+/+}$) and STEP KO (*Ptpn5*$^{-}$

/-) mice, we used 2 age groups: one group consists of mice with age from the beginning of the 6th week to the end of 7th week (P42-P55) which is defined as 6 to 7 weeks of age. The second group consists of mice with age from the beginning of the 8th week to the end of 12th week (P56-P90), which is defined as 8 to 12 weeks of age. Mice weighed 15 to 26 g when KA injections were performed in the laboratory under the bright light. Mice were returned to their home cage and monitored for their behavioral seizures every 10 min for the first 2 hours (h) using a modified Racine scale [4], which consists of seven stages: (Stage-0) normal behavior, (Stage-1) immobility, rigidity, (Stage-2) head bobbing, (Stage-3) rearing, forelimb clonus, (Stage-4) continuous rearing/falling, (Stage-5) tonic-clonic seizure, (Stage-6) death. Mice were euthanized at 2 h post KA injection after seizure scoring was completed. Cumulative seizure scores were calculated as the sum of all Racine stage scores at each 10-minute (min) interval over a 120-min time period. To calculate the percentage of mice that reached Stage-5 (% SE) or Stage-6 (% Death) per treatment group, the number of KA-injected mice that reached Stage-5 or Stage-6, respectively, was divided by the total number of mice in that group.

To measure the effect of STEP inhibitor TC-2153 on seizure propensity, both male and female C57BL/6J mice at 8 to 12 weeks of age were injected with either vehicle control (saline containing 2.8% DMSO or TC-2153 (Sigma Aldrich, 10 mg/kg in saline containing 2.8% DMSO) as described [5]. At 3 h post injection, mice were given either saline or KA (30 mg/kg, a single i.p. injection) and monitored for behavioral seizures as described above. Saline injection resulted in the Stage-0 seizure score in every time point in all tested males (vehicle: n = 13, TC-2153: n = 12) and females (vehicle: n = 12, TC-2153: n = 12). Based on the G*Power 3.1 analysis (power of 80%, α-error of 0.05, and effect size of 0.8), we used >12 mice per treatment for all tested groups except for OVX females (total 13 mice including 6 for vehicle, 7 for TC-2153) upon considering the robust effects of OVX on blocking anti-seizure effects of TC-2153 as well as saline-injected mice upon considering the lack of saline response.

Whole brain lysate preparation and western blotting

A separate cohort of C57BL/6J mice at 8-12 weeks old received i.p. injections with either vehicle control or TC-2153 (10 mg/kg). At 3 h post injection, mice were anesthetized by isoflurane inhalation and rapidly decapitated. Their brains were removed, dissected for hippocampi, and

stored in −80°C. The hippocampi of C57BL/6J mice were biochemically fractionated to the supernatant (S2) and the membrane (P2) fractions (0.5 mg/mL) as described [6]. In brief, two hippocampi per mouse were homogenized in ice-cold homogenization buffer (solution A) containing (in mM): 320 sucrose, 1 NaHCO3, 1 MgCl2, 0.5 CaCl2, 0.4 HEPES (pH 7.4) and Halt protease inhibitors (Thermo Fisher Scientific). After centrifuging 1,400g for 10 min at 4°C, the homogenate supernatant (S1) was separated from insoluble tissue and nuclear pellet (P1). The S1 fraction was then centrifuged at 13,800g for 10 min at 4°C. The supernatant (S2) was removed, and the remaining pellet (P2 membrane fraction) was resuspended in ice-cold solution B containing (in mM): 160 sucrose, 6 Tris-HCl, 0.5% Triton-X (pH 8.0) and Halt protease inhibitors. The S2 fraction is enriched with cytosolic soluble proteins. The P2 fraction is enriched with transmembrane proteins and membrane-bound proteins. BCA assay (Pierce) analysis was performed to determine protein concentrations across samples, which were subsequently normalized to 0.5 mg/mL in Solution A (pH 7.4). The S2 and P2 fractions were stored at −80°C until use.

The S2 or P2 fractions (6 μg per sample) were mixed with 5X SDS sample buffer and heated at 75°C for 15 min. Lysate samples were run on SDS-polyacrylamide gel electrophoresis (SDS-PAGE) gels and transferred to polyvinyl difluoride (PVDF) membrane (Millipore). Immunoblot analysis was performed as described [6, 7] with the following modifications. Each blot was blocked in 5% bovine serum albumin (BSA) and 0.1% Tween-20 in Tris buffered saline (TBS) for 1 h and then incubated in primary antibodies with washing buffer (1% BSA and 0.1% Tween-20 in TBS) overnight at 4°C. Primary antibodies used include $STEP_{61}$ (#4396, Cell Signaling, 1:1000), anti-GluN2B (AB1557P, Millipore, 1:1,000), anti-GluN2B-$pTyr^{1472}$ (P1516-1472, PhosphoSolutions, 1:500), anti-ERK1/2 (#4695, Cell Signaling, 1:1,000), anti-ERK1/2-$pTyr^{202/204}$ (#9106, Cell Signaling, 1:2000), and GAPDH (#2118, Cell Signaling, 1:1000). After incubating in HRP-conjugated secondary antibody in washing buffer for 1 h, the blots were exposed to enhanced chemiluminescence substrate (ECL, Thermo Fisher Scientific) for 1 min. The luminescent signals were detected using an iBright imaging processor. Densitometric quantification was performed with ImageJ Software (National Institutes of Health) as previously described [6, 7]. The band intensity of a protein of interest was divided by the GAPDH band intensity. The ratio of vehicle-treated control group was taken as 100%, and the ratio of TC-2153-treated

group was normalized to the ratio of vehicle-treated control to obtain the % of relative protein expression.

GCaMP6s imaging

Acute hippocampal slices were prepared from male and female Thy1-GCaMP6s mice (Jax.org stock 024275) at 4-11 weeks of age. These mice contain genetically encoded calcium indicator GCaMP6s [8]. In brief, Thy1-GCaMP6s mice were anesthetized with isoflurane and rapidly decapitated. Both male and female mice were used. The brain was quickly removed and placed in ice-cold sucrose based cutting solution consisting of the following (mM): 25 $NaHCO_3$, 200 sucrose, 10 glucose, 2.5 KCl, 1.3 NaH_2PO_4, 0.5 $CaCl_2$ and 7 $MgCl_2$. Coronal hippocampus slices were cut at 200 μm using a vibrating microtome (Leica VT1000S). Slices were then transferred to basal artificial cerebrospinal fluid (ACSF) consisting of the following (in mM): 125 NaCl, 26 $NaHCO_3$, 2.5 KCl, 1 NaH_2PO_4, 1.3 $MgCl_2$, 2.5 $CaCl_2$ and 12 glucose, equilibrated at 35°C for 30 min, and then maintained at room temperature for 1 h before calcium imaging. Cutting solution and ACSF were saturated with 95% O_2 and 5% CO_2. All experiments were performed at 32°C. Slices were incubated with either vehicle control (0.14% DMSO) or TC-2153 (10 μM) for 1 hour as they recovered at room temperature.

Time lapse fluorescence images of GCaMP6s (size: 640 x 404 pixel) at the CA1, CA3, and DG regions were acquired in ACSF for 1 min at 3.6 frame per second with 25 ms exposure time, and 3x3 binning using a Zeiss Axio Observer microscope with a Zeiss AxioCam 702 mono Camera and ZEN Blue 2.6 software, and were stored with no further modification as ZVI and 16-bit TIFF files. Slices were then incubated with KCl (15 μM) in ACSF for 2 min and imaged for another 1 min. Images from 10-60 sec were analyzed for mean fluorescence intensity (F) in DG, CA1, and CA3 using ImageJ (NIH). $\Delta F/F = (F-Fmin)/Fmin$ was computed as described [8], where ΔF indicates the difference between the initial intensity in ACSF and the intensity after KCl stimulation. $\Delta F/F$ was normalized to ACSF.

Hippocampal neuronal culture and western blotting

Primary dissociated hippocampal cultures were prepared from E18 Sprague-Dawley rat embryos as described [7] and plated at high density (330 cells/mm^2) onto poly L-lysine-coated (0.1 mg/mL) 30 mm cell culture dishes. Application of TC 2153 at 1-10 μM for 1 h has been previously demonstrated to increase Tyr-phosphorylation of multiple STEP substrates in primary cortical cultured neurons with minimal toxicity, although TC-2153 has an IC50 of 24.6 nM *in vitro* [5]. To maximally inhibit STEP, neurons at 9-10 *days in vitro* (DIV) were treated for 1 h with vehicle control (0.14% DMSO) or TC 2153 (10 μM).

Following pharmacological treatment, hippocampal cultured neurons were lysed in ice-cold RIPA buffer (200 μL per dish) which contained protease inhibitor cocktail and phosphatase inhibitor cocktail (Thermo Fisher Scientific). The resulting lysate samples (12 μL) were subjected to immunoblot analysis as described [7] with primary antibodies including $STEP_{61}$ (#4396, Cell Signaling, 1:1000), anti-GluN2B (AB1557P, Millipore, 1:1,000), anti-GluN2B-$pTyr^{1472}$ (P1516-1472, PhosphoSolutions, 1:500), anti-ERK1/2 (#4695, Cell Signaling, 1:1,000), anti-ERK1/2-$pTyr^{202/204}$ (#9106, Cell Signaling, 1:2000), HCN1 (#APC-056, Alomone, 1:1000), HCN2 (#75-111, Neuromab, 1:1000), and GAPDH (#2118, Cell Signaling, 1:1000). Densitometric quantification, following normalization to GAPDH was performed with ImageJ software (National Institutes of Health) as described [6, 7].

Electrophysiology

For recording in dissociated cultured rat hippocampal neurons, we pre-treated with TC 2153 (10 uM) or DMSO in the coverslip containing DIV 8-10 for 60 min before recording. Then, the coverslip was transferred to the recording chamber in external solution containing (in mM): 125 NaCl, 26 $NaHCO_3$, 2.5 KCl, 1 NaH_2PO_4, 1.3 $MgCl_2$, 2.5 $CaCl_2$, and 12 Dextrose, bubbled with 95% O_2 and 5% CO_2 (310–315 mOsm, pH 7.2 to 7.3 with KOH). The pyramidal neurons were visually identified using an upright microscope (Axio scope, Carl Zeiss Microimaging, Thornwood, NY, USA). The whole-cell patch-clamp recordings were carried out at 30–32°C in external solution containing the synaptic transmission blockers CNQX (20 μM), DL-AP5 (100 μM) and bicuculline (20 μM) for action potential (AP) and Sag voltage and rebound voltage under

current clamp mode. Recording pipettes were pulled from glass capillaries with an outer diameter of 1.5 mm on micropipette puller (P-97; Sutter Instruments, Novata, CA, USA), and had a resistance of 3–5 MΩ when filled with internal solution containing (in mM): 130 potassium methylsulfate, 10 KCl, 5 Tris-phosphocreatine, 10 HEPES, 4 NaCl, 4 Mg_2ATP, and 0.4 Na_2GTP. (290–295 mOsm, pH 7.2 to 7.3 with KOH) [9, 10]. RMP was measured in current-clamp 2 min after achieving the whole-cell configuration to let the internal solution diffused enough into the cytosol.

Neurons were held at -60 mV. The AP firing rates (Hz) were measured upon delivering constant current pulses of 500 ms ranging from 0 to 200 pA in 10 pA increments with a step interval of 10 sec. Neurons were omitted if the resting membrane potential was more depolarized than −50 mV, or if no APs were discharged. Sag voltages were measured upon delivering constant current pulses of 500 ms ranging from - 200 to 0 pA in 20 pA increments. Whole-cell recordings were made using a Multiclamp 700B amplifier (Molecular Devices). Electrophysiological recordings were filtered at low-pass Bessel at 10 kHz and digitized at 10 kHz. Data was acquired and analyzed with a Digidata 1440A interface (Molecular Devices) and the pClamp suite of software (version 10.6; Molecular Devices). Recording analyses were performed using Clampfit software (version 10.7; Molecular Devices).

The instantaneous AP firing rate at each current pulse was calculated as a reciprocal of the interspike intervals (ISI), measured as the time between the first and second AP peaks (i.e. 1/interspike interval) as previously described [9, 10]. The AP threshold was measured as the membrane potential at which dV/dt of the AP exceeded 10 mV/ms. The AP height was calculated as the difference between the AP peak amplitude and the AP threshold. The 10–90% rise time and decay time were determined by calculating the difference between the time of 10% and 90% of the AP peak amplitude, respectively. The AP half width was measured as the width at half-maximal AP amplitude. Fast afterhyperpolarization (fAHP) was measured from trains of APs elicited by 100-pA current injection as the difference between the AP threshold and minimum voltage after the AP peak. The AP latency was assessed as the time between onset of current injection to peak of the first ensuing AP. Rheobase current was quantified as the minimal depolarizing current step sufficient to elicit an AP as described [9, 10]. Input resistance of the neuron was measured by dividing the average voltage deflection of the membrane potential by a hyperpolarizing 10 pA current step (500 ms) from -50 pA to -10 pA.

Voltage clamp recording of hyperpolarization activated current (I_h) was performed as described [11]. I_h was activated by changing the holding potential at -60 mV through a range from -60 mV to -120 mV in 5 mV decrements under voltage clamp in external solution containing CNQX (20 μM), DL-AP5 (50 μM), bicuculline (10 μM) and TTX (0.5 μM). Each test potential was maintained for 1 s. The net I_h conductance was measured as the difference between the steady-state current at the end of the test potential and the minimum current measured within 100 ms. The normalized conductance (G/Gmax) was plotted as a function of voltage steps. No corrections were made for liquid junction potentials. The I_h currents were then fit to a Boltzmann distribution of the following form: $y=y\ max/[1/exp.(V_{1/2}-V)/k]$, where V is the test potential, $V_{1/2}$ the half-activation potential, and k the slope factor.

Supplementary References

1. Kilkenny, C., et al., *Animal research: reporting in vivo experiments: the ARRIVE guidelines.* Br J Pharmacol, 2010. **160**(7): p. 1577-9.
2. Zhang, Y., et al., *Genetic reduction of striatal-enriched tyrosine phosphatase (STEP) reverses cognitive and cellular deficits in an Alzheimer's disease mouse model.* Proc Natl Acad Sci U S A, 2010. **107**(44): p. 19014-9.
3. Kim, E.C., et al., *Heterozygous loss of epilepsy gene KCNQ2 alters social, repetitive and exploratory behaviors.* Genes Brain Behav, 2020. **19**(1): p. e12599.
4. Levesque, M. and M. Avoli, *The kainic acid model of temporal lobe epilepsy.* Neurosci Biobehav Rev, 2013. **37**(10 Pt 2): p. 2887-99.
5. Xu, J., et al., *Inhibitor of the tyrosine phosphatase STEP reverses cognitive deficits in a mouse model of Alzheimer's disease.* PLoS Biol, 2014. **12**(8): p. e1001923.
6. Jang, S.S., et al., *Seizure-Induced Regulations of Amyloid-beta, STEP61, and STEP61 Substrates Involved in Hippocampal Synaptic Plasticity.* Neural Plast, 2016. **2016**: p. 2123748.
7. Jang, S.S., et al., *Regulation of STEP61 and tyrosine-phosphorylation of NMDA and AMPA receptors during homeostatic synaptic plasticity.* Mol Brain, 2015. **8**(1): p. 55.
8. Dana, H., et al., *Thy1-GCaMP6 transgenic mice for neuronal population imaging in vivo.* PLoS One, 2014. **9**(9): p. e108697.
9. Kim, E.C., et al., *Reduced axonal surface expression and phosphoinositide sensitivity in Kv7 channels disrupts their function to inhibit neuronal excitability in Kcnq2 epileptic encephalopathy.* Neurobiol Dis, 2018. **118**: p. 76-93.
10. Lee, K.Y., et al., *N-methyl-D-aspartate receptors mediate activity-dependent down-regulation of potassium channel genes during the expression of homeostatic intrinsic plasticity.* Mol Brain, 2015. **8**: p. 4.
11. Bonin, R.P., et al., *Hyperpolarization-activated current (In) is reduced in hippocampal neurons from Gabra5-/- mice.* PLoS One, 2013. **8**(3): p. e5867

CHAPTER 3: INVESTIGATING THE EFFECTS OF SPONTANEOUS RECURRENT SEIZURE DEVELOPMENT IN A HOMOZYGOUS STEP KO STRAIN AND CCI-INDUCED TBI ON STEP EXPRESSION IN THE HIPPOCAMPUS

3.1 Background

Upregulation of Striatal-enriched protein tyrosine phosphatase (STEP), gene name *PTPN5*, has been shown in numerous models of neurological disorders. Upregulation of STEP is found in postmortem tissue of Alzheimer's (AD) patients as well as animal models of AD [1-3]. Significant increases in $STEP_{61}$ levels have been found in the postmortem anterior cingulate cortex and dorsolateral prefrontal cortex of schizophrenia patients, as well as inducible mouse model of schizophrenia upon treatments with psychotomimetic NMDAR antagonists MK-801/Dizocilpine and a dissociative hallucinogenic drug, phencyclidine [4]. $STEP_{61}$ levels are also shown to be elevated in the cortex of both putative risk gene neuregulin 1 knockout ($Nrg1^{+/-}$) and the receptor tyrosine kinase ErbB2/4 (which is signaled by Nrg1) knockout mouse model of schizophrenia, and in human induced pluripotent stem cells (hiPSC)-derived forebrain neurons and Ngn2-induced excitatory neurons from two independent schizophrenic patient cohorts [5].

Notably, age-dependent increases in STEP levels are found in heterozygous knock-out mice of superoxide dismutase ($SOD2^{+/-}$), which plays an anti-apoptotic role in countering oxidative stress and inflammation in aging, cancer, and neurodegenerative disorders [6]. A follow-up investigation of the role of $STEP_{61}$ in oxidative stress caused by traumatic brain injury (TBI) demonstrates that increased $STEP_{61}$ levels and accompanies decreased protein and current levels of synaptic NMDARs in C57Bl/6 and $SOD2^{+/-}$ mice, whereas treatment of STEP inhibitor TC-2153 partially reduced this effect [7], suggesting that the increase in $STEP_{61}$ level and/or activity may serve as an early biomarker of synaptic damage due to trauma. This is crucial, since trauma to the brain, such as TBI and *status epilepticus* (SE), is one of the most common risk factors that leads to the development of temporal lobe epilepsy (TLE) [8].

Our recent publication [9] showed that the administration of TC-2153 at 3 h prior to i.p. injection of kainic acid (30 mg/kg) leads to significantly less seizure severity in C57Bl/6J mice compared to

vehicle control (see Chapter-2). We also show that TC-2153 significantly reduces intrinsic excitability and I_h of cultured rat hippocampal neurons (see Chapter-2). However, whether the anti-seizure effect of TC-2153 is due to its specific inhibition of STEP or its direct inhibition of other proteins such as HCN channels that underlie I_h is unknown. Furthermore, whether hippocampal $STEP_{61}$ contributes to the development of TLE is unknown.

In this chapter, we first tested if the anti-seizure effect of TC-2153 requires STEP by utilizing KA-induced acute SE model in homozygous *PTPN5*$^{-/-}$ (STEP KO) mice. We found that the effect of TC-2153 in reducing severity of kainate (KA)-induced seizures was abolished in both male and female STEP KO mice, indicating that anti-seizure effect of TC-2153 requires STEP. As a first step to investigate whether hippocampal $STEP_{61}$ contributes to the development of TLE, we next investigated if TBI changes $STEP_{61}$ expression and/or activity using the Cortical Controlled Impact (CCI) model of TBI. Our preliminary findings show that TBI increases $STEP_{61}$ protein expression by 14 days post TBI in both the hippocampus and cortex.

To test if this increase in hippocampal $STEP_{61}$ persists during epileptogenesis and if hippocampal $STEP_{61}$ contributes to the development of spontaneous seizures in TLE, I used the repeated, low-dose kainate (RLD-KA) model of TLE in STEP KO mice and wild-type (WT) mice. In this RLD-KA model of TLE, KA-induced SE induces damage to the hippocampus, and ultimately produces spontaneous convulsive seizures over a 7 day period post-insult [10] that originate from the hippocampus and become generalized over time [8]. I have collected the brain tissues at 1, 2, 4, 7, 14, and 21 day post KA-induced SE, but was unable to process the tissues for western blot analysis of $STEP_{61}$ level and activity. However, based on our TBI-induced increase in hippocampal $STEP_{61}$ expression, I expect to see a persistent increase in the level and activity of $STEP_{61}$ during epileptogenesis as well as when spontaneous recurrent seizures occur in the RLD TLE model. Here, I present the progress of these 3 outlined projects as shown below.

3.2 Methods

Acute KA-induced seizures in STEP KO mice after vehicle or TC-2153 treatment.

All animal procedures were approved by the Institutional Animal Care and Use Committee of the University of Illinois at Urbana Champaign and conformed to the ARRIVE Guidelines. Both male

and female *Ptpn5* homozygous knock-out mice (*Ptpn5*$^{-/-}$) [3], wild-type mice (*Ptpn5* $^{+/+}$), (Jax.org, Stock Number: 000664) were used for seizure studies at 9-11 weeks old. Behavioral seizures were induced in mice by intraperitoneal (i.p.) injection of saline or a high, single dose of KA, (30 mg/kg, Abcam) [11] and monitored using modified Racine scale for 2 hours (h) [12]. To test the effects of TC-2153, C57BL/6J mice received KA at 3 h post i.p. injections with either vehicle control (saline containing 2.8% DMSO) or TC-2153 (10 mg/kg in saline containing 2.8% DMSO, Sigma Aldrich). This treatment was previously demonstrated to increase Tyr-phosphorylation of STEP substrates in the cortex [1].

The Cortical Controlled Impact (CCI) model of TBI.

The animals were administered with Carprofen (0.5 mg/kg, i.p.) and 2-3% isoflurane. Body temperature was maintained at 37 °C on a heating pad and monitored during the surgery. Depth of anesthesia was observed by a gentle toe pinch without causing any injury. The hair on the heads of the anesthetized mice was removed with Nair and skin was cleaned with betadine. Then, the animals' heads were fixed in a stereotaxic frame and TBI was induced using the CCI technique. A midline skin incision was performed to expose the skull and craniotomy over the left somatosensory cortex was performed in both sham and CCI animals. To produce the recapitulative effects of induced TBI, the impact was delivered to the mice at a strike velocity of 3.5 m/sec with a dwell time of 400 msec at a depth of 1.0 mm. The area of craniotomy was sutured, lidocaine (2.5%) or prilocaine (2.5%) and Neosporin were applied as topicals on the injury site. The animals were monitored until recovery from anesthesia and over the next 14 consecutive postoperative days.

Transcardial perfusion, hippocampal slice, and immunohistochemistry

Our postdoc Dr. Eung Chang Kim fixed and collected neural tissue at time point 14 days post-CCI. To make the slices, the mice were deeply anesthetized using isoflurane and transcardially perfused with ice-cold 1x PBS (approximately 15-20ml or until all blood is clear) then with ice-cold 2% PFA (pH 6; about 20ml or until mouse is rigid). The brain was then harvested and placed in 5 ml of cold 2% PFA (pH 6) in a 50 ml conical tube and stored for 1 hour (h) at 4°C. The brain was cryoprotected with 30% w/v sucrose overnight (or until brain sinks in solution) at 4°C. The brain was frozen using isopentane on dry ice, embed in OCT and stored at -80°C. Slice sections of

30um of the desired area (hippocampus) were taken and collected on glass slides (Superfrost plus Microscope slide, Fisher, Cat # 22-037-246).

On Day 1 of immunostaining, the slides were washed twice with 1X PBS (300 ul/slice) for 5 min and then fix the with fixation buffer (300 ul/slice) for 30 min at room temperature. Slices were then permeabilized with 0.3% Triton-X-100/1X PBS for 1 h at room temperature. The slices were then blocked (10% NGS / 0.3% Triton-X in 1X PBS), labeled with 300 ul of anti-STEP Ms (Cell Signaling #4396S, 1:100), anti-GFAP Ms (Neuromab #75-240, 1:200) and anti-NeuN Rb (Cell Signaling #24307, 1:250) primary antibodies and incubated overnight while rotating at 4°C. On Day 2, slices were washed and secondary antibodies were added at 1:200 dilution in incubating solution (3% NGS / 0.3% Triton-X in PBS) and incubated in 500 ul of secondary antibody overnight at 4°C. On Day 3, the slices were washed and then transferred to slides. Once the slides were partially dry, DAPI was added (1:200) in PBS and a coverslip for 1 h at room temperature. Slides were stored at 4°C. The slices were imaged using our Zeiss Axio Observer microscope with a Zeiss AxioCam 702 mono Camera and ZEN Blue 2.6 software. Images were acquired using a 63x objective. Fluorescence images of the slices will be acquired using the same exposure time and analyzed with ImageJ software (National Institutes of Health).

Immunohistochemical analysis

Fluorescence images of the slices were acquired using the same exposure time and the average mean intensities of each image were analyzed with ImageJ (National Institutes of Health). Student *t*-test was used to determine significance. The p value (< 0.05) will be considered statistically significant.

The RLD-KA model of TLE in STEP KO mice and wild-type (WT) mice

All animal procedures were approved by the Institutional Animal Care and Use Committee of the University of Illinois at Urbana Champaign and conformed to the ARRIVE Guidelines. Both male and female *Ptpn5* homozygous knock-out mice (*Ptpn5*$^{-/-}$, or STEP KO) [3] (Jax.org, Stock Number: 000664) and wild-type mice bred on a C57BL/6J background were used for seizure studies at 6-8 weeks old. To test if $STEP_{61}$ levels and activity change in the hippocampus during the development of spontaneous seizures, we employed the RLD-KA mouse model of chronic TLE as described [13], where wild-type and STEP KO mice were given one dose of either saline or KA (5 mg/kg, i.p.)

every 30 min until the animal reaches a stage 5 score on the modified Racine scale (Fig. 3.3). Once the animal entered stage 5, behavioral seizure scores were monitored continuously for 120 min. Immediately following the scoring period, Diazepam (10 mg/kg, i.p.) was administered to allow seizures to subside. Neural tissue was collected at 1, 2, 4, 7, 14, and 21 days post-KA (Table 3.2). Spontaneous recurrent seizures in mice are always non-convulsive according to the literature [11], so the time points according to interictal spike recordings from the ipsilateral and contralateral hippocampus are crucial. Prior to the onset of the first spontaneous seizure and within one week after SE, abnormalities in EEG recordings of kainate-injected rodents occur. The 1-7 d post-KA time point allows us to examine changes in $STEP_{61}$ during the latent period after injection [11]; 14 d post-insult allows us to investigate the changes occurring after spontaneous seizure onset is established [14], and 21 d post-insult lies within the time frame when recurrent spontaneous recurrent seizures are produced [10, 13].

Seizure Score Analysis

Statistical analyses were performed using the Student's two-tailed *t* test to determine statistical significance at each 10 min time interval of the 120 min seizure scoring period, as well as to assess significance of cumulative seizure scores, RLD-KA injection amount, and average time of SE onset. Data are reported as mean ± SEM. The priori value (p) < 0.05 was considered statistically significant.

3.3 Results

TC-2153 does not alter seizure severity in homozygous STEP KO mice of both sexes.

We first tested if the anti-seizure effect of TC-2153 requires STEP by utilizing a KA-induced acute SE model in a homozygous $PTPN5^{-/-}$ (STEP KO) mouse strain. Mice were used at 9-11 weeks of age for consistency, since our previously published study investigated the effects of TC-2153 in C57BL/6J mice at 8-12 weeks of age [9].

We found that the effect of TC-2153 (10 mg/kg, i.p.) in reducing severity of kainate (KA)-induced seizures was abolished in both male and female STEP KO mice (Fig. 3.1B), which indicates that the anti-seizure effect of TC-2153 requires STEP. In addition, differences in cumulative seizure

scores were not significant in either sex (Fig. 3.1C). There was a slight 9.09% SE increase in vehicle-injected STEP KO males compared to the group that received TC-2153, while the % SE was the same in both female groups. The % death in males increased 18.18% in the TC-2153-injected group compared to control, while in females there was a 22.22% increase in the vehicle-injected group.

Controlled Cortical Impact (CCI) leads to TBI induction and changes in STEP expression in the hippocampus.

To assess the effects of neuronal injury on STEP levels expressed within the hippocampus, we used the CCI model of TBI induction to produce the focal injury (Fig. 3.2A). CCI is used as a model of posttraumatic epilepsy to induce similar pathology to injury-induced epilepsy. It has been shown to onset the development of spontaneous posttraumatic seizures within 24 h, as well as structural and functional network changes in the murine dentate gyrus associated with TLE, by 71-d post-injury [15]. Specifically, spontaneous convulsive seizures are exhibited in approximately 40% of mice within weeks post-CCI induced severe injury, while they are observed in about 9-20% of mice after moderate CCI injury [15, 16]. In addition, many mice develop seizures and hippocampal pathology by 8 weeks post-CCI induced injury [17].

CCI is a common model of brain trauma that uses a controlled piston to induce reproducible and well-controlled injury [18]. Animals were subjected to either sham or CCI procedure during stereotaxic craniotomy (Fig. 3.2A) and were transcardially perfused 14 d later. The brains were immediately collected, fixed, and cryosectioned. Slices were immunostained using anti-STEP Ms (Cell Signaling #4396S), anti-GFAP Ms (Neuromab, #75-240) and anti-NeuN Rb (Cell Signaling #24307). In hippocampal sections that received CCI, we observed higher ipsilateral GFAP and STEP expression (Fig. 3.2B). It is established that upregulated GFAP expression by astrocytes significantly increases from 1 d up to 4 weeks after brain injury due to cortical contusion [19]. NeuN and DAPI were observed to maintain similar levels of expression compared to sham control, despite the cortical impact and diminished expression of NeuN and DAPI in the cortex (Fig. 3.2B). These results confirm that our CCI model worked in animals that received the traumatic cortical impact procedure and that CCI leads to TBI-induced changes in STEP expression in the hippocampus.

Our preliminary data demonstrates that CCI leads to a visible increase in STEP-expressing neurons in the CA2 region on both ipsilateral and contralateral sides (Fig. 3.3A). Further analysis of the average STEP mean intensity over the number of cells in each hippocampal region showed that animals subjected to CCI express significantly higher levels of STEP compared to sham animals (Fig. 3.3B). These results are consistent with previous findings demonstrating that increased levels of total STEP expression are observed in $SOD2^{+/-}$ mouse models of oxidative stress and inflammation [6], as well as a follow-up study that specifically observed increased $STEP_{61}$ and higher STEP activity after being subjected to TBI by using the CCI method [7]. Further investigation of subsequent time points post-TBI induction as well as immunostaining of STEP and its activity should be pursued to assess the progression of STEP expression as a follow-up to these experiments.

Homozygous loss of STEP does not significantly delay the onset of SE in RLD-KA model.

Kainate is one of the most commonly used drugs to induce SE in rodents – however, this model poses several challenges such as high mortality rate, inconsistent seizure response, and resistance to kainate-induced neurotoxicity by intraperitoneal (i.p.) injection, particularly in the C57BL/6J strain of mice [11]. Recently, it has been shown that using repeated low doses of kainate via i.p. injection can mitigate some of these risks [13, 20]. The use of repeated low doses of kainate at 5 mg/kg via i.p. injection at 30 min intervals until C57BL/6J mice reach stage 5 seizures (based on a Racine scale) has been reported to successfully produce immediate epileptogenesis at less than 1-5 days post-SE as demonstrated by continuous video-electrography (EEG) recording for 4-18 weeks [13]. To do this, the study identified two forms of seizures: behavioral convulsive seizures (CS) and electrographic nonconvulsive seizures (NCS), where spontaneous behavioral CS episodes decreased after four weeks of SE, but the spontaneous NCS were recurrent during up to the 18-week observation period. There was also found to be a mortality reduction from 21% to 6% and decreased seizure variability observed between animals when compared to groups receiving a single high dose (20 mg/kg, i.p.) of kainate [20]. For these reasons, we found this repeated low-dose method of seizure induction to be an ideal model for studying the effects of spontaneous recurrent seizures on STEP expression, as well as to investigate the effects of the RLD model in a genetic STEP knockout strain of mice bred on a C57BL/6J background.

To this end, our first goal was to demonstrate the efficacy of the RLD-KA model in both WT and STEP KO mice at 6 to 8 weeks of age, as well as to analyze the effects on both strains after SE onset (Fig. 3.4A).

Since our previous results using a single high dose of kainate (30 mg/kg, i.p.) demonstrated an apparent age- and sex-dependent difference in homozygous STEP KO mice, we hypothesized that RLD would recapitulate these outcomes [9]. The repeated low-dose KA was given to the mice to achieve SE. We determined the number of KA injections required in order to reach SE (Fig. 3.4B) as well as the average amount of time leading up to the onset of SE in each experimental group (Fig. 3.4C). Seizures were monitored for 120 min immediately once SE was reached. Seizure score analyses were performed investigating the outcomes of STEP KO mice of combined sex compared to WT mice of combined sex, female STEP KO compared to female WT, and male STEP KO compared to male WT. An increased trend in severity was observed in STEP KO females compared to WT females (Fig. 3.4D) – however, it is important to note that the female sample number is small (n=5) and is subject to change with the addition of later samples. The number of kainate injections administered per mouse, and average time of the SE onset after the final low dose of kainate, and cumulative seizure scores were not significantly different (Fig. 3.4B-C, 3.4E).

Sensitivity to RLD-KA model based on a sex-dependent manner is observed in both WT and STEP KO mice.

Mice that were used to assess the effectiveness of RLD-KA model in Fig. 3.4 were also compared by sex in Fig. 3.5. The number of KA injections administered per mouse is slightly higher in females from both WT and STEP KO mice – females also showed a slightly elevated trend in the average time of SE onset after receiving the final KA injection (Fig. 3.5A-B). Intriguingly, WT females displayed a significant reduction in seizure severity, whereas WT males experienced an average of stage 4-5 seizures throughout the majority of the scoring period. A decreased trend in seizure severity was also observed in STEP KO females compared to males (Fig. 3.5C). Significantly increased cumulative seizure scores were also reflected in WT females compared to males, while a higher trend was seen in STEP KO males compared to females (Fig.

3.5D). These trends suggest that females exert a modest resistance to RLD-induced seizures compared to their male counterparts.

Hippocampal and cortical tissue were harvested and frozen in -80°C at time points 1d, 2d, 4d, 7d, and 21d post-SE onset to mark the progression of STEP expression, as well as its activity, through the period of epileptogenesis (days 1-10) and up to the point of spontaneous seizure development, which typically develop approximately 11 days post-kainate injection. The 2-7 d post-insult time point will allow us to examine changes in $STEP_{61}$ during the latent period after injection [11]; 14 d post-insult allows us to investigate the changes occurring after spontaneous seizure onset is established [14], and 21 d post-insult lies within the time frame (30-60 d) when spontaneous recurrent seizures occur in both ipsilateral and contralateral sides of the injection site [11]. Below is a table of all sets of neural tissue I have personally collected for analysis – in the future, our lab will fractionate and western blot these tissues to analyze hippocampal levels of STEP expression, as well as its activity and substrate phosphorylation. These findings will determine whether STEP is upregulated during the progression of spontaneous seizures in a RLD-KA model of TLE.

RLD kainate injection method successfully induces SE with extremely low mortality and spontaneous recurrent seizures using video recording to assess behavioral convulsive seizures.

High mortality rate is a large problem when considering the use of the kainate injection model [11]. Out of the WT mice (n=38) that underwent induced SE for these experiments, there was a death rate of 0.05%, while for STEP KO mice (n=10) the death rate rested at 0%. This was quite an improvement, considering the WT and STEP KO mice that received 30 mg/kg (i.p.) kainate injections in our previous study experienced death rates that ranged between 20-70% [9]. Spontaneous recurrent seizure activity was monitored and scored based on the following table (Table 3.1) from 1-hour video recordings per mouse taken 21 days post-SE.

For monitoring spontaneous seizure at 21 d post-SE, STEP WT (n=1) and STEP KO (n=7) mice were subjected to RLD-KA, and STEP WT (n=1) and STEP KO (n=3) mice were subjected to RLD-saline. We found that 5 out of 7 STEP KO mice that underwent RLD-KA injections exhibited at least one score of 8 (wild jumping) within a 60 min scoring period, where two of those animals

also experienced intervals of behavioral arrest. No seizure stage phenotypes were observed in STEP KO mice that received saline (n=3) or in WT mice that received saline or kainate (n=1 each). Separate observations that could not be indicated with a score were that all RLD-KA injected mice displayed persistent hyperactivity and excessive grooming compared to mice that received saline. Though not all animals subjected to RLD-KA injections experienced spontaneous seizures, it is important to note that repeated low doses of kainate are reported result in infrequent seizure activity specifically in C57BL/6J mice – however, pathological signs of temporal lobe epilepsy such as hippocampal cell death, widespread astrogliosis, and astrocyte expression of mGluR5 are still produced [10]. In order to reach sufficient sample size for power analysis as well as confirm interictal spike activity, we must repeat these experiments with behavioral seizure scoring and electroencephalography (EEG) recording.

3.4 Discussion and Future Directions

STEP is highly expressed not only in the hippocampus, but also in the pituitary in a developmental manner [21]. A recent study has investigated the role of STEP in promoting follicle-stimulating hormone (FSH) secretion, where genetic knockout or pharmacological inhibition of STEP using acute inhibitor TC-2153 was shown to reduce FSH release in the whole pituitary. They found that PTPN5 expression is also found to be heavily reduced in the pituitary after ovary removal (OVX) [22]. It is known that FSH is released from the pituitary and binds to its receptor on the female ovary, where one of its main roles is the regulation of estrogen secretion [23]. It is possible that genetic deletion or inhibition of STEP consequently effects levels of estrogen by dysregulation of FSH. Our previous findings showed that sex- and age-dependent differences were observed in STEP KO mice that received a single high dose of kainate (30 mg/kg, i.p.) compared to their WT littermates [9]. The mice were consolidated into two age groups – 6-to-7 and 8-to-12 weeks of age – considering the significant sex hormone-dependent neurological changes the animals undergo in the hippocampus during the 6^{th} to 8^{th} week of development [24, 25]. These critical alterations in hippocampal circuitry and synapse formation may influence the animal's sensitivity to KA and could explain the sex-related differences in our data. It is also important to acknowledge that the STEP KO "n" is low (n=5 for females and n=7 for males) when broken out by sex. These results are subject to change after increasing the number of data points. In the future, it would be

interesting to investigate whether seizure severity in either sex is differentially affected in 8-to-12-week-old WT and STEP KO mice.

In regard to choosing an RLD-KA injection model to study the onset and development of temporal epilepsy pathology and spontaneous recurrent seizures, there are notable advantages and disadvantages in this paradigm. Benefits of this model include its low mortality rate and reliable ability to induce behavioral and electrographic SE over a 7-d period, as well as the ability to produce interictal spiking in the cortex [10]. This model also produces features indicative of TLE pathology (hippocampal cell death, widespread astrogliosis, and astrocyte expression of mGluR5), as well as the ability to produce interictal spiking in the cortex [10]. What sets our particular protocol apart (using 5 mg/kg, i.p.) from other RLD-KA injection paradigms is that it has the ability to produce spontaneous recurrent seizures over an 8 week period [10]. However, the disadvantage lies in that the presentation of these spontaneous seizures is quite rare, therefore it does not ultimately produce a robust epilepsy phenotype. On the other hand, in terms of the translation of this model to test for potential ASDs, there are several factors to consider. Specifically, when kainate is injected systemically, the neuronal damage that is observed is more widespread – particularly in limbic regions [26] and few studies have been conducted testing the effects of ASDs on spontaneous recurrent seizure development after systemic administration of kainate in rats [27-29], and are proven to be quite complicated and laborious due to 1) the infrequent and variable spontaneous seizure activity demonstrated in rodents, and 2) the rapid elimination of the drug in rodents when compared to humans [30]. Overall, this type of model suggests low predictive validity in the ability to reliably screen for a potential ASD or therapeutic.

In contrast, an intrahippocampal kainate (IHP-KA) injection model proves to be more efficient way to produce spontaneous seizures that remain focal and rarely generalize to tonic-clonic seizures [31]. IHP-KA injection in mice will produce acute, nonconvulsive or mild clonic SE prior to the onset of spontaneous seizures within 2 weeks to 2 months from the insult [31]. Histopathological features such as hippocampal sclerosis and gliosis are recapitulated as well, which are hallmarks observed in human TLE [31-34]. Considering its effectiveness in reliably producing spontaneous seizure recurrence after the initial insult using IHP-KA injection, this will be the optimal model to test the effect of TC-2153 on recurrent seizure development and activity. In support of its predictive validity, this model of mesial TLE is now pharmacologically

characterized [32, 35, 36] and has been implemented in the Differentiation phase of the Epilepsy Therapy Screening Program (NINDS/NIH). The ultimate advantage of this model for use in drug screening is the occurrence of highly frequent electrographic seizures in the hippocampus, where drugs can be tested on spontaneous seizures with only short periods of EEG recording [30, 37]. In addition, these frequent seizures are resistant to several ASDs, thus rendering this model ideal for novel drug discovery with higher efficacy against drug-resistant focal seizures [30, 35].

It will be necessary to investigate the changes in $STEP_{61}$ level during spontaneous seizure development in TLE by RLD-KA injection. Throughout the period of spontaneous seizure development, our lab expects to see increasing levels of $STEP_{61}$ expression. Preliminary data collected by our previous lab technician, Han Gil Jeong, also demonstrates that levels of $STEP_{61}$ are upregulated at 24 hours (h) post-intraperitoneal (i.p.) injection of kainate (Abcam, 30 mg/kg). This data suggests that seizure occurrence may upregulate $STEP_{61}$ expression. Our future plan is to perform RLD-KA injection of C57Bl/6J mice and collect neural tissue at 1, 2, 4, 7, 14, and 21 days post-KA as well as to perform immunohistochemistry to stain hippocampal slices using anti-NeuN, anti-STEP, and DAPI antibodies, image the slices using an epifluorescent microscope, and analyze STEP intensity levels, both ipsilaterally and contralaterally. Finally, our lab would like to confirm the levels of active STEP expression at each stage of spontaneous seizure development using phosphorylated STEP antibody by performing hippocampal fractionation and Western blot.

In addition, our lab plans to use video electroencephalography (EEG) to assess spontaneous seizure development in STEP KO and WT mice following RLD-KA injection model of TLE. Upon repeated, low dose (5 mg/kg, i.p.) kainate injection, it has been demonstrated that peak occurrence of spontaneous seizures is evident during 4 to 6 weeks post-insult [13]. Therefore, in combined consideration with our previous findings that behavioral spontaneous seizures are observed at 21 d post-insult, we would expect to see both behavioral CS and NCS using EEG produced in both STEP KO and WT mice. Our lab plans to perform behavioral convulsive seizure recording of STEP KO and WT mice at 28-to-42 d post-insult by scoring seizures for 120 min. based on a modified Racine scale, as well as monitor EEG activity of nonconvulsive seizures to determine the occurrence in STEP KO and WT mice at 28-to-42 d post-insult.

3.5 Conclusion

Overall, we found that TC-2153 does not alter seizure severity in homozygous STEP KO mice of either sex. This reveals to us that TC-2153 is acting through STEP specifically, and not any other off-target proteins. We also found that by using the CCI method of TBI induction as a model of posttraumatic epilepsy, this sustained injury produces observed changes in STEP expression in all regions of the hippocampus. Alternatively, using the RLD-KA injection model that induces SE and temporal lobe epilepsy pathology did not significantly delay the onset of SE in homozygous STEP KO mice. However, we did observe extremely low mortality rates and spontaneous recurrent seizures at 21 d post-SE onset using video recording to assess behavioral convulsive seizures in our mice subjected to RLD-KA injections, in addition to a sex-dependent sensitivity to the RLD-KA model in both WT and STEP KO mice.

Figures

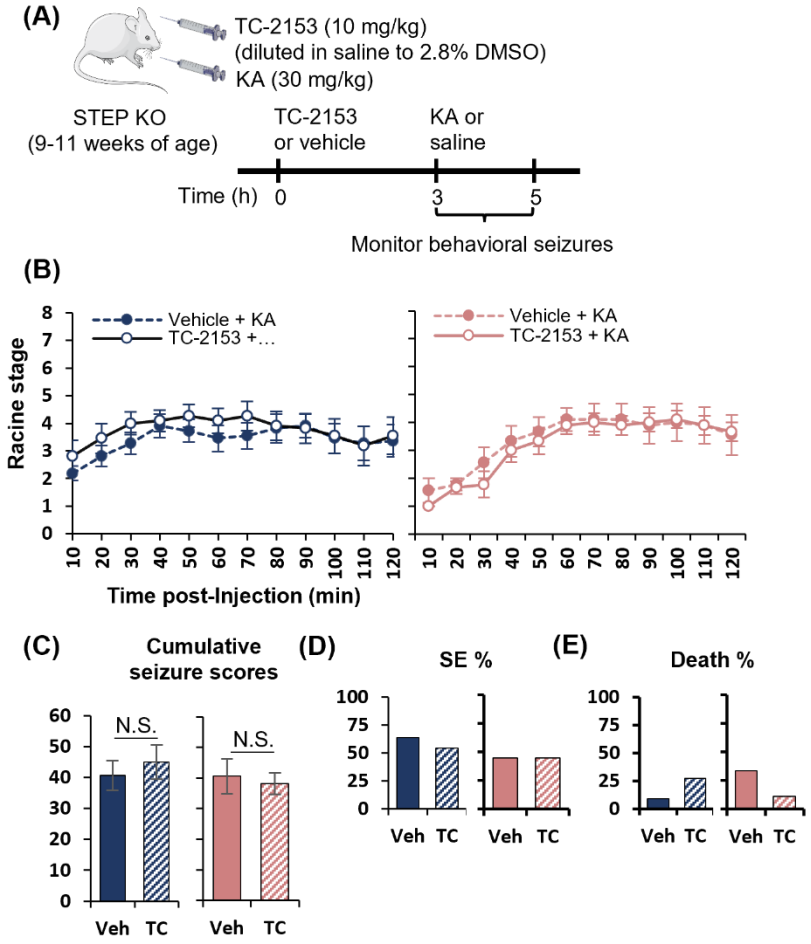

Figure 3.1: TC-2153 treatment does not significantly affect KA-induced seizure severity in adult STEP KO mice compared to vehicle control. **(A)** Experimental schematic of kainic acid (KA)-induced seizure severity in 9- to 11-week-old male and female STEP KO mice at 3 h post intraperitoneal (i.p.) injection with STEP inhibitor TC-2153 (10 mg/kg in saline containing 2.8% DMSO) or vehicle control (saline containing 2.8% DMSO). Behavioral seizures were monitored using modified Racine scale (Fig. 3.4). **(B)** TC-2153-treated STEP KO males (n=11) shows no significant difference in seizure stage or severity compared to vehicle treatment (n=11). Similarly, STEP KO females (n=9) show no significant difference compared to vehicle control (n=9). **(C)** Cumulative seizure scores. Two-tailed Student t-test results are shown (N.S. = not significant). **(D-E)** Percentage (%) of mice that achieved Stage 5 **(D)** and Stage 6 **(E)**. Two-tailed Student *t*-test was performed to assess significance. Data shown as mean ± SEM.

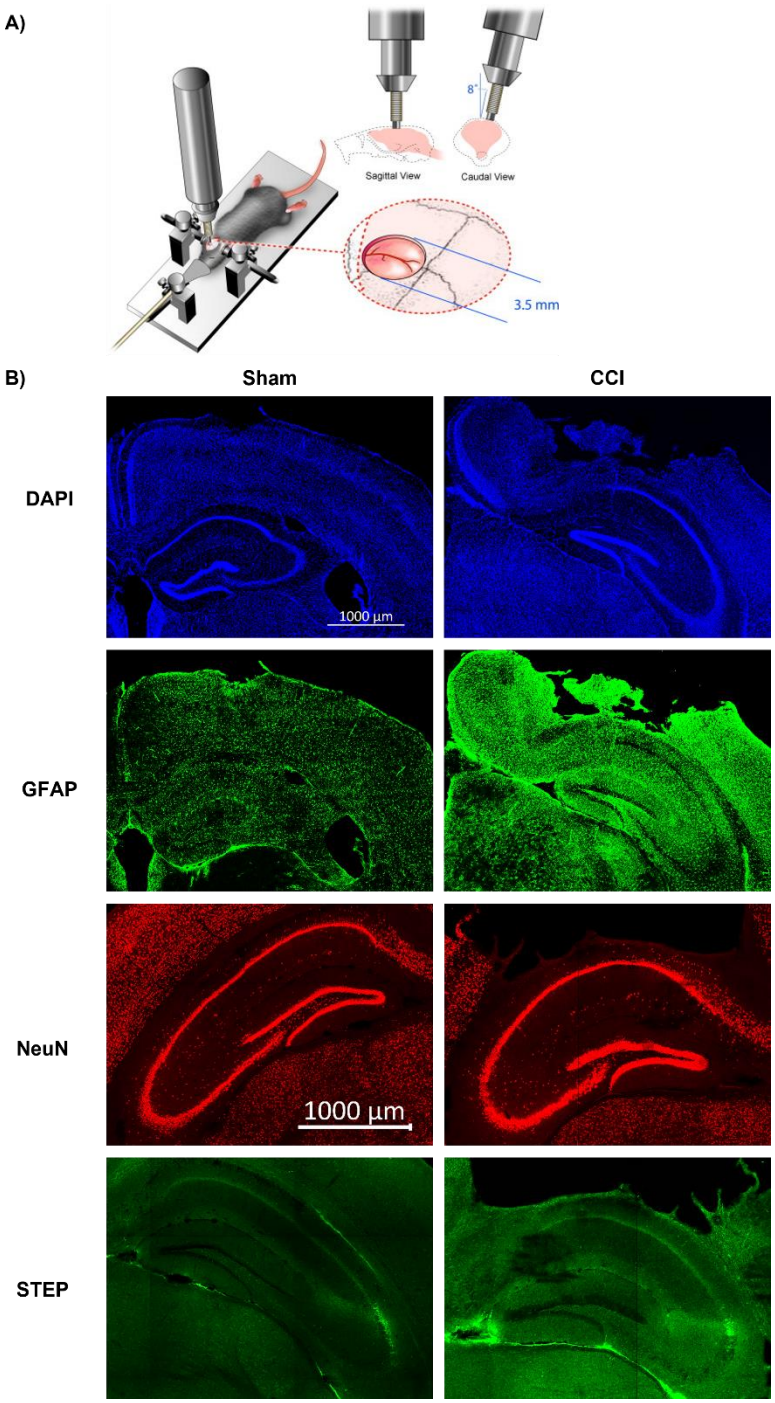

Figure 3.2: CCI model of TBI induction leads to changes in STEP expression in the entire hippocampus. **(A)** Experimental schematic of CCI performed on stereotaxic mouse (image courtesy of [38]). **(B)** Representative 10x tile scan images taken of the entire hippocampus in male mice (22 weeks of age) after either sham or CCI procedure.

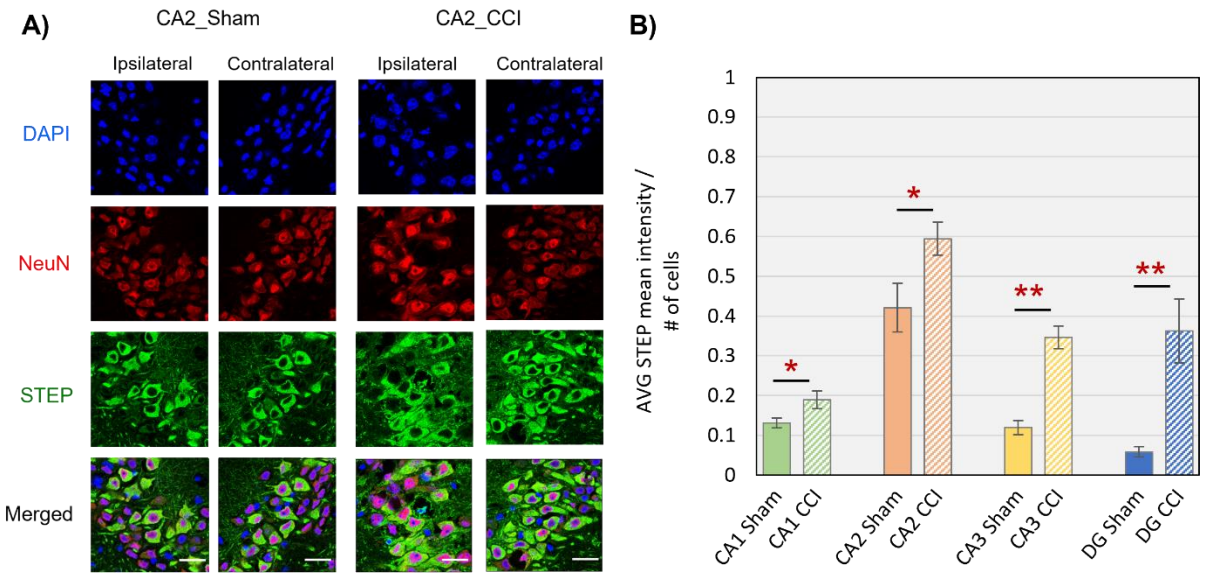

Figure 3.3: Changes in STEP expression in the hippocampus 14 days post-TBI induction. **(A)** Representative image of the CA2 region immunohistochemically stained using DAPI, NeuN, and STEP antibodies. Images were taken using a 63x objective (scale bar = 20 μm). **(B)** Analysis of the average mean intensities expressed by STEP in each region of the hippocampus (CA1 sham n=7, CA1 CCI n=8;.CA2 sham n=11, CA2 CCI n=7; CA3 sham n=4, CA3 CCI n=8; DG sham n=6, DG CCI n=7). Data shown as mean ± SEM. Student *t*-test results are shown (*$p<0.05$, **$p<0.02$).

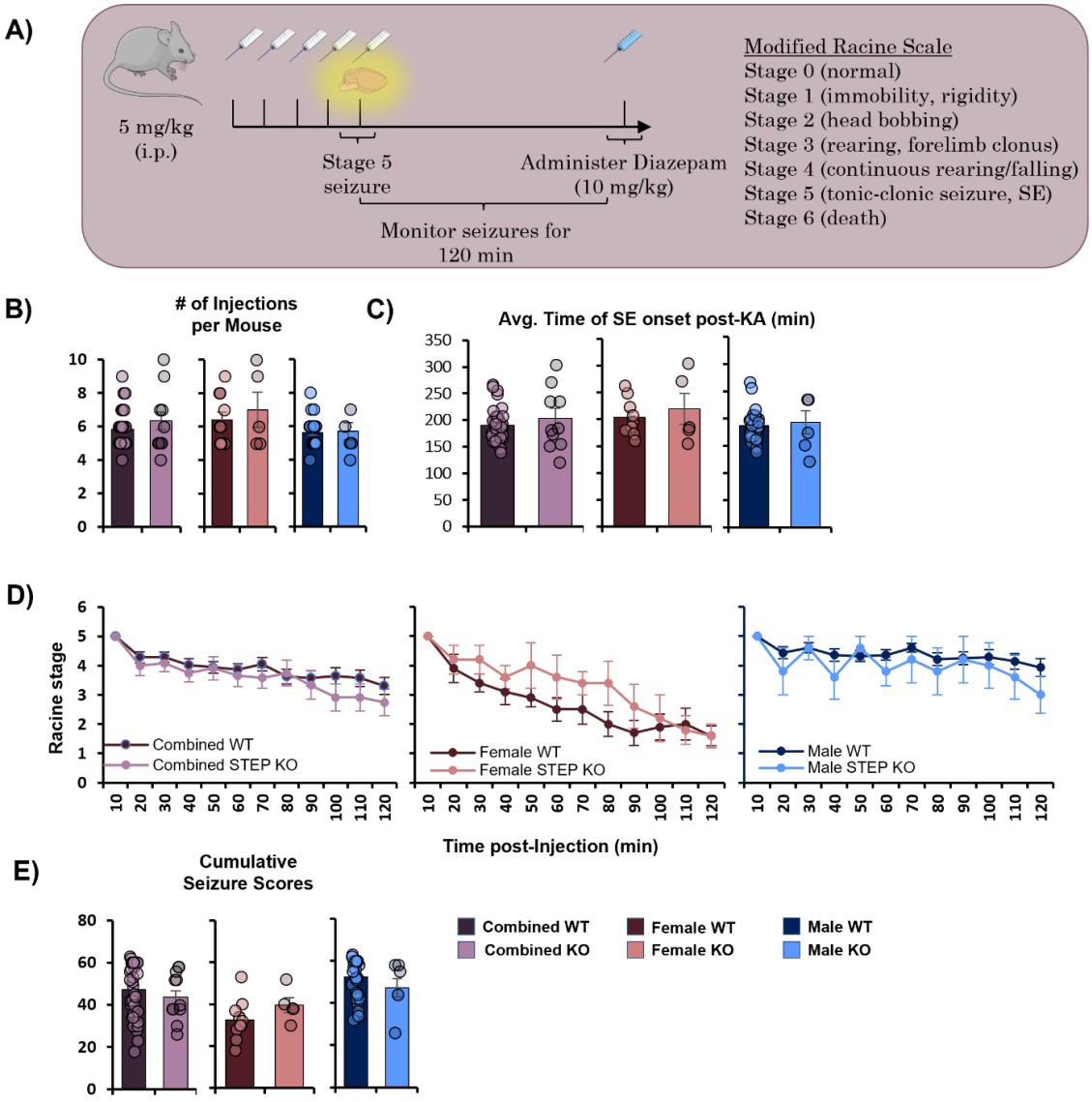

Figure 3.4: Homozygous loss of STEP does not significantly delay the onset of SE in CLD-KA model. **(A)** Initial SE induction timeline. WT or STEP KO mice were injected with 5 mg/kg (i.p.) of kainate at every 30 min time interval until the onset of a stage 5 seizure (tonic-clonic seizure, SE). Immediately upon SE, the behavioral CS were scored (according to the modified Racine scale) at every 10-minute time interval for a total of 120 min. At the end of the scoring period, the animal received a 10 mg/kg (i.p.) dose of Diazepam to allow seizures to subside. **(B)** Number of KA injections each mouse received prior to SE onset. **(C)** Average time of SE onset following KA injection. No significant differences observed in each group. **(D)** Combined sex data shows no significant difference (combined WT n=38, combined STEP KO n=12). STEP KO females (n=5) appear to show an increased trend in seizure severity compared to WT female mice (n=10), while STEP KO males (n=7) appear to display no difference compared to WT males (n=28). Combined, we also see that the STEP KO compared to WT seizure severity is not significant. **(E)** Cumulative seizure scores. No significant differences observed in each group. Two-tailed Student *t*-test was performed to assess significance. Data shown as mean ± SEM.

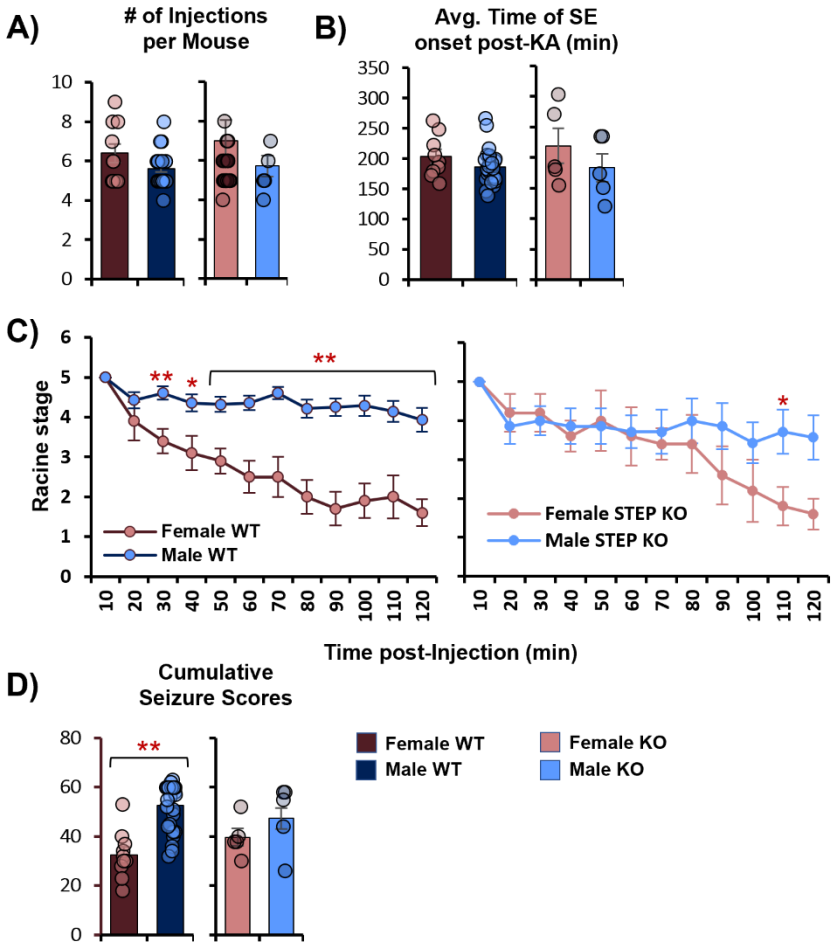

Figure 3.5: Sensitivity to CLD-KA model based on a sex-dependent manner is observed in both WT and STEP KO mice. **(A)** Number of KA injections each mouse received prior to SE onset. **(B)** Average time of SE onset following KA injection. No significant differences observed in each group. **(C)** Female WT mice (n=10) experience significantly lower induced seizure severity compared to WT males (n=28), while female STEP KO mice (n=5) demonstrate a decreased trend in seizure severity from 70-120 min. of scoring period compared to STEP KO males (n=7). Two-tailed Student t-test results are shown (*p<0.05, **p<0.02). **(D)** Cumulative seizure scores. Male WT mice show significantly higher cumulative scores on average compared to female WT, whereas STEP KO males only show a slightly increased trend in severity. Two-tailed Student t-test results are shown (**p<0.02). Data shown as mean ± SEM.

Tables

Table 1

Behavior	Score	Stage	Duration of behavior
None	0	0	N/A
Behavioral arrest (5+ s)	1	1–2	5–60 s
Single head and neck jerk	2	3	5–10 s
Multiple head and neck jerks	3	3	5–15 s
Severe head and neck jerks (no rearing)	4	3	5–20 s
Clonic seizure (sitting)	5	4–5	10–30 s
Clonic seizure (lying on side)	6	6	10–30 s
Clonic seizure (forelimb and hindlimb)	7	6	10–60 s
Violent clonic seizure (wild jumping)	8	6	10–60 s
Tonic extension	9		5–10 s
Death	10		Immediately after TE

The tonic–clonic seizure scale described here was adapted from Luttjohann et al. (2009). The score indicates seizure progression purely based on observed behavior while the stage indicates the stage designated by Luttjohann et al. where behavior was correlated with EEG measurements of PTZ-induced seizures in rats. Stages were subdivided for blinded assessment, but combined for genotype comparison and statistical analysis into three main groups to reflect the behavior most commonly observed in apoE4 TR mice: Behavioral arrest (score=1), head and neck jerks (score=2–4), clonus (score=5–10).

Table 3.1: Courtesy of Hunter et al., 2012 – "Emergence of a seizure phenotype in aged apolipoprotein epsilon 4 targeted replacement mice."

Wild-type	1d time point	2d time point	4d time point	7d time point	21d time point
Saline	N=7 (4 males, 3 females)	N=6 (6 males)	N=6 (1 female, 5 males)	N=7 (5 males, 2 females)	N=1 (male)
KA	N=7 (4 males, 3 females)	N=7 (7 males)	N=7 (2 females, 5 males)	N=7 (5 males, 2 females)	N=1 (female)

STEP -/-	1d time point	2d time point	4d time point	7d time point	21d time point
Saline	N=0	N=0	N=0	N=0	N=0
KA	N=0	N=0	N=0	N=0	N=4 (2 male, 2 female)

Table 3.2: CLD kainate-injected hippocampal and cortical tissue samples collected at time points 1d, 2d, 4d, 7d, and 21d post-SE onset to be used for future immunostaining.

References

1. Xu, J., et al., *Inhibitor of the tyrosine phosphatase STEP reverses cognitive deficits in a mouse model of Alzheimer's disease.* PLoS Biol, 2014. **12**(8): p. e1001923.
2. Xu, J., et al., *Striatal-enriched protein tyrosine phosphatase in Alzheimer's disease.* Adv Pharmacol, 2012. **64**: p. 303-25.
3. Zhang, Y., et al., *Genetic reduction of striatal-enriched tyrosine phosphatase (STEP) reverses cognitive and cellular deficits in an Alzheimer's disease mouse model.* Proc Natl Acad Sci U S A, 2010. **107**(44): p. 19014-9.
4. Carty, N.C., et al., *The tyrosine phosphatase STEP: implications in schizophrenia and the molecular mechanism underlying antipsychotic medications.* Transl Psychiatry, 2012. **2**: p. e137.
5. Xu, J., et al., *Inhibition of STEP61 ameliorates deficits in mouse and hiPSC-based schizophrenia models.* Mol Psychiatry, 2018. **23**(2): p. 271-281.
6. Carvajal, F.J., et al., *Age-related NMDA signaling alterations in SOD2 deficient mice.* Biochim Biophys Acta Mol Basis Dis, 2018. **1864**(6 Pt A): p. 2010-2020.
7. Carvajal, F.J. and W. Cerpa, *Regulation of Phosphorylated State of NMDA Receptor by STEP61 Phosphatase after Mild-Traumatic Brain Injury: Role of Oxidative Stress.* Antioxidants (Basel), 2021. **10**(10).
8. Spencer, S.S., *When should temporal-lobe epilepsy be treated surgically?* Lancet Neurol, 2002. **1**(6): p. 375-82.
9. Walters, J.M., et al., *Pharmacological inhibition of STriatal-Enriched protein tyrosine Phosphatase by TC-2153 reduces hippocampal excitability and seizure propensity.* Epilepsia, 2022.
10. Umpierre, A.D., et al., *Repeated low-dose kainate administration in C57BL/6J mice produces temporal lobe epilepsy pathology but infrequent spontaneous seizures.* Exp Neurol, 2016. **279**: p. 116-126.
11. Levesque, M. and M. Avoli, *The kainic acid model of temporal lobe epilepsy.* Neurosci Biobehav Rev, 2013. **37**(10 Pt 2): p. 2887-99.
12. Racine, R.J., J.G. Gartner, and W.M. Burnham, *Epileptiform activity and neural plasticity in limbic structures.* Brain Res, 1972. **47**(1): p. 262-8.
13. Puttachary, S., et al., *Immediate Epileptogenesis after Kainate-Induced Status Epilepticus in C57BL/6J Mice: Evidence from Long Term Continuous Video-EEG Telemetry.* PLoS One, 2015. **10**(7): p. e0131705.
14. Mouri, G., et al., *Unilateral hippocampal CA3-predominant damage and short latency epileptogenesis after intra-amygdala microinjection of kainic acid in mice.* Brain Res, 2008. **1213**: p. 140-51.
15. Hunt, R.F., S.W. Scheff, and B.N. Smith, *Posttraumatic epilepsy after controlled cortical impact injury in mice.* Exp Neurol, 2009. **215**(2): p. 243-52.
16. Hunt, R.F., S.W. Scheff, and B.N. Smith, *Regionally localized recurrent excitation in the dentate gyrus of a cortical contusion model of posttraumatic epilepsy.* J Neurophysiol, 2010. **103**(3): p. 1490-500.
17. Hunt, R.F., J.A. Boychuk, and B.N. Smith, *Neural circuit mechanisms of post-traumatic epilepsy.* Front Cell Neurosci, 2013. **7**: p. 89.
18. Osier, N. and C.E. Dixon, *Mini Review of Controlled Cortical Impact: A Well-Suited Device for Concussion Research.* Brain Sci, 2017. **7**(7).

19. Hausmann, R., et al., *Immunohistochemical investigations on the course of astroglial GFAP expression following human brain injury.* Int J Legal Med, 2000. **113**(2): p. 70-5.
20. Tse, K., et al., *Advantages of repeated low dose against single high dose of kainate in C57BL/6J mouse model of status epilepticus: behavioral and electroencephalographic studies.* PLoS One, 2014. **9**(5): p. e96622.
21. Kim, H.J., et al., *Identification of estradiol/ERalpha-regulated genes in the mouse pituitary.* J Endocrinol, 2011. **210**(3): p. 309-21.
22. Wang, H., et al., *PTPN5 promotes follicle-stimulating hormone secretion through regulating intracellular calcium homeostasis.* FASEB J, 2021. **35**(8): p. e21756.
23. Dorrington, J.H. and D.T. Armstrong, *Effects of FSH on gonadal functions.* Recent Prog Horm Res, 1979. **35**: p. 301-42.
24. Bell, M.R., *Comparing Postnatal Development of Gonadal Hormones and Associated Social Behaviors in Rats, Mice, and Humans.* Endocrinology, 2018. **159**(7): p. 2596-2613.
25. Sisk, C.L. and J.L. Zehr, *Pubertal hormones organize the adolescent brain and behavior.* Front Neuroendocrinol, 2005. **26**(3-4): p. 163-74.
26. Levesque, M., M. Avoli, and C. Bernard, *Animal models of temporal lobe epilepsy following systemic chemoconvulsant administration.* J Neurosci Methods, 2016. **260**: p. 45-52.
27. Ali, A., et al., *A once-per-day, drug-in-food protocol for prolonged administration of antiepileptic drugs in animal models.* Epilepsia, 2012. **53**(1): p. 199-206.
28. Grabenstatter, H.L., S. Clark, and F.E. Dudek, *Anticonvulsant effects of carbamazepine on spontaneous seizures in rats with kainate-induced epilepsy: comparison of intraperitoneal injections with drug-in-food protocols.* Epilepsia, 2007. **48**(12): p. 2287-95.
29. Grabenstatter, H.L., et al., *Use of chronic epilepsy models in antiepileptic drug discovery: the effect of topiramate on spontaneous motor seizures in rats with kainate-induced epilepsy.* Epilepsia, 2005. **46**(1): p. 8-14.
30. Loscher, W., *Animal Models of Seizures and Epilepsy: Past, Present, and Future Role for the Discovery of Antiseizure Drugs.* Neurochem Res, 2017. **42**(7): p. 1873-1888.
31. Bouilleret, V., et al., *Recurrent seizures and hippocampal sclerosis following intrahippocampal kainate injection in adult mice: electroencephalography, histopathology and synaptic reorganization similar to mesial temporal lobe epilepsy.* Neuroscience, 1999. **89**(3): p. 717-29.
32. Riban, V., et al., *Evolution of hippocampal epileptic activity during the development of hippocampal sclerosis in a mouse model of temporal lobe epilepsy.* Neuroscience, 2002. **112**(1): p. 101-11.
33. Blumcke, I., et al., *Histopathological Findings in Brain Tissue Obtained during Epilepsy Surgery.* N Engl J Med, 2017. **377**(17): p. 1648-1656.
34. Li, J., et al., *Dynamic and Sex-Specific Changes in Gonadotropin-Releasing Hormone Neuron Activity and Excitability in a Mouse Model of Temporal Lobe Epilepsy.* eNeuro, 2018. **5**(5).
35. Duveau, V., et al., *Differential Effects of Antiepileptic Drugs on Focal Seizures in the Intrahippocampal Kainate Mouse Model of Mesial Temporal Lobe Epilepsy.* CNS Neurosci Ther, 2016. **22**(6): p. 497-506.

36. Klein, S., M. Bankstahl, and W. Loscher, *Inter-individual variation in the effect of antiepileptic drugs in the intrahippocampal kainate model of mesial temporal lobe epilepsy in mice.* Neuropharmacology, 2015. **90**: p. 53-62.
37. Guillemain, I., P. Kahane, and A. Depaulis, *Animal models to study aetiopathology of epilepsy: what are the features to model?* Epileptic Disord, 2012. **14**(3): p. 217-25.
38. Onyszchuk, G., et al., *A mouse model of sensorimotor controlled cortical impact: characterization using longitudinal magnetic resonance imaging, behavioral assessments and histology.* J Neurosci Methods, 2007. **160**(2): p. 187-96.

APPENDIX A: INVESTIGATING THE MOLECULAR PATHOGENETIC EFFECTS OF SELECTED EPILEPTIC ENCEPALOPATHY MUTATIONS IN HELICES A AND B OF $K_V7.2$ [2]

A.1 Background

This work was performed in collaboration with Drs. Eung Chang Kim and Jiaren Zhang in my lab, Dr. Hee Jung Chung's lab, in the Department of Molecular and Integrative Physiology at the University of Illinois in Urbana-Champaign.

Epilepsy is a common seizure disorder that is caused by excessive neuronal excitability characterized by seizures, which are abnormal and uncontrolled discharges of action potentials [1]. Genetic factors, including ion channel mutations that occur as early as infancy, are estimated to account for approximately 40% of all epilepsies [2]. Of these ion channels, neuronal K_V7/KCNQ potassium (K^+) channels act as critical players in epilepsy – their agonist (ezogabine, retigabine) suppresses seizures in animal models and was utilized clinically as an antiseizure drug until 2017 [3-5]. Inherited and *de novo* mutations in the *Kcnq2* gene encoding the $K_V7.2$ subunit are associated with early-onset epileptic disorders, including benign familial neonatal epilepsy (BFNE) and epileptic encephalopathy (RIKEE database: www.rikee.org). This study in particular explores the molecular pathogenetic effects of selected epileptic encephalopathy mutations (R333W, M518V, K526N, and R532W) in helices A and B of $K_V7.2$. These mutations were specifically investigated because they 1) cause early-onset epileptic encephalopathy with drug refractory seizures, profound psychomotor delay, and other behavioral comorbidities including autism; 2) to compare the effects

[2] Title: Reduced axonal surface expression and phosphoinositide sensitivity in Kv7 channels disrupts their function to inhibit neuronal excitability in Kcnq2 epileptic encephalopathy.

Authors: Eung Chang Kim, Jiaren Zhang, Weilun Pang, Shuwei Wang, Kwan Young Lee, John P. Cavaretta, Jennifer Walters, Erik Procko, Nien-Pei Tsai, and Hee Jung Chung

Contributions: Western blotting, quantification, analysis, and assisted with the creation of main figure I.1E and I.2A-B.

Published in Neurobiology of Disease volume 118, 76-93 (2018)

of mutations buried within calmodulin contact sites (M518V in helix B) to those located at the periphery (R333W in helix A, K526N in helix B, and R532W in helix B-C linker).

A.2 Voltage-dependent activation of K_v7.2 channels is decreased by R532W mutation in helix B-C linker and abolished by M518V mutation in helix B

Dr. Kim's whole-cell path clamp recordings showed that epileptic encephalopathy mutations in helices A and B of K_v7.2 affect voltage-dependent activation of K_v7.2 channels in CHO hm1 cells. Specifically, mutation R532W decreased voltage-dependent activation, while mutation M518V abolished voltage-dependent activation. My contribution was performing the immunoblotting with anti-K_v7.2 N-terminal antibodies on CHO hm1 lysate expressing K_v7.2 WT, R333W, A343D, M518V, K526N, and R532W. These immunoblots showed that the total protein expression of K_v7.2-A343D and K_v7.2-M518V was comparable to K_v7.2 WT. In addition, decreased Kv7.2-R333W expression and increased K_v7.2-K526N expression was observed. Although K_v7.2-R532W total expression was comparable to K_v7.2 WT, Dr. Kim showed that K_v7.2-R532W generated 40% less outward K^+ currents, with a right shift in voltage dependence at -10 mV to +10 mV and found that R532W significantly slowed channel activation. Altogether, these findings revealed that M518V and R532W mutations significantly impaired current expression of K_v7.2 channels.

A.3 K_v7.2-M518V proteins undergo ubiquitination and proteasome-dependent degradation, whereas Kv7.3 coexpression prevents this degradation

Here, my immunoblots and analysis demonstrated that there was accelerated degradation of K_v7.2 proteins containing M518V or A343D mutation in HEK293T cells by 24 h post transfection, although both WT and mutant K_v7.2 proteins were equally expressed at 10 h post transfection. Dr. Zhang's work investigating the immunoprecipitation of K_v7.2 or mutant Kv7.2 cotransfected with HA-ubiquitin showed that K_v7.2-M518V proteins were heavily ubiquitinated. The full immunostaining of this figure conducted by Dr. Kim revealed that the M518V mutation decreased K_v7.2 expression by about 50%, while treatment with proteasome inhibitor MG132 blocked this degradation.

A.4 Materials

Western Blot

Equal amounts of protein were loaded, and electrophoresis was performed in NuPAGE 4–12% gradient bis-tris polyacrylamide protein gels (Thermo Fisher). Proteins were transferred to PVDF membrane and blocked with 5% milk in phosphate-buffered saline with Tween-20 for 1 hour. Membranes were then incubated overnight with primary antibody at 4 °C. Antibodies used include anti-KCNQ2 (Alomone, APC-050; Neuromab, N26A/23) and anti-GAPDH (Cell Signaling, 2118). Blots were washed and incubated with secondary antibody for 1 hour at room temperature. After washing, the secondary antibody was visualized by Pierce ECL chemiluminescence reagents (Thermo Fisher).

Statistical analysis

All analyses are reported as mean ± SEM. The Student *t*-test was performed to identify the statistically significant difference with a priori value $(p) < 0.05$ between 2 groups.

Figures

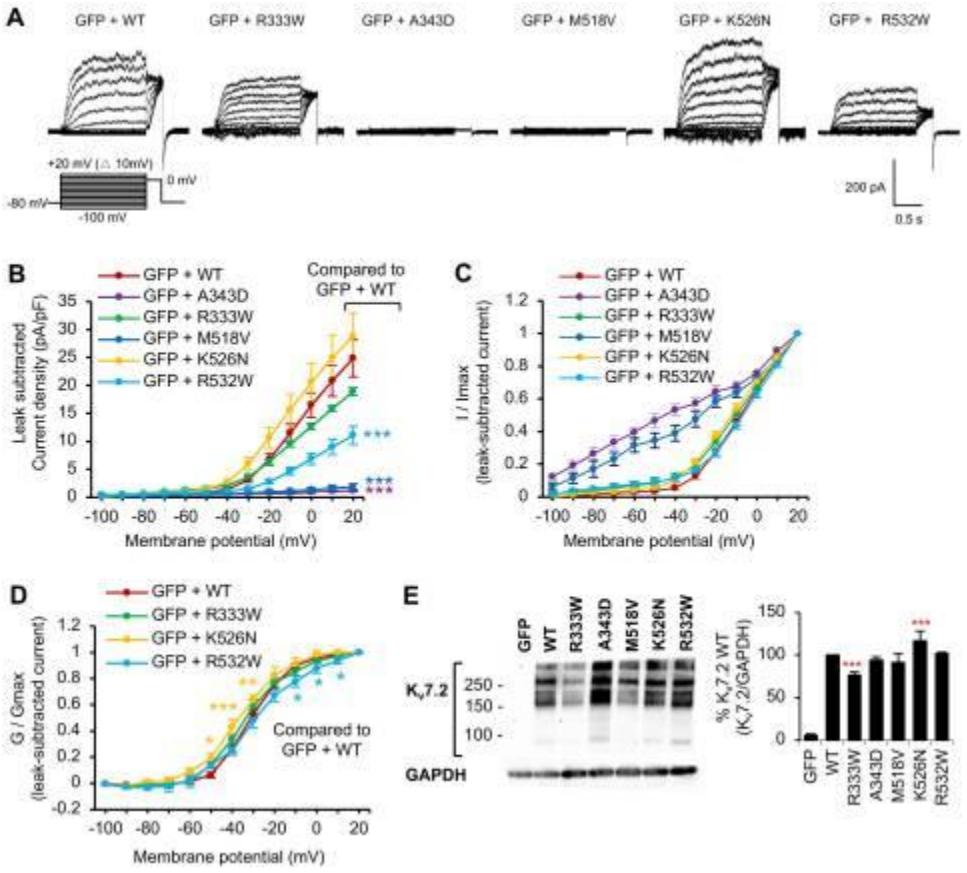

Figure A.1: Voltage-dependent activation of Kv7.2 channels is decreased by R532W mutation and abolished by M518V mutation. Whole cell voltage clamp recording of macroscopic K+ currents from CHO hm1 cells transfected with GFP and Kv7.2 WT or Kv7.2 containing epileptic encephalopathy mutations. The cells were held at −80 mV. Currents were evoked by depolarization for 1.5 s from −100 mV to +20 mV in 10 mV increments, followed by a step to 0 mV for 300 ms. **(A)** Representative traces of currents from which leak currents were subtracted at all voltage steps. Leak current was defined as non-voltage-dependent current from GFP-transfected cells. **(B-D)** Average peak current densities **(B)**, normalized currents **(C)**, and normalized conductance (G / Gmax) **(D)** were quantified using leak subtracted currents at all voltage steps. The number of transfected cells that were analyzed: GFP (n=9), GFP and Kv7.2 WT (n=11), R333W (n=12), A343D (n=12), M518V (n=8), K526N (n=14), or R532W (n=18). **(E)** Immunoblotting with anti-Kv7.2 N-terminal antibodies on the lysate from CHO hm1 cells expressing Kv7.2 WT (n=4), R333W (n=12), A343D (n=4), M518V (n=4), K526N (n=4), or R532W (n=4). GAPDH served as a loading control. Data shown represent the Ave ± SEM (*p<0.05, **p<0.01, ***p<0.005).

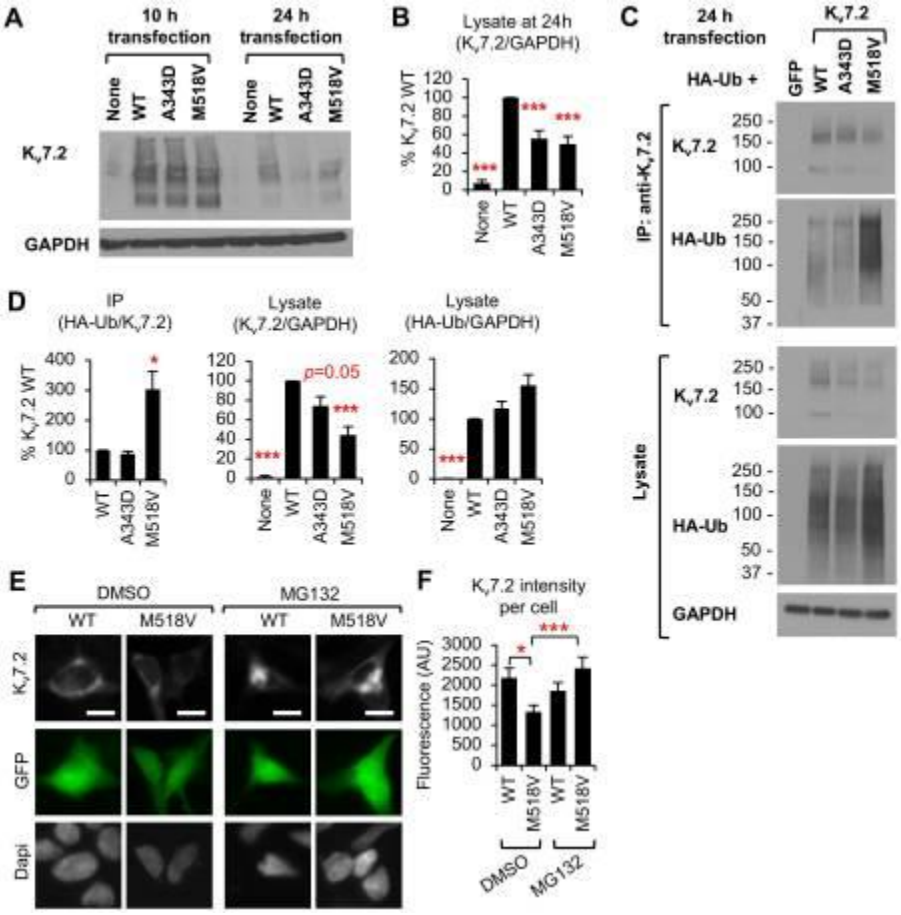

Figure A.2: M518V mutation causes ubiquitination and proteasome-dependent degradation of Kv7.2. **(A-B)** Immunoblot analyses of Kv7.2 WT, or mutant Kv7.2 (A343D and M518V) in HEK293T cells at 10 h and 24 h post transfection. Representative immunoblots **(A)**. Quantification at 24 h post transfection for n=4 independent experiments. **(B). (C-D)** Immunoprecipitation of Kv7.2 WT or mutant Kv7.2 (A343D and M518V) from HEK293T cells cotransfected with HA-ubiquitin. Representative immunoblots **(C).** Quantification of coIP and lysate **(D)** are shown for n=4 independent experiments. **(E-F)** Immunocytochemistry of HEK293T cells showing total Kv7.2 WT or Kv7.2-M518V proteins after 24 h treatment with vehicle control DMSO (1% v/v) or MG132 (1 μM). Dapi staining shows nuclei. **(E)** Representative images with scale bars: 10 μm. **(F)** Background subtracted mean intensity of total Kv7.2 fluorescence per transfected cell for DMSO+WT (n=20), DMSO+M518V (n=21), MG132+WT (n=22), MG132+M518V (n=22). Data shown represent the Ave ± SEM (*p<0.05, **p<0.01, ***p<0.005).

References

1. Fisher, R.S., et al., *Epileptic seizures and epilepsy: definitions proposed by the International League Against Epilepsy (ILAE) and the International Bureau for Epilepsy (IBE).* Epilepsia, 2005. **46**(4): p. 470-2.
2. Guerrini, R. and J. Noebels, *How can advances in epilepsy genetics lead to better treatments and cures?* Adv Exp Med Biol, 2014. **813**: p. 309-17.
3. Blackburn-Munro, G., et al., *Retigabine: chemical synthesis to clinical application.* CNS Drug Rev, 2005. **11**(1): p. 1-20.
4. Gunthorpe, M.J., C.H. Large, and R. Sankar, *The mechanism of action of retigabine (ezogabine), a first-in-class K+ channel opener for the treatment of epilepsy.* Epilepsia, 2012. **53**(3): p. 412-24.
5. Large, C.H., et al., *The spectrum of anticonvulsant efficacy of retigabine (ezogabine) in animal models: implications for clinical use.* Epilepsia, 2012. **53**(3): p. 425-3.

APPENDIX B: POLYCYSTIN 2 IS INCREASED IN DISEASE TO PROTECT AGAINST STRESS-INDUCED CELL DEATH [3]

B.1 Background

In a separate collaboration with Yale University [1], I investigated the expression of the Polycystin 2 (PC2) protein in both soluble and membrane-bound tissue fractions (respectively) of saline versus kainate-injected C57Bl/6J mice to study expression of these proteins in non-seizure compared to seizure-induced models [2]. Polycystin-2 (PC2 or TRPP1, formerly TRPP2) is a Transient Receptor Potential (TRP) channel most well-known for its associated pathology. When mutated, PC2 causes autosomal dominant polycystic kidney disease (ADPKD), a debilitating condition leading to bilateral renal cyst formation and eventual kidney failure [3]. Located primarily on the endoplasmic reticulum (ER) and primary cilia of all cell and tissue types [4-7], PC2 is a calcium (Ca^{2+})-permeant cation channel whose expression level directly affects Ca^{2+} release from the ER [4]. PC2 is thought to play a key role in regulating Ca^{2+}-regulated homeostasis and signaling pathways [8]. Given the importance of PC2 in ADPKD development, most studies of PC2 focus on its function in the kidney. However, the ubiquitous expression of PC2 in all cell types suggests that it is important in maintaining Ca^{2+} homeostasis in tissues beyond the kidney. Indeed, beyond ADPKD, the polycystins have been linked to multiple pathologies involving dysregulated Ca^{2+} and stress, including the development of liver [9] and pancreatic [10] cysts and cerebral aneurysms [11, 12] to name a few. We found that levels of PC2 increase in disease states with ER and oxidative stress and that PC2 up-regulation particularly occurred under pathological conditions in stressed brains.

[3] Title: Polycystin 2 is increased in disease to protect against stress-induced cell death

Authors: Allison L. Brill, Tom T. Fischer, Jennifer M. Walters, Arnaud Marlier, Lorenzo R. Sewanan, Parker C. Wilson, Eric K. Johnson, Gilbert Moeckel, Lloyd G. Cantley, Stuart G. Campbell, Jeanne M. Nerbonne, Hee Jung Chung, Marie E. Robert & Barbara E. Ehrlich

Contributions: Kainate injection experiments, tissue collection, western blotting, and assisted with the creation of both main and supplemental figures.

Published in Scientific Reports volume 10, Article number: 386 (2020)

B.2 PC2 expression is increased in stressed brains

Expression of PC2 in the brain led us to test whether its abundance is also altered with stress in the central nervous system. As a model of pathologically altered Ca^{2+} signaling and cell stress in the brain [13, 14], we used kainic acid to induce acute seizures in mice [15]. Systemic injections of kainate cause epileptiform seizures in the hippocampus and induce hippocampus-restricted neuropathology comparable to that seen in patients with temporal lobe epilepsy [15]. Mice were injected intraperitoneally with saline (Sal) or kainic acid (KA; Fig. SII.1A), and their seizures scored according to a modified Racine scale every 10 minutes for 120 minutes (Fig. II.1A, Table SII.1). Hippocampal lysates collected from randomly-paired, weight- and age-matched mice were found to have increased expression of PC2 in epileptic compared to saline-treated brains (Fig. II.1B). *Pkd2* and *Nfe2l2* mRNA expression was likewise tested from hippocampi of saline- and KA-treated mice and found to be significantly increased with KA induction of epileptic seizures (Fig. II.1C, SII.1B).

From the samples we treated and provided, it was then determined whether this increase was translatable to human disease by investigating if PC2 expression correlates with stress in human brains. Using the RNA-Seq dataset provided by the Allen Institute Ivy Glioblastoma Atlas Project [16], and examined *PKD2* expression in 3 different glioblastoma structures (hyperplastic blood vessels, microvascular proliferation, and leading edge). Leading edge (LE) samples showed relatively low amounts of *PKD2* expression, whereas hyperplastic blood vessels (HBV) and microvascular proliferation (MVP) samples expressed relatively high amounts of *PKD2* (Fig. II.1D). These findings correlated with differential expression of the ISR genes *NFE2L2* and *ATP2A2* in the different glioblastoma structures (Fig. SII.1C,D), indicating altered ISR levels amongst these structures. We then used correlation analysis (correlation $\geq 70\%$) and found that, like in human hearts, *PKD2* levels positively correlated with *NFE2L2* in human brains (Fig. II.1E; correlation = 76.8%), but not with *ATP2A2* (Fig. SII.1E).

To our surprise, we also discovered that our PC2 protein was expressing as a spliced variant form of PC2 called PKD2Δ7, which is mainly expressed in the brain as opposed to the kidney. PKD2Δ7 is a TRPP2 (Transient Receptor Protein Polycystin 2) channel variant. The repercussions of PKD2Δ7 expression in neurons could result in neurite outgrowth inhibition, act as a mediator of

excitatory postsynaptic conductance, or, most significantly, could be a contributing factor to the clustering of intracranial aneurysms reportedly seen in patients with ADPKD [2].

B.3 Materials and Methods

Antibodies

Anti-PC2 (sc-47734; for immunoblotting) was purchased from Santa Cruz Biotechnology and anti-GAPDH (#2118) antibodies was purchased from Cell Signaling Technology. Kainic acid (ab120100) were purchased from Abcam.

Animal Studies

The Yale University and University of Illinois at Urbana-Champaign Institutional Animal Care and Use Committees (IACUC) approved the animal housing conditions and the experimental procedures conducted in this study. All experiments were performed in accordance with relevant guidelines and regulations. C57BL/6J mice were kept under standard laboratory conditions with free access to food and water. All animal experiments were performed in a blinded manner.

Kainic acid-induced acute seizure mouse model

At 8–10 weeks of age, male C57BL/6 J mice (Jackson Laboratory, Stock Number: 000664) received an i.p. injection of kainic acid (30 mg/kg body weight) or an equal volume of 0.9% saline as described [17]. Mice were returned to their cages and monitored for behavioral seizures every 10 minutes for 2 hours following injection. Behavioral seizures were scored according to a modified Racine scale as described previously [18, 19] At 24 hours post injection, mice were euthanized by CO_2 inhalation and brains stored at −80 °C until use.

Brain lysate preparation

The dissected brain regions per mouse were homogenized in ice-cold homogenization buffer (Solution A) containing (in mM): 320 sucrose, 1 $NaHCO_3$, 1 $MgCl_2$, 0.5 $CaCl_2$, 0.4 HEPES (pH 7.4) and Halt protease inhibitors (Thermo Fisher Scientific) as previously described [17]. After centrifuging at 1400 x g for 10 minutes at 4 °C, the homogenate supernatant (S1) was separated from insoluble tissue and nuclear pellet (P1). The S1 fraction was then centrifuged at 13,800 x g for 10 min at 4 °C. The supernatant with cytosolic soluble proteins (S2) was removed, and the remaining pellet with transmembrane proteins and membrane-bound proteins (P2 membrane fraction) was resuspended in ice-cold solution B containing (in mM): 160 sucrose, 6 Tris-HCl, 0.5% Triton-X (pH 8.0) and Halt protease inhibitors. Pierce BCA assay (Thermo Fisher Scientific) was performed to normalize protein concentrations to 1 mg/ml in Solution B (pH 7.4). The S1, S2, and P2 fractions were stored at −80 °C until use.

Western blot

Lysates of mouse hippocampi were prepared as described above and the P2 fractions were run for western blotting. Equal amounts of protein were loaded, and electrophoresis was performed in NuPAGE 4–12% gradient bis-tris polyacrylamide protein gels (Thermo Fisher). Proteins were transferred to PVDF membrane and blocked with 5% milk in phosphate-buffered saline with Tween-20 for 1 hour. Membranes were then incubated overnight with primary antibody at 4 °C. Blots were washed and incubated with secondary antibody for 1 hour at room temperature. After washing, the secondary antibody was visualized by Pierce ECL chemiluminescence reagents (Thermo Fisher).

Statistical analysis

For animal-based experiments, data were calculated from at least three biological replicates. Where appropriate, one-way analysis of variance (ANOVA) with multiple comparisons or non-parametric Mann Whitney U test was applied. Data are presented as (1) mean ± SD, or (2) median

with range, as stated in the figure legend. In all experiments, $p < 0.05$ was considered statistically significant. *$p < 0.05$, **$p < 0.01$, ***$p < 0.001$, and ****$p < 0.0001$.

Main Figure

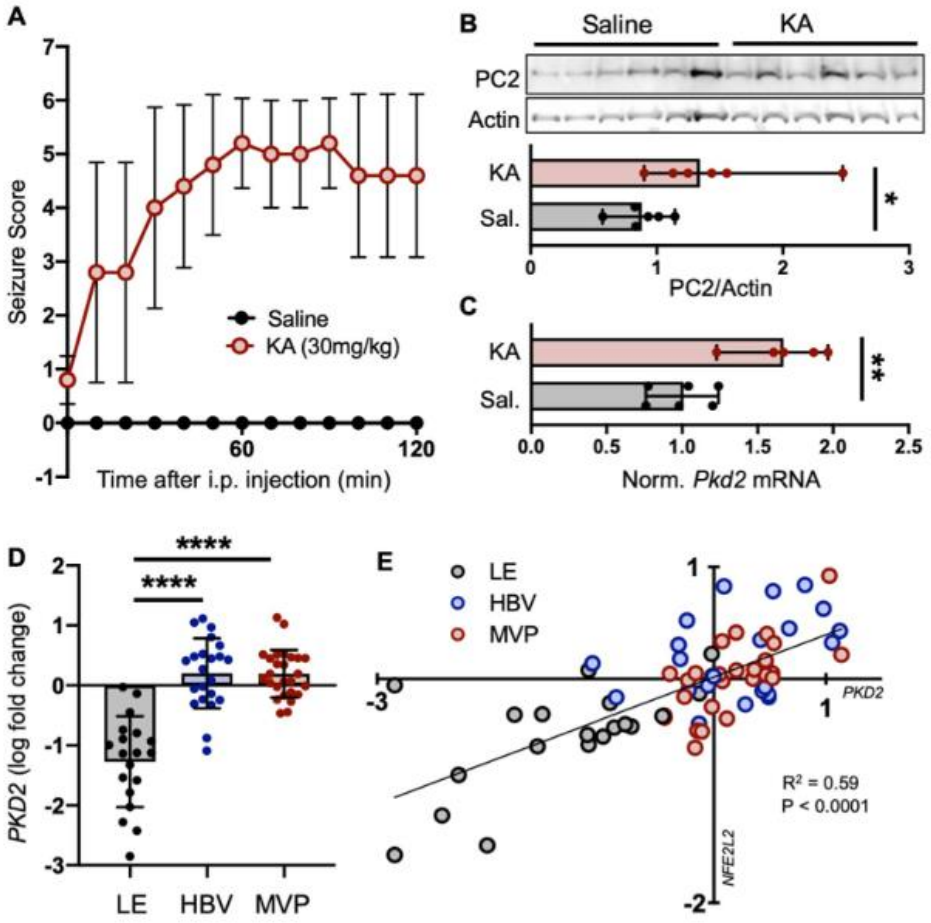

Figure B.1: PC2 is increased in stressed brains. Mice were given injections of saline (Sal) or kainic acid (KA) to induce epileptic seizures and oxidative stress in the brain. (**A**) Seizure scores following injections were measured according to a modified Racine scale. Data shown are mean ± SD of 6 mice per group. (**B**) TOP: Hippocampal tissue was collected and immunoblotted for PC2 24 hours following injections. Each lane represents one biological replicate; sample size n = 6 per group. BOTTOM: Quantification of PC2 protein abundance in Saline and KA-treated hippocampi, normalized to actin. *$p < 0.05$ as determined by Mann Whitney U test. Data presented as median with range. Sample size n = 6 biological replicates per group. (**C**) Normalized mRNA expression of Pkd2 in hippocampi from mice injected with saline or KA. GAPDH used as internal control. Sample number Saline n = 6, KA n = 5. **$p < 0.01$ as determined by Mann Whitney U test. Data presented as median with range. (**D**) RNA-Seq FPKM values from different structures (LE, leading edge; HBV, hyperplastic blood vessel; MVP, microvascular proliferation) of human glioblastoma samples were $\log_2$ transformed and their fold change determined. PKD2 transcripts were increased in HBV and MVP samples compared to LE. ****$p < 0.0001$ as determined by one-way ANOVA. Data presented as mean ± SD. (**E**) Linear regression analysis demonstrated that the ISR gene NFE2L2 significantly correlates with PKD2 in human glioblastoma tissues.

Supplementary Figures

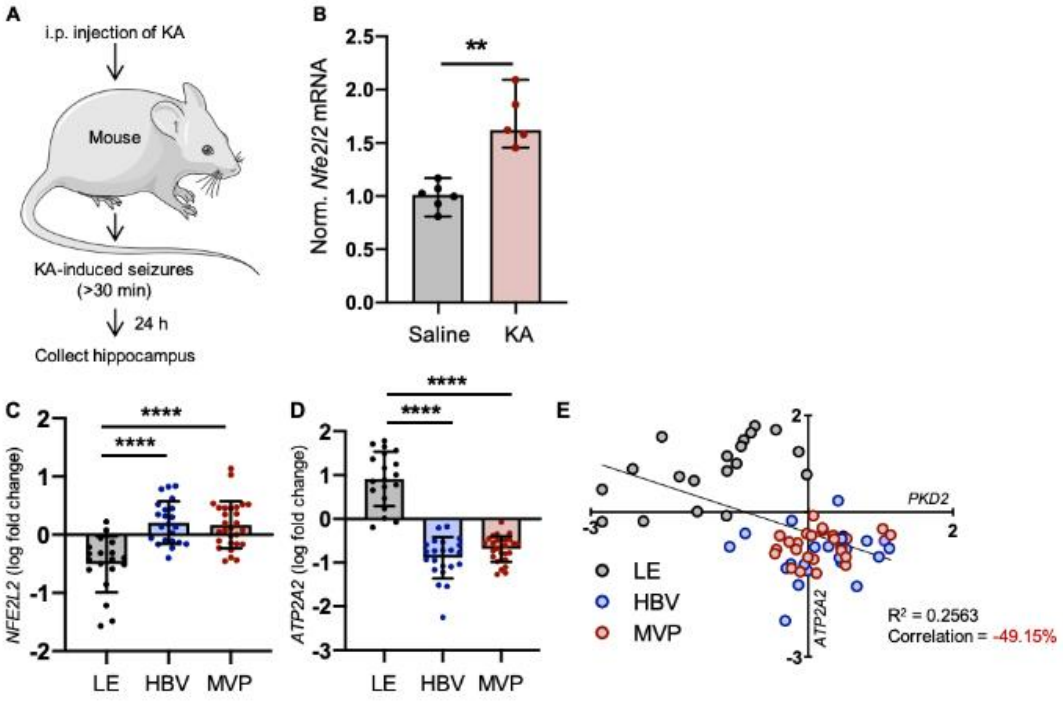

Supplementary Figure B.1: (A) Schematic of the experimental procedure using kainic acid to induce epileptic seizures in mice. (B) Fold change of Nfe2l2 mRNA in hippocampi of saline- or KA-treated mice. **p<0.01 as determined by Mann Whitney U test. Data presented as median with range. Sample size Saline n=6, KA n=5. (C,D) Log fold change of the ISR genes NFE2L2 and ATP2A2 in LE versus HBV and MVP tumor samples from human glioblastoma. ****p<0.0001 as determined one-way ANOVA. (E) ATP2A2 does not correlate with PKD2 expression at the cutoff of 70% correlation or higher.

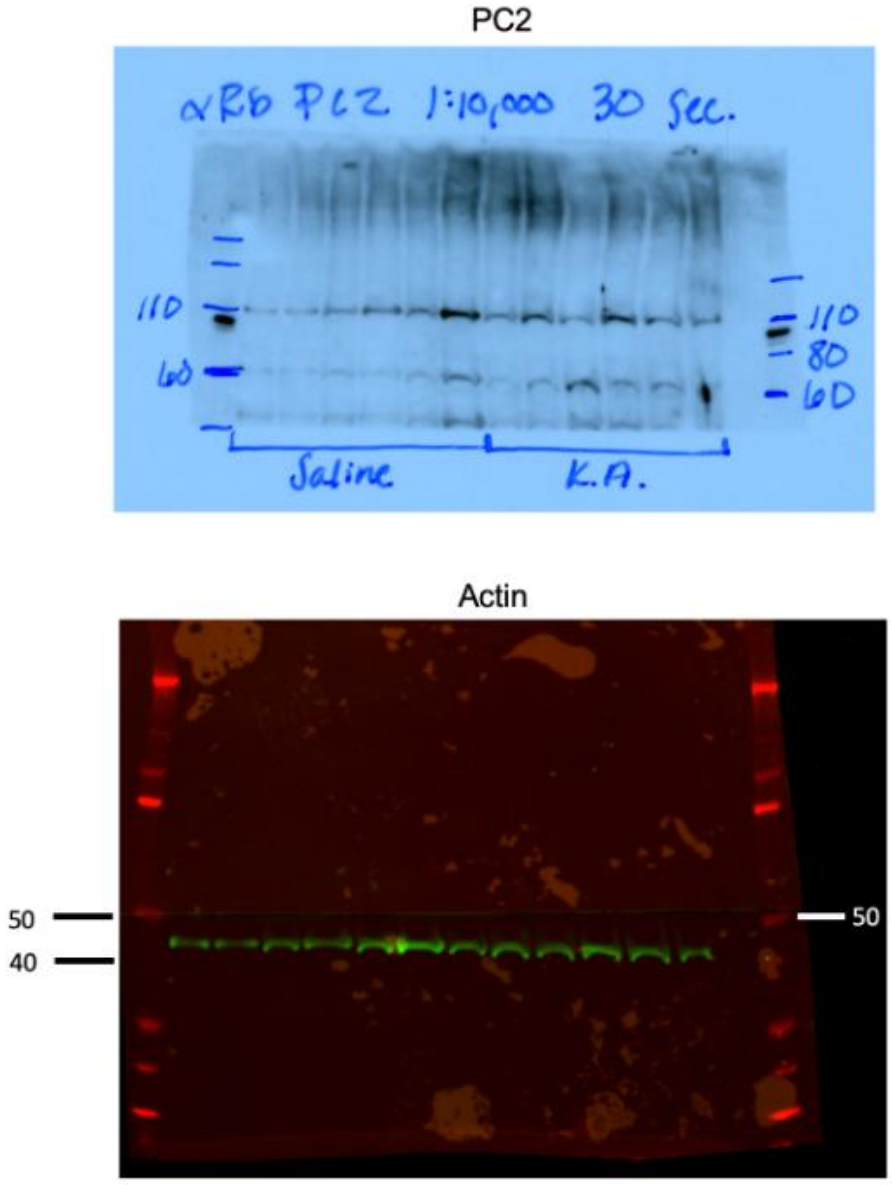

Supplementary Figure B.2: (A) Schematic of the experimental procedure using kainic acid to induce epileptic seizures in mice. (B) Fold change of Nfe2l2 mRNA in hippocampi of saline- or KA-treated mice. **p<0.01 as determined by Mann Whitney U test. Data presented as median with range. Sample size Saline n=6, KA n=5. (C,D) Log fold change of the ISR genes NFE2L2 and ATP2A2 in LE versus HBV and MVP tumor samples from human glioblastoma. ****p<0.0001 as determined one-way ANOVA. (E) ATP2A2 does not correlate with PKD2 expression at the cutoff of 70% correlation or higher.

Supplementary Table

Supplementary Table 6

	Treatment											
	Saline						Kainic Acid (30 mg/kg body weight)					
Sample	1	2	3	4	5	6	7	8	9	10	11	12
Weight (g)	23.5	22	21	20	20	20	20.4	21	23	19	22	22
Behavior Score (average)	0	0	0	0	0	0	2.4615	3.5385	2.9231	3.3077	5.4615	5.4615

Supplementary Table B.1: Recorded sample numbers, weights, and behavioral scores of saline and kainate-injected mice.

References

1. Brill, A.L., et al., *Polycystin 2 is increased in disease to protect against stress-induced cell death.* Sci Rep, 2020. **10**(1): p. 386.
2. Hackmann, K., et al., *A splice form of polycystin-2, lacking exon 7, does not interact with polycystin-1.* Hum Mol Genet, 2005. **14**(21): p. 3249-62.
3. Cornec-Le Gall, E., et al., *PKD2-Related Autosomal Dominant Polycystic Kidney Disease: Prevalence, Clinical Presentation, Mutation Spectrum, and Prognosis.* Am J Kidney Dis, 2017. **70**(4): p. 476-485.
4. Koulen, P., et al., *Polycystin-2 is an intracellular calcium release channel.* Nat Cell Biol, 2002. **4**(3): p. 191-7.
5. Thul, P.J., et al., *A subcellular map of the human proteome.* Science, 2017. **356**(6340).
6. Uhlen, M., et al., *Proteomics. Tissue-based map of the human proteome.* Science, 2015. **347**(6220): p. 1260419.
7. Uhlen, M., et al., *Towards a knowledge-based Human Protein Atlas.* Nat Biotechnol, 2010. **28**(12): p. 1248-50.
8. Cantiello, H.F., et al., *Polycystin-2 as a signal transducer.* Adv Exp Med Biol, 2004. **559**: p. 235-44.
9. Chauveau, D., F. Fakhouri, and J.P. Grunfeld, *Liver involvement in autosomal-dominant polycystic kidney disease: therapeutic dilemma.* J Am Soc Nephrol, 2000. **11**(9): p. 1767-1775.
10. Kim, J.A., et al., *Pancreatic Cysts in Autosomal Dominant Polycystic Kidney Disease: Prevalence and Association with PKD2 Gene Mutations.* Radiology, 2016. **280**(3): p. 762-70.
11. Chang, M.Y. and A.C. Ong, *Autosomal dominant polycystic kidney disease: recent advances in pathogenesis and treatment.* Nephron Physiol, 2008. **108**(1): p. p1-7.
12. Vlak, M.H., et al., *Prevalence of unruptured intracranial aneurysms, with emphasis on sex, age, comorbidity, country, and time period: a systematic review and meta-analysis.* Lancet Neurol, 2011. **10**(7): p. 626-36.
13. Evans, M.C., T. Griffiths, and B.S. Meldrum, *Kainic acid seizures and the reversibility of calcium loading in vulnerable neurons in the hippocampus.* Neuropathol Appl Neurobiol, 1984. **10**(4): p. 285-302.
14. Gluck, M.R., et al., *CNS oxidative stress associated with the kainic acid rodent model of experimental epilepsy.* Epilepsy Res, 2000. **39**(1): p. 63-71.
15. Ben-Ari, Y. and R. Cossart, *Kainate, a double agent that generates seizures: two decades of progress.* Trends Neurosci, 2000. **23**(11): p. 580-7.
16. Puchalski, R.B., et al., *An anatomic transcriptional atlas of human glioblastoma.* Science, 2018. **360**(6389): p. 660-663.
17. Baculis, B.C., et al., *Prolonged seizure activity causes caspase dependent cleavage and dysfunction of G-protein activated inwardly rectifying potassium channels.* Sci Rep, 2017. **7**(1): p. 12313.
18. Boehringer, R., et al., *Chronic Loss of CA2 Transmission Leads to Hippocampal Hyperexcitability.* Neuron, 2017. **94**(3): p. 642-655 e9.
19. Racine, R., V. Okujava, and S. Chipashvili, *Modification of seizure activity by electrical stimulation. 3. Mechanisms.* Electroencephalogr Clin Neurophysiol, 1972. **32**(3): p. 295-9.

APPENDIX C: INVESTIGATING THE EFFECTS OF TC-2153 ON THE EVOKED ACTIVITY OF NEURONS DERIVED FROM MOUSE NEURAL PROGENITOR CELLS

C.1 Background

Temporal Lobe Epilepsy (TLE) is the most common form of focal-onset epilepsy in adults [1]. Current antiseizure drugs (ASDs) are ineffective for ~75% of the patients with advanced mesial TLE, leading to severe consequences including hippocampal sclerosis, high mortality rate, cognitive decline, depression, and temporal lobe resection [1]. This underscores the critical need for the discovery of a novel ASD.

Emerging evidence from our published work (Chapter-2) and other studies suggests that Striatal Enriched protein tyrosine Phosphatase (STEP) may be a molecular target for seizure treatment in TLE. STEP is expressed throughout the brain, with the exception of the cerebellum [2]. However, only membrane-bound $STEP_{61}$ is expressed in the hippocampus and neocortex [3] where it dephosphorylates N-Methyl-D-aspartic acid receptor (NMDAR) and α-amino-3-hydroxy-5-methyl-4-isoxazolepropionic acid receptor (AMPAR), the key glutamate receptors that mediate fast excitatory synaptic transmission. $STEP_{61}$ also dephosphorylates and inactivates protein kinases including extracellular signal-regulated kinase 1 and 2 (ERK1/2), p38, Fyn, and Pyk2 [2].

Previous studies have reported that deletion of STEP gene *PTPN5* results in resistance to pilocarpine-induced seizures [4] and diminishes audiogenic seizures in a fragile X syndrome (FXS) mouse model [5]. In Chapter-2, I have also shown that acute pharmacological inhibition of STEP using selective small molecule STEP inhibitor TC-2153 (8-(trifluoro-methyl)-1,2,3,4,5-benzopentathiepin-6-amine-hydrochloride) both reduces network activity of acute mouse hippocampal slices and dampens severity of seizures in C57Bl/6J male and female mice against a single systemic injection of kainic acid (KA) [6], which induces *status epilepticus* (SE) [7]. We also show that TC-2153 treatment also decreased action potential firing rate, sag voltage, and hyperpolarization-induced current (I_h) of cultured rat hippocampal neurons, indicating that TC-2153 downregulates the intrinsic neuronal excitability [6].

Although our findings demonstrate that the acute inhibition of STEP by TC-2153 decreases excitability of cultured hippocampal neurons and hippocampal slices in a murine model, the

imminent question we must ask now, is whether TC-2153 application will decrease the excitability of *human neurons*? Based on our findings, we hypothesize that TC-2153 will reduce the activity of cortical-like excitatory neurons derived from human-induced pluripotent stem cells (hiPSCs). Before pursuing hiPSCs with the collaboration with Dr. Jack Parent (University of Michigan), we first collaborated with Dr. Hyunjoon Kong's lab to investigate the effects of TC-2153 on excitatory pyramidal neurons derived from mouse neural progenitor/stem cells (NPSCs) as part of my internship through the Miniature Brain Machinery Research Traineeship program (supported by the National Science Foundation under grant #1735252).

Mouse NPSCs provide an excellent model to study the neural development process, as well as neurological disorders. Approximately 99% of mouse genes are matched by a corresponding sequence in the human genome [8]; though mice are similar to humans at a fundamental level, there are clear biological differences and limitations of only studying a murine model. The mouse NPSC differentiation to excitatory cortical neurons/astrocytes and their maintenance served as a critical stepping stone to polish my skills in handling stem cell differentiation and the formulation of our future direction to study the effects of TC-2153 on neurons derived from human iPSCs. I was trained under Dr. Kong's graduate student Kai-Yu Huang for mouse NPSC expansion and differentiation into excitatory pyramidal neurons, as well as astrocytes.

C.2 Materials and Methods

Mouse NPSC culture and differentiation

Mouse cortical stem cells were seeded and plated on 3 cm glass-bottom dishes (Cellvis, D35-20-1.5-N) according to the monolayer system procedure. Dishes were treated with 1 µg/mL Bovine Fibronectin solution (R&D Systems, Catalog # 1030-FN). To promote stem cell attachment and spreading and incubated 3 hours (h) to overnight at 37 °C and 5% CO2. Once seeded at the appropriate density (2.5E-6 cells) in Completed Base Media (DMEM/F12, glucose, glutamine, $NaHCO_3$, N-2 Plus Media Supplement [R&D Systems, Catalog # AR003]) supplemented with growth factors 1000X Recombinant Human EGF (R&D Systems, Catalog #236-EG) and 1000X Recombinant Human FGF basic (R&D Systems, Catalog #233-FB or 4114-TC), the cells were incubated at 37 °C and 5% CO2. After cells become adherent (3 h to overnight) and replace the

media with fresh Completed Base Media supplemented with growth factors. Each day, the cells were supplemented with 1000x stock of each growth factor, as well as replace the media every second day. Once the cells reach 70-80% confluency, cells were passaged as described: media was removed from the dishes, add 3 ml of Buffered Ca2+/Mg2+-free Hank's Balanced Salt Solution (HBSS) (1X) and incubated at room temperature for 15-45 min until the cells round up. The cells were transferred and centrifuged down for 5 min at 200 x g. After collecting the supernatant, cells were resuspended in Completed Base Media with growth factors, were counted using a hemocytometer, and seeded at the appropriate density once more to maintain the line. The cells were once more be incubated at 37 °C and 5% CO2 and maintained until they reached the desired confluency. To differentiate the cells, Complete Base Media was added *without* the growth factors, and replaced fresh media daily

Immunocytochemistry

For permeabilized immunostaining, the neurons were fixed in 4% paraformaldehyde/4% sucrose in Phosphate buffered saline (PBS), permeabilized in 0.2% Triton X-100 in PBS, and for incubated overnight at 4°C with primary antibodies. To test if the mouse NPSCs have successfully differentiated into neurons, I will use rabbit anti-MAP2 antibody (Cell Signaling, #4542) at a 1:500 dilution. To test for the expression of astrocytes in my culture, I will use mouse anti-GFAP antibody (N206A/8) (Neuromab, 75-240) at a 1:500 dilution. I will then incubate with secondary antibodies as described [9]. Images of the cells will be taken with our Zeiss Axio Observer microscope with a Zeiss AxioCam 702 mono Camera and ZEN Blue 2.6 software.

Drug treatment and calcium imaging

To examine the effects of TC-2153 on mouse cortical stem cell-derived differentiated neuronal excitability, I performed calcium imaging in neurons differentiated from mouse cortical stem cells using a calcium dye indicator. To do this, mouse NPSCs were expanded and differentiated (as described above) in 3 cm glass-bottom dishes (Cellvis, D35-20-1.5-N) for imaging. Once the differentiated neurons were 9 *days in vitro* (DIV), I incubated the cells with either vehicle control of DMSO or TC-2153 (1 or 5 μM) for 1 h and were stored at 37°C and 5% CO2. Immediately after drug incubation, I applied Oregon Green™ 488 BAPTA-1-AM (Invitrogen, cat #O6807) and stored the dishes in the 37 °C tissue culture incubator for 30 minutes. Neurons were then incubated in basal artificial cerebrospinal fluid (ACSF) for 1 min, imaged, and then introduced to potassium

chloride (KCl) (15 mM, to raise extracellular potassium and thus increase neuronal activity) for 2 min immediately before imaging. The treated neurons were imaged using our Zeiss Axio Observer microscope with a Zeiss AxioCam 702 mono Camera and ZEN Blue 2.6 software. Specifically, images were taken under a 20x objective at 500 ms exposure time using 75% intensity, 3x3 binning, and will be set for a duration time of 30 s with no intervals.

C.3 Results

Differentiation of neuron-rich and astrocyte-rich cultures derived from mouse NPSCs

To verify successful differentiation of mouse NPSC differentiation to neuron-rich and astrocyte-rich cultures, I performed immunocytochemistry using neuronal somatodendritic marker MAP2 (microtubule associated protein 2) and astrocyte marker with GFAP (glial fibrillary acidic protein), respectively, and counterstained with DAPI (4′,6-diamidino-2-phenylindole) (Fig. C.1). To test the effect of TC-2153 on cultures derived from mouse NPSCs, calcium imaging was performed on both neuron-rich and astrocyte-rich cultures using Oregon Green™ 488 BAPTA-1-AM calcium dye (Invitrogen, cat #O6807). Cultures were treated with either DMSO or TC-2153 (1 and 5 μM) for 1 h prior to imaging. a 15 mM KCl bath was introduced to the cultures to induce activity (Fig. C.1B). After incubating the cultures with 15 mM KCl for 2 min to induce KCl-mediated depolarization, we found that TC-2153 is observed to reduce evoked activity in both neuron-rich and astrocyte-rich culture. Cells were seeded at the appropriate density in 3 cm glass bottom dishes (2.5E-6 cells) and checked two days later to confirm 70-80% confluency. To induce differentiation, the cell media was changed to remove the growth factors and routinely replace the media each day until DIV 9. For a "neuron-rich culture", cells were differentiated and maintained as described in the *Methods* – to create an "astrocyte-rich neuronal culture", 2% horse serum was added to induce astrocytic differentiation. Differentiated cells were used for experimental purposes at DIV 9 (Fig. C.1A) – for immunocytochemistry, the process began on DIV 9 and were finally imaged at DIV 11 (Fig. C.1C).

Immunostaining revealed that the mouse NPSCs cultured without horse serum show MAP2-positive neurons, yet little GFAP-positive astrocytes (Fig. C.2). In contrast, the mouse NPSCs cultured with 2% horse serum displayed significantly more MAP2-positive neurons and GFAP-positive astrocytes compared to those cultured without horse serum (Fig. C.2). Herein, we will

denote the mouse NPSCs cultured without horse serum as “neuron-rich culture”, and the mouse NPSCs cultured with 2% horse serum as “astrocyte-rich neuronal culture”. In neuron-rich culture, we observe a lower number of neurons with more dendritic processes. In contrast, whereas we see a higher number of neurons lacking dendrites in astrocyte-rich neuronal culture showed a higher number of neurons which show thinner and shorter dendritic processes compared to the neurons in neuron-rich culture. These results indicate successful differentiation of mouse NPSCs into neuronal culture, and the culturing with 2% horse serum in the media increases astrocytes.

TC-2153 (1 μM)-treated astrocyte-rich culture derived from mouse NPSCs show reduced excitability compared to control.

To test whether TC-2153 exhibits an effect on KCl-induced activity of either neuron-rich or astrocyte-rich cultures derived from mouse NPSCs, we investigated the basal and evoked activity of differentiated cells after either dimethylsulxofide (DMSO) or TC-2153 (1 μM) application by performing calcium imaging. Once the differentiated neurons reached DIV 9, the cells were incubated with either vehicle control of DMSO or TC-2153 (1 μM) for 1 h as they are stored at 37°C and 5% CO2. This 1 h treatment using a low dose (1 μM) of TC-2153 was shown not to induce neuronal death in DIV 18-21 primary cortical cells cultured from E18 rat embryos [10]. Immediately after drug incubation, Oregon Green™ 488 BAPTA-1-AM (Invitrogen, cat #O6807) was applied to the cultures and the dishes were stored in the 37 °C tissue culture incubator for 30 min. For calcium imaging, the cells were then incubated in basal artificial cerebrospinal fluid (ACSF) for 1 min, imaged for 30 s to capture basal level activity, and then introduced to 15 mM KCl (to raise extracellular potassium and thus increase neuronal activity) for 2 min immediately before imaging for 30 s to capture evoked activity.

In the first calcium imaging trial, the spontaneous activity and KCL-evoked activity of mouse NPSC-derived cells from the neuron-rich culture (containing no horse serum) were assessed after DMSO and TC-2153 (1 μM) treatment. In DMSO-treated neurons, the Oregon Green™ 488 calcium signal activity observed before KCl treatment were similar to the activity observed after KCl treatment. These findings were unexpected, since KCl treatment should increase the activity of the neuron-rich culture. Comparably, the calcium signals in TC-2153-treated neuron-rich

culture were similar between before and after KCl treatment. These findings suggest that the neuron-rich culture in this first imaging trail might have had poor neuronal health, considering there was no increase in signal after the introduction of KCl (Fig. C.3B-C).

To promote neuronal health and number (See Fig.C.1 and C.4), we next differentiated mouse NPSCs to astrocyte-rich cultures (containing 2% horse serum) and repeated the calcium imaging experiment to assess the activity of the cells after DMSO and TC-2153 (1 μM) treatment. First, I observed that the rate of Oregon Green™ signal activity in astrocyte-rich neuronal culture was higher compared to that in neuron-rich culture, both before and after treatment with KCl, suggesting that astrocyte-rich neuronal culture was healthier and exhibited higher basal activity. In DMSO-treated culture, the KCL treatment increased the number of cells exhibiting calcium signals (Fig. C.4B). In TC-2153-treated culture, application of 15 mM KCl did not increase Oregon Green signals (Fig. C.4C), indicating that TC-2153 treatment inhibits KCL-evoked activity in astrocyte-rich neuronal culture derived from mouse NPSCs compared to the DMSO vehicle control.

TC-2153 (5 μM)-treated astrocyte-rich cultures display less excitability, lower cell number.

To investigate whether a higher concentration of TC-2153 is required to achieve a more significant reduction in neuronal activity, we repeated the calcium imaging experiments after treating neuron-rich culture and astrocyte-rich neuronal culture with a higher TC-2153 concentration of 5 μM (Fig. C.5 and C.6). In DMSO-treated neuron-rich culture, the Oregon Green™ 488 signal activity evoked after KCl application was similar to the basal activity (before KCl), with the exception that flashes of signal after KCl treatment were more intense and sustained for a longer period of time (see white arrowheads in Fig. C.5B). In neuron-rich culture treated with TC-2153 (5 μM), the calcium activity was slightly reduced upon KCL treatment compared to that before the treatment. We also observed that neuron-rich culture treated with TC-2153 (5 μM) had a much lower number of cells compared to the culture treated with DMSO (Fig. C.5C). However, it is unclear whether TC-2153 (5 μM) induced cell death or the cell density of this particular dish was unevenly plated. In addition, only glial cells were observed to display activity in TC-2153-treated dishes (Fig. C.5C).

In contrast to the neuron-rich culture, the basal calcium activity of astrocyte-rich culture before KCl treatment was robust after DMSO or TC-2153 treatment (Fig. C.6B), consistent with the higher number of cells in astrocyte-rich neuronal culture compared to neuron-rich culture (Fig. C.5B-C). This reaffirms that the presence of more glia likely stabilizes the health and function of the neurons. After KCl treatment, the rate of calcium signal activity in DMSO-treated culture remained high, yet the fluorescence signal itself was slightly weaker (Fig. C.6B), suggesting potential photobleaching. In TC-2153-treated astrocyte-rich neuronal culture, we observed weaker calcium signals and their rate of activity after KCl treatment compared to those before KCL treatment (Fig C.6C), suggesting that TC-2153 treatment at 5 μM reduces excitability compared to DMSO control.

DMSO and TC-2153-treated (1 μM) neuron-rich and astrocyte-rich cultures appear unhealthy, with further reduction in GFAP expression in TC-2153-treated astrocyte-rich culture.

To test if TC-2153 treatment affects the health of mouse NPSC-derived neural cells, we performed immunostaining on two separate sets of neuron-rich culture which have been treated with either DMSO vehicle control or TC-2153 (1 μM or 5 μM) for 1 h, but did not undergo calcium imaging. In the first experiment, the MAP2-positive neurons in the neuron-rich culture appeared to be visibly damaged as they show dispersed and fractured dendrites and soma regardless of DMSO or 1 μM TC-2153 treatment. (Fig. C.7), suggesting that these neurons are unhealthy. Similar results were obtained for the astrocyte-rich neuronal culture (Fig. C.8).

In second independent experiment, the MAP2-positive neuronal dendrites and soma in the neuron-rich culture were less fractured and beaded (Fig. C.9) compared to those from the first experiment (Fig. C.7). Similarly, a marked difference is also observed in high levels of GFAP-expressing astrocytes and MAP2-positive neurons were observed in the astrocyte-rich neuronal culture regardless of DMSO or 5 μM TC-2153 treatment. in the second experiment (Fig. C.10). Thus, there appears to be a culture-to-culture variability between the cells in experiment #1 and experiment #2.

C.4 Discussion and Future Directions

My preliminary calcium imaging experiments demonstrate that application of 1 μM TC-2153 induced a decreasing trend in spontaneous activity but did not block KCl-evoked activity in mouse NPSC-derived neuron-rich culture (Fig. C.3B-C). In mouse NPSC-derived neuron- and astrocyte-rich culture, application of 1 μM TC-2153 induced a decreasing trend in both spontaneous and evoked activity (Fig. C.3 and C.4). Better neuronal health and survival in neuron- and astrocyte-rich culture compared to neuron-rich culture (Fig. C.3) could underlie our ability to see the effect of 1 μM TC-2153 in reducing both spontaneous and evoked activity. Application of 5 μM TC-2153 also induced a decreasing trend in spontaneous activity as well as KCl-evoked activity both neuron-rich (Fig. C.5C) and astrocyte-rich cultures (Fig. C.6C). The overall health of the cells after higher concentration of TC-2153 used in experiment #2 did not appear to significantly detract from the overall health of either neuronal or astrocytic cultures.

My first set of preliminary immunocytochemical staining data showed that cells stained with MAP2 from neuron-rich cultures treated with either DMSO or 1 μM TC-2153 were both fractured and damaged, reflecting poor neuronal health (Fig. C.7). In astrocyte-rich culture, MAP2 expression in neurons from both DMSO and TC-2153 treatment groups were observed to have less fragmentation (Fig. C.8). One possibility is that direct application of TC-2153 to this culture (especially if these cells were in a vulnerable state to begin with) was too overwhelming and induced cellular stress and death. These NPSC-derived cells are quite young (DIV 9) and are not yet part of an established, strengthened neural network. Notably, our previous study demonstrated the effects of TC-2153 in KCl-evoked hippocampal excitability of acute slice [6], where one of the advantages of this model is to study the drug's effects on an established neuronal circuit. A future alternative method would be to use cultured neurospheres as opposed to stem-cell derived neural cells. The brain is a complex organ and its development, structure, and function rely heavily on interactions between numerous cell types (i.e. neurons, glia, oligodendrocytes, etc.) [11]. Neurospheres offer a more mature, complex 3D organoid model that recapitulate these multicellular interactions and would be a more appropriate model for neurotoxicity testing.

In my second set of immunocytochemical staining data, neuron-rich culture treated with DMSO or 5 μM TC-2153 both exhibited high MAP2 expression with much less fracture, intact cell bodies, and highly developed neurites, as well as high GFAP expression (Fig. C.9). Astrocyte-rich culture

also demonstrated more robust MAP2 expression and GFAP expression (Fig. C.10). Neurons expressed in astrocyte-rich culture appear to have less fragmentation and healthier neurites, even when treated with TC-2153 (5 μM). However, even though we do observe improved overall health of neurons treated with TC-2153 (5 μM), there are still many cells with beaded/shortened neurites. This suggests that direct application of TC-2153 may have detrimental effects on young stem cell-derived mouse NPSCs, in contrast to the rat hippocampal neuronal culture which was resilient to 10 μM TC-2153 treatment [6]. To address this, it will be necessary to systematically analyze the dose effect on the health of stem cell-derived neurons, whether from mouse NPSCs or human iPSCs.

Approximately 99% of mouse genes are matched by a corresponding sequence in the human genome [8]; though mice are similar to humans at a fundamental level, there are clear biological differences and limitations of only studying a murine model. My experiments investigating the effects of TC-2153 on mouse NPSC-derived neuron-rich and astrocyte-rich cultures greatly enriched my knowledge in working with stem cell-derived models, including how to maintain, differentiate, and culture mouse NPSCs. This knowledge, as well as the troubleshooting that occurred along the way, will be beneficial when starting our work growing and maintaining hIPSCs to further study the effects of TC-2153 in a human-derived model. I propose a number of follow-up studies with two specific aims for the future graduate students who will pursue this project.

To further understand the specific impact TC-2153 has on human cells, our lab plans to investigate its effects on human iNeurons – excitatory, cortical-like neurons generated by forced expression of NGN2 or NGN1 and 2 in hIPSCs. Based on my preliminary findings that TC-2153 may affect the health of neurons derived and cultured from stem cells (Fig. C.7-C.10) differently from rat embryonic hippocampal cultured neurons [6], our lab will first successfully grow iNeurons to maturity (21 days) and test the dose-dependent effect of TC-2153 on their health in this Aim. The human iNeurons at DIV 2 are ready from our collaborator Dr. Jack Parent, MD (Michigan Neuroscience Institute, University of Michigan) and stored in our cryotank. These neurons will be thawed out and cultured for at least 21 days so that they have mature synaptic connections according to the detailed protocols provided by Dr. Wei Niu in Dr. Parent's lab (this protocol is attached at the end of this chapter). To see if the iNeuron culture is successfully differentiated into

cortical-like neurons and to examine the percentage of astrocytes, iNeuron culture will be subjected to immunocytochemical analysis at DIV 21 (3 weeks) using primary antibodies for neuronal marker MAP2, glia marker GFAP, and DAPI as in Figures C.7-C.10. To verify that iNeurons are successfully differentiated into cortical-like glutamatergic excitatory neurons with mature synaptic connections, immunostaining will be performed for presynaptic marker VGLUT1 (vesicular glutamate transporters 1) and postsynaptic marker PSD-95 (postsynaptic density protein 95). To test if these human iNeurons express $STEP_{61}$, we will also immunostain the neurons for $STEP_{61}$. Finally, our lab will test the effect of TC-2153 on iNeuronal health by treating human iNeuron culture at DIV 21-28 (3-4 weeks) with 1-5 uM TC-2153 and vehicle controls for 1 h, and subjected to MTT assay used to measure cellular metabolic activity as an indicator of cell viability, proliferation, and cytotoxicity (Sigma-Aldrich, Cat. # 11465007001). Immunostaining with MAP2, GFAP, and DAPI will also be performed to correlate MTT results.

Our second aim will be to investigate the effects of TC-2153 on reducing activity of cortical-like neurons derived from hiPSCs. Our hypothesis is that TC-2153 will impose a similar reduction on the excitability of these iPSC-derived human excitatory neurons compared to our previous findings. Our previous findings demonstrate that TC-2153 application reduces intrinsic excitability, as well as decreases I_h current, in cultured rat pyramidal hippocampal neurons [6], while TC-2153 demonstrates potential to reduce the KCl-evoked activity of neuron-rich and astrocyte-rich culture derived from mouse NPSCs (Fig. C.3-C.6). Once we have the range of TC-2153 concentration that does not affect the health, our lab will test if TC-2153 has an effect on KCl-evoked activity by calcium imaging as shown in Figures C.3-C.6. Our lab plans to accomplish this by investigating the basal (spontaneous) and KCl-evoked activity of human iNeurons after either DMSO or TC-2153 (1-5 μM) application using Oregon Green™ 488 BAPTA-1-AM (Invitrogen, cat #O6807) to visualize, image, and analyze calcium signals. $\Delta F/F = (F-F_{min})/F_{min}$ will be computed as described [12], where ΔF indicates the difference between the initial intensity in ACSF and the intensity after KCl stimulation. ΔF/F will be normalized to ACSF. Our lab will also assess the effect of TC-2153 on the spontaneous and KCl-evoked activity of human iNeurons by performing multi-electrode array (MEA) recordings on cultures incubated in ACSF with either DMSO as vehicle control or TC-2153 (5 μM).

C.5 Conclusion

Overall, our first experiment showed that TC-2153 (1 μM)-treated astrocyte-rich culture derived from mouse NPSCs showed reduced excitability compared to control – however, both the DMSO and TC-2153-treated (1 μM) neuron-rich and astrocyte-rich cultures appear unhealthy, with further reduction in GFAP expression in TC-2153-treated astrocyte-rich culture. Our second experiment demonstrated that TC-2153 (5 μM)-treated astrocyte-rich cultures displayed less excitability, as well as a lower cell number. The differentiation of neuron-rich and astrocyte-rich cultures derived from mouse NPSCs was also successful, with each culture containing a noticeably higher amount of the desired cell type.

Figures

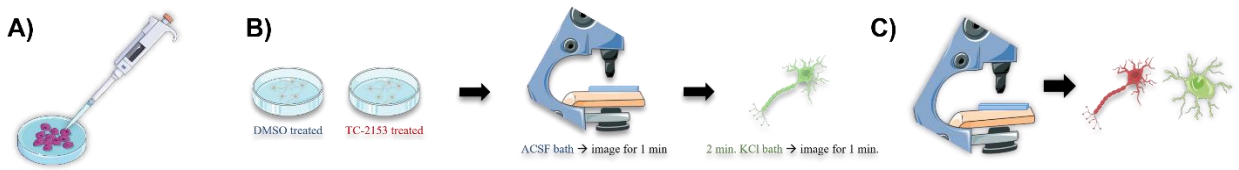

Figure C.1: Experimental schematic. **(A)** Stem cell generation and differentiation. **(B)** Calcium imaging of both neuron-rich and astrocyte-rich cultures differentiated from mouse-derived cortical stem cells after treatment of either DMSO or TC-2153. **(C)** Immunocytochemical staining of both culture sets to confirm desired cell type.

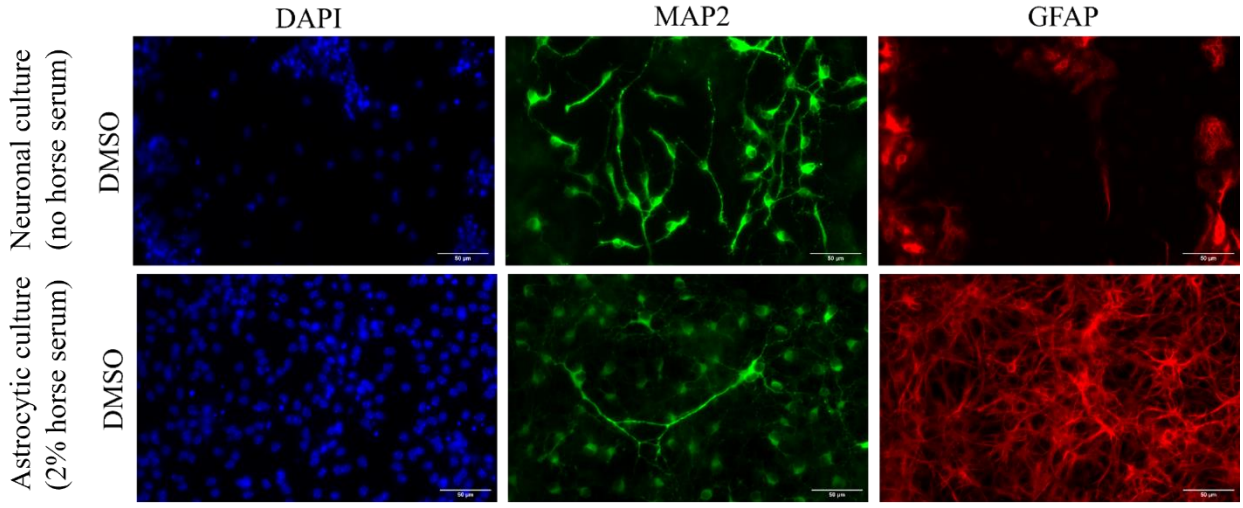

Figure C.2: Immunocytochemically stained neuron-rich and astrocyte-rich mouse NPSCs (containing 2% horse serum in 1x PBS). Imaged using a 20x objective with a 1.6x Tubelens. Images were taken after calcium imaging of KCl-evoked activity.

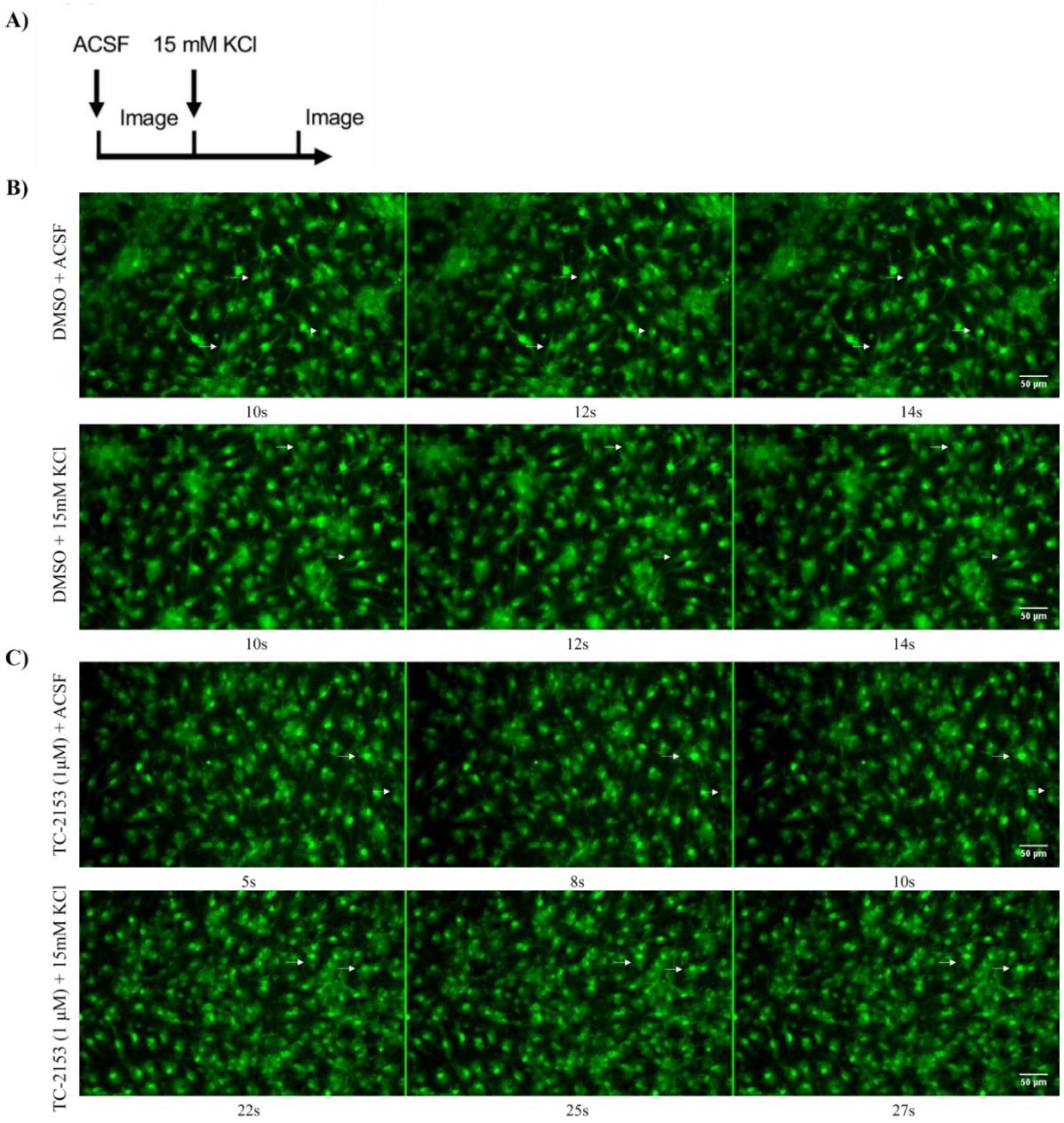

Figure C.3: Effects of TC-2153 (1 μM) in neuron-rich culture. **(A)** Experimental schematic of calcium imaging on neuron-rich cultures (containing no horse serum) derived from mouse NPSCs at DIV 9. The cells were incubated with DMSO or TC-2153 (1 μM) for 1 h, followed by a 30 min incubation with Oregon Green™ 488, and finally subjected to calcium imaging first in ACSF and then after 2 min of 15 mM KCl application. **(B)** Images taken of DMSO-treated cells before KCl treatment in ACSF (first panel) and after 2 min KCl treatment (second panel). **(C)** Images taken of TC-2153-treated cells before KCl treatment in ACSF (third panel) and after 2 min KCl treatment (fourth panel). White arrowheads indicate single cell activity fluctuations in each time frame. Imaged using a 20x objective with a 1.0x Tubelens. Time stamps marked beneath each image indicate when the image was taken during the 30 sec recording.

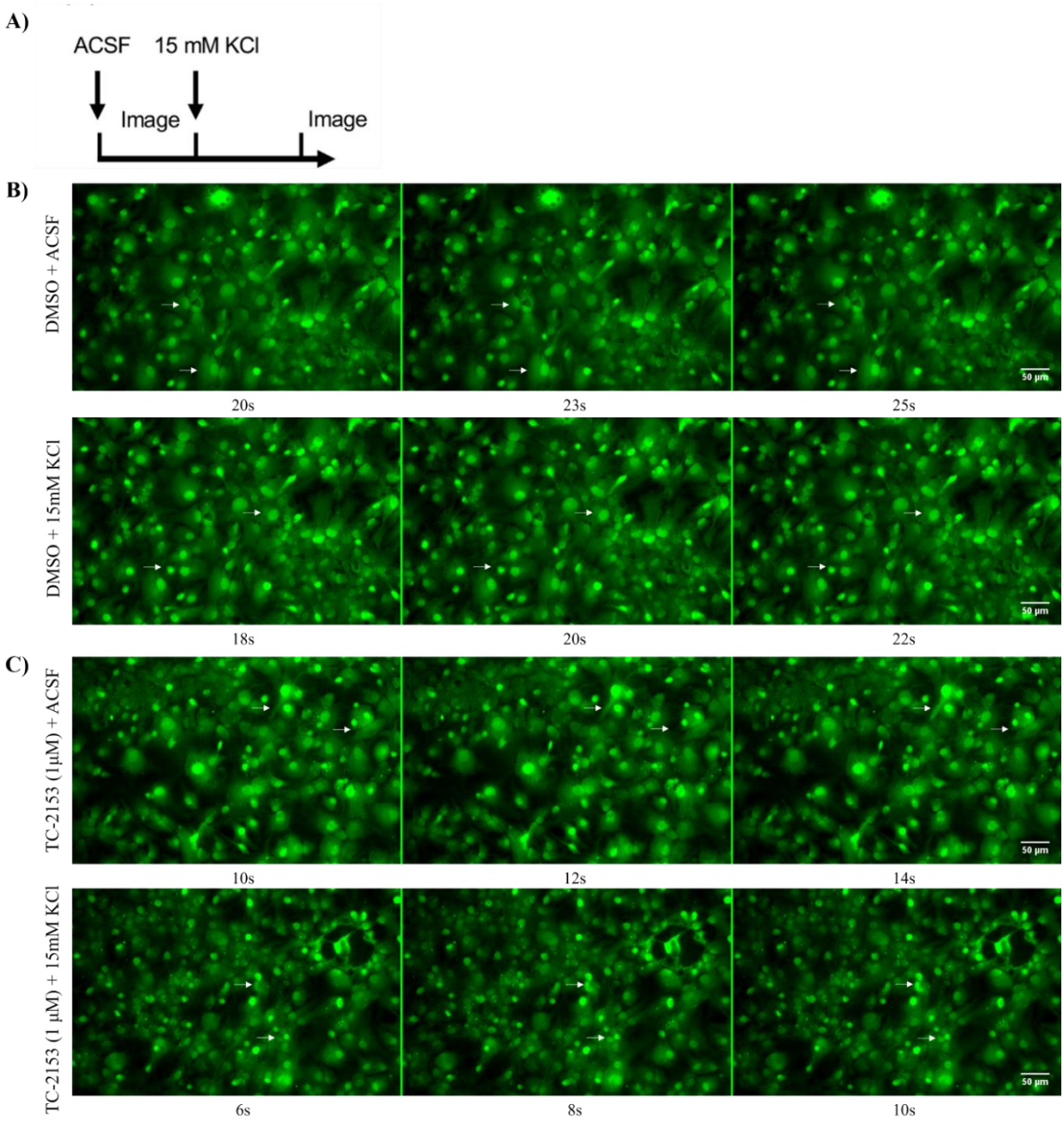

Figure C.4: Effects of TC-2153 (1 µM) in astrocyte-rich culture. **(A)** Experimental schematic of calcium imaging on astrocyte-rich cultures (containing 2% horse serum) derived from mouse NPSCs at DIV 9. The cells were incubated with DMSO or TC-2153 (1 µM) for 1 h, followed by a 30 min incubation with Oregon Green™ 488, and finally subjected to calcium imaging first in ACSF and then after 2 min of 15 mM KCl application. **(B)** Images taken of DMSO-treated cells before KCl treatment in ACSF (first panel) and after 2 min KCl treatment (second panel). **(C)** Images taken of TC-2153-treated cells before KCl treatment in ACSF (third panel) and after 2 min KCl treatment (fourth panel). White arrowheads indicate single cell activity fluctuations in each time frame. Imaged using a 20x objective with a 1.0x Tubelens. Time stamps marked beneath each image indicate when the image was taken during the 30 sec recording.

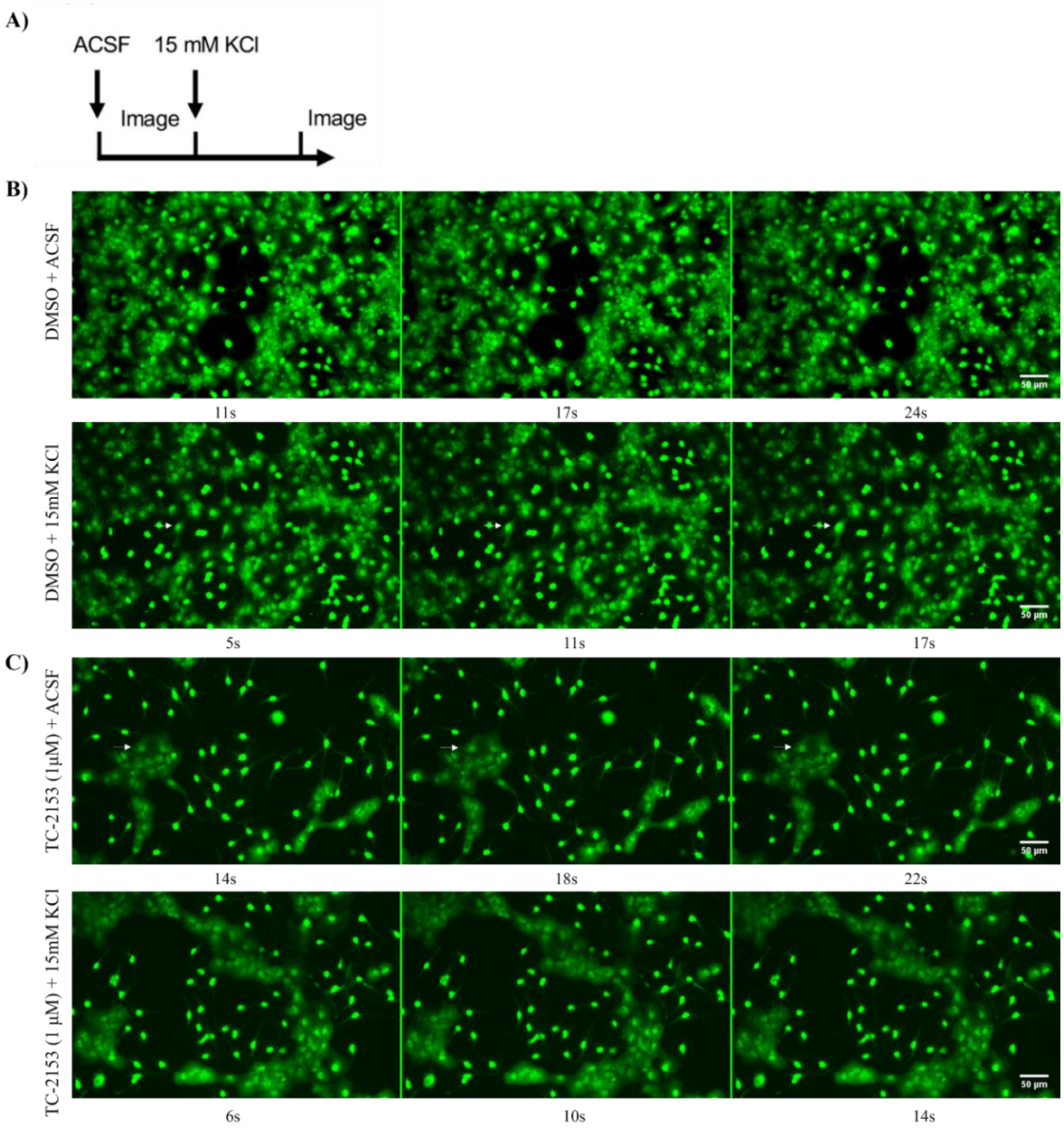

Figure C.5: Effects of TC-2153 (5 μM) in neuron-rich culture. **(A)** Experimental schematic of calcium imaging on neuron-rich cultures (containing 2% horse serum) derived from mouse NPSCs at DIV 9. The cells were incubated with DMSO or TC-2153 (5 μM) for 1 h, followed by a 30 min incubation with Oregon Green™ 488, and finally subjected to calcium imaging first in ACSF and then after 2 min of 15 mM KCl application. **(B)** Images taken of DMSO-treated cells before KCl treatment in ACSF (first panel) and after 2 min KCl treatment (second panel). **(C)** Images taken of TC-2153-treated cells before KCl treatment in ACSF (third panel) and after 2 min KCl treatment (fourth panel). White arrowheads indicate single cell activity fluctuations in each time frame. Imaged using a 20x objective with a 1.0x Tubelens. Time stamps marked beneath each image indicate when the image was taken during the 30 sec recording.

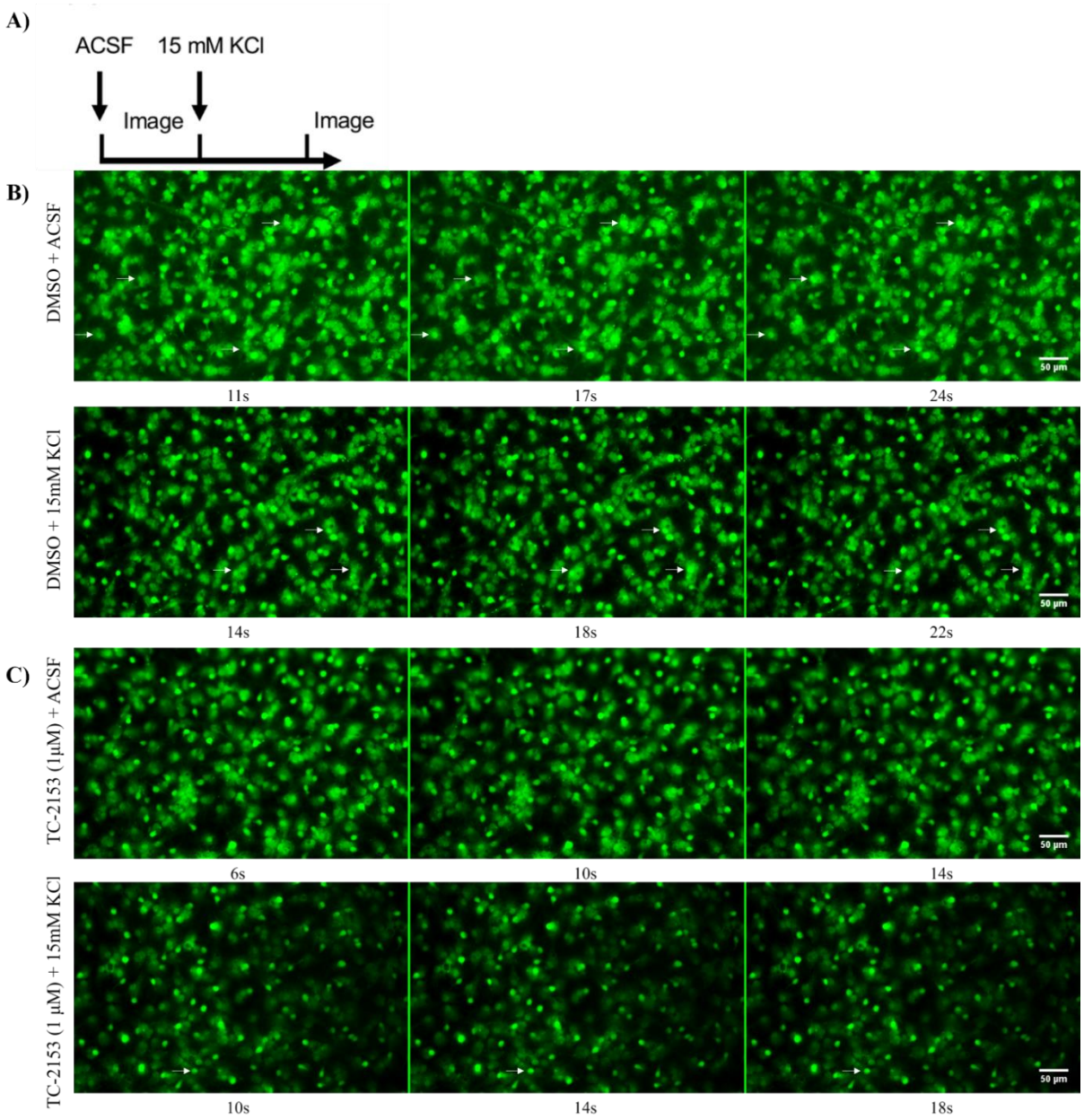

Figure C.6: Effects of TC-2153 (5 μM) in astrocyte-rich culture. **(A)** Experimental schematic of calcium imaging on astrocyte-rich cultures (containing 2% horse serum) derived from mouse NPSCs at DIV 9. The cells were incubated with DMSO or TC-2153 (5 μM) for 1 h, followed by a 30 min incubation with Oregon Green™ 488, and finally subjected to calcium imaging first in ACSF and then after 2 min of 15 mM KCl application. **(B)** Images taken of DMSO-treated cells before KCl treatment in ACSF (first panel) and after 2 min KCl treatment (second panel). **(C)** Images taken of TC-2153-treated cells before KCl treatment in ACSF (third panel) and after 2 min KCl treatment (fourth panel). White arrowheads indicate single cell activity fluctuations in each time frame. Imaged using a 20x objective with a 1.0x Tubelens. Time stamps marked beneath each image indicate when the image was taken during the 30 sec recording.

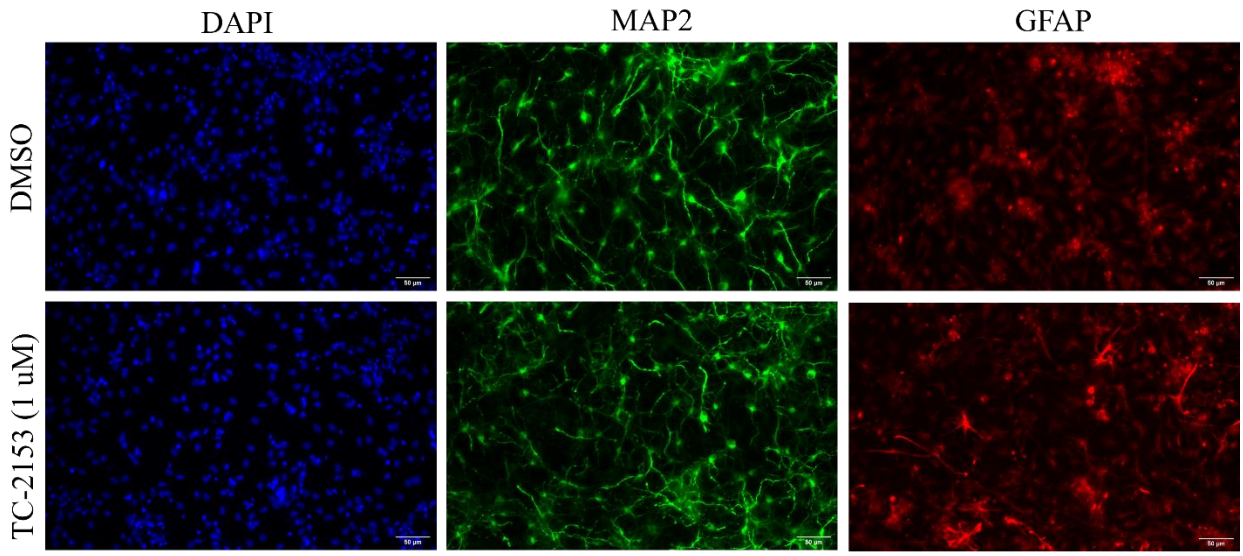

Figure C.7: Experiment #1 immunocytochemically stained neuron-rich culture derived from mouse NPSCs (containing no horse serum in 1x PBS). Imaged using a 20x objective with a 1.0x Tubelens. These cells were not previously calcium imaged and were used for the sole purpose of performing immunocytochemistry.

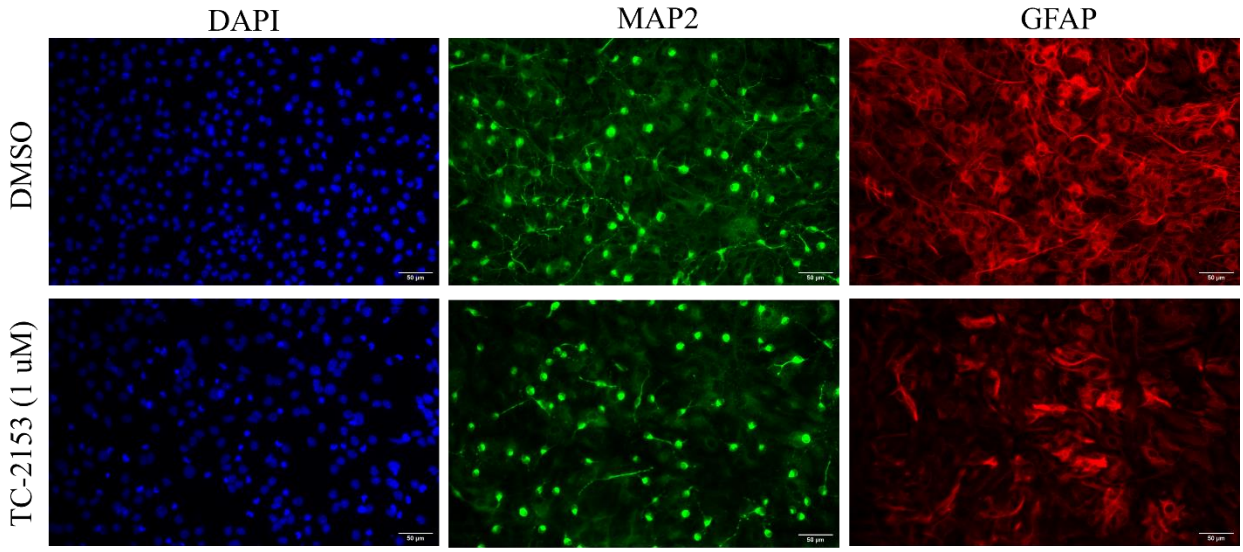

Figure C.8: Experiment #1 immunocytochemically stained astrocyte-rich culture derived from mouse NPSCs (containing 2% horse serum in 1x PBS). Imaged using a 20x objective with a 1.0x Tubelens. These cells were not previously calcium imaged and were used for the sole purpose of performing immunocytochemistry.

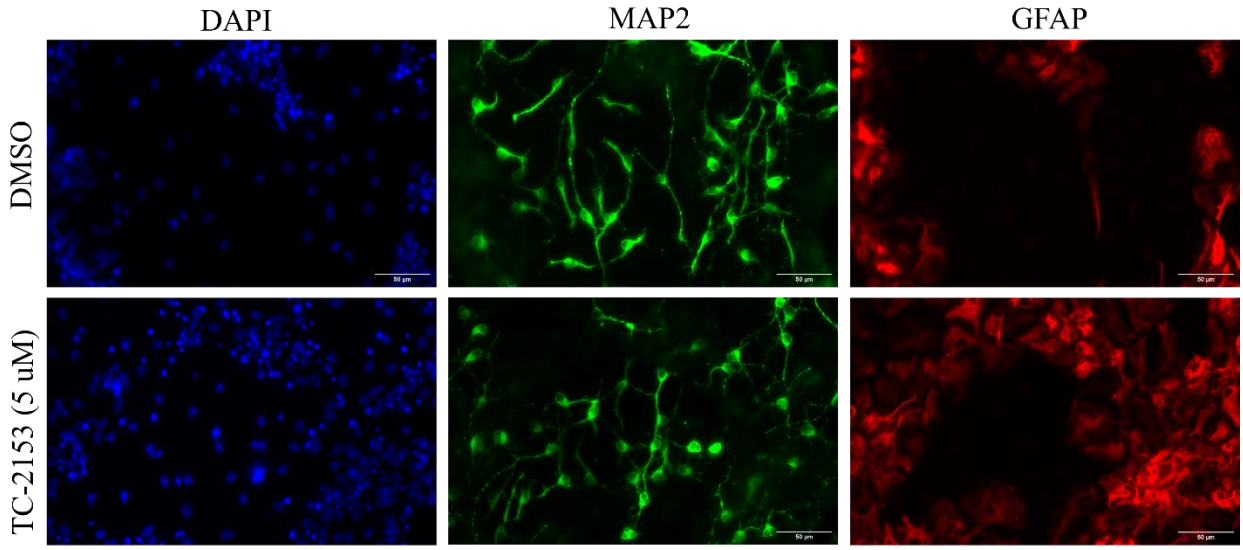

Figure C.9: Experiment #2 immunocytochemically stained neuron-rich culture derived from mouse NPSCs (containing no horse serum in 1x PBS). Imaged using a 20x objective with a 1.6x Tubelens. Cells were fixed (from dishes indicated in Fig. 5B-C) and immunostained immediately after calcium imaging experiment was complete. Images were taken 2 d later.

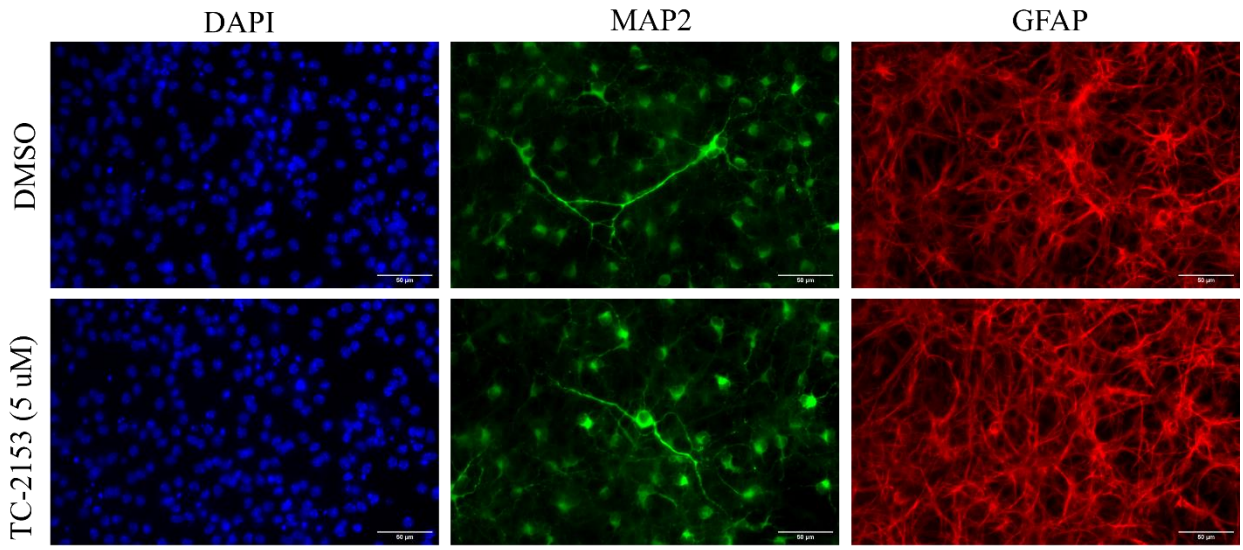

Figure C.10: Experiment #2 immunocytochemically stained astrocyte-rich culture derived from mouse NPSCs (containing 2% horse serum in 1x PBS). Imaged using a 20x objective with a 1.6x Tubelens. Cells were fixed (from dishes indicated in Fig. 5B-C) and immunostained immediately after calcium imaging experiment was complete. Images were taken 2 d later.

References

1. Spencer, S.S., *When should temporal-lobe epilepsy be treated surgically?* Lancet Neurol, 2002. **1**(6): p. 375-82.
2. Goebel-Goody, S.M., et al., *Therapeutic implications for striatal-enriched protein tyrosine phosphatase (STEP) in neuropsychiatric disorders.* Pharmacol Rev, 2012. **64**(1): p. 65-87.
3. Boulanger, L.M., et al., *Cellular and molecular characterization of a brain-enriched protein tyrosine phosphatase.* J Neurosci, 1995. **15**(2): p. 1532-44.
4. Briggs, S.W., et al., *STEP regulation of seizure thresholds in the hippocampus.* Epilepsia, 2011. **52**(3): p. 497-506.
5. Chatterjee, M., et al., *STEP inhibition reverses behavioral, electrophysiologic, and synaptic abnormalities in Fmr1 KO mice.* Neuropharmacology, 2018. **128**: p. 43-53.
6. Walters, J.M., et al., *Pharmacological inhibition of STriatal-Enriched protein tyrosine Phosphatase by TC-2153 reduces hippocampal excitability and seizure propensity.* Epilepsia, 2022.
7. Levesque, M. and M. Avoli, *The kainic acid model of temporal lobe epilepsy.* Neurosci Biobehav Rev, 2013. **37**(10 Pt 2): p. 2887-99.
8. Mouse Genome Sequencing, C., et al., *Initial sequencing and comparative analysis of the mouse genome.* Nature, 2002. **420**(6915): p. 520-62.
9. Cavaretta, J.P., et al., *Polarized axonal surface expression of neuronal KCNQ potassium channels is regulated by calmodulin interaction with KCNQ2 subunit.* PLoS One, 2014. **9**(7): p. e103655.
10. Xu, J., et al., *Inhibitor of the tyrosine phosphatase STEP reverses cognitive deficits in a mouse model of Alzheimer's disease.* PLoS Biol, 2014. **12**(8): p. e1001923.
11. Sandstrom, J., et al., *Development and characterization of a human embryonic stem cell-derived 3D neural tissue model for neurotoxicity testing.* Toxicol In Vitro, 2017. **38**: p. 124-135.
12. Dana, H., et al., *Thy1-GCaMP6 transgenic mice for neuronal population imaging in vivo.* PLoS One, 2014. **9**(9): p. e108697.

APPENDIX D: iNEURON DIFFERENTIATION PROTOCOL
(PiggyBac vectors)
(Modified by Louis Dang)

Protocol courtesy from Dr. Jack Parent lab at the University of Michigan

Day -1

Plate cells at $5x10^5$ cells using accutase per well of a 6 well plate (use Matrigel coated plates) with Y27632 (**cat# 1293823; vendor Biogems or Cayman; 13031**) (final concentration 10 uM) in E8 (**cat# No. 05940 and vendor STEMCELL Technology** or mTeSR1 (**cat# #85850 and vendor STEMCELL Technology**) media. Use 3-6 wells/line. If plating 96-well MEA plate on day 2, will likely need at least 6 wells/line.

Day 0

Remove old E8 or mTeSR1 media and replace with E8 or mTeSR1 media containing 1 ug/ml doxycycline (make a 500x 0.5 mg/mL stock from the 20 mg/mL concentrated stock)

Day 1

Change media, E8 or mTeSR1 with 1 ug/mL dox

Day 2

Remove old E8 or mTeSR1 media and replace with E8 or mTeSR1 media containing 1 ug/ml dox.

For MEA recording: coat plates with 0.2% PEI in borate buffer overnight.
Wash PEI-coated plates 4x with H20. Let dry in hood (lid off). Coat with laminin, 1:100 (~10 ug/mL) in DMEM/F12 at 37 C x 2 hours.

For short-term culture (less than 2 weeks): coat with Matrigel (**cat# 354234 and vendor Corning**) or geltrex (**cat#A1413302 and vendor Fisher**) 1:100 in DMEM/F12 (**cat# 11330-032 and vendor Invitrogen**) at 37 C x 2 hours.

Optional: If you plan to do ICCs on these neurons, you can use chamber-slide (**Lab-Tek II Chamber slide 8-well; ThermoFisher #154534**). Occasionally I used 4-well plates (**Thermo Scientific Nunclon surface No. 144444**) and put coverslips inside each well of 4-well plate.

Passage cells using accutase:

Remove old mTeSR1 media
Wash with PBS
Add 0.5 mL of warmed Accutase (**cat# A1110501 and vendor Fisher**) per well
Put at 37 deg for 4-7 mins
Add 2 mL of mTeSR per well, and gently triturate.
Collect cell suspension in 15 mL tubes
Spin 300g x 5 mins
Aspirate off media/accutase
Resuspend in 1 mL of 3N+A (B27 with Vitamin A)+ Y27632 (final concentration 10uM) + Dox (final concentration 1ug/ml) (Ratio/recipe found below)
Cell count

Freeze down cells and/or continue differentiation (these cells are considered postmitotic)

For regular plating:

*Standard thawing protocol in tissue culture is used for frozen iNeurons – but COUNT the cells before plating them down.

Replate single cell suspension at $2x10^5$ cells/mL onto PEI/laminin or matrigel coated dishes in 3N+A+Y+Dox.

If collecting samples for RT-qPCR, could plate up to $4x10^5$ cells/mL

For 6-well plate, use 2ml per well.

If collecting samples for western blot, could plate up to $3x10^6$ cells in 10cm coated dishes, use 10ml per dish.

For 96-well MEA plating:

Remove the number of cells needed to plate MEA with some excess medium
Spin 300g x 5 mins
Resuspend at $3x10^7$ cells/mL, in 3N+A+Y+Dox with 1:100 laminin
Plate 5 uL dots in center of each well
Put 5 mL of H20 around edge of plate to keep humidity
Put in 37 deg incubator for 30 mins
Gently add 3N+Y+Dox to wells (150 uL/well for 96-well plate)

For other type plates:

50K/250 uL on Mattek (**MatTek Corp, P35G-1.5-14-C**): for electrophysiology recording

50K/250 uL per well of Labtek (**ThermoFisher #154534**): for ICC

150K/5uL with 1:100 laminin on 96-MEA plate

Day 3-7 (Thaw cells from this step (Day 3), then proceed from here**)**

Change medium daily with 3N+A (B27 with Vitamin A) + dox – leave a thin layer of media so neurons don't dry out.

For MEA recording: Around day 5-7 add rat glia (1 vial per differentiation, typically 30K cells/mL of media)

Day 8

Remove all media from dish and add BrainPhys (**BP; cat# 05790, Stemcell technologies**) with SM1 (**Stemcell technologies Catalog # 05711**)/N2 **(#17502-048, Life technologies**) /0.5x Pen-Strep (50 units/mL of Pen and 50 units/mL of Strep) medium containing 20 ng/ml BDNF (**PeproTech; 450-02**), 20 ng/ml GDNF (**PeproTech; 450-10**). Optional: 0.4mM dbcAmp, which prevents cell proliferation (**Sigma; D0627-1**)

Day 9+

Feed M/W/F with 50% volume of BP+SM1/N2/P/S/BDNF/GDNF(and optional dbcAMP), with MEA recordings on these days – take half the media out, then add in half feeding media.

Optional: Add 1:1000 geltrex to help neurons to stick to the plate during each medium change

For MEA recording: around day 9-14 (usually on a Friday), infect with CamKIIa-GFP **lentivirus** (1:200-500 final dilution)

Day 21: Fix Labteks for ICCs

Day 21-28: Do electrophysiology. Some lab members do it on ~day35.

3N+A recipe:

Media:
3N+A medium: 1:1 mixture of N2 and B27 (with vitamin A) media

N2 medium

500 mL	Component
487.5 mL	DMEM/F12 with HEPES (**cat# 11330-032 and vendor Gibco/Invitrogen**)
5 mL	NEAA (**11140-050, Thermo fisher**)
5 mL	N2 (**#17502-048, Life technologies**)
2.5 mL	Pen/Strep (**15140122, Invitrogen**)
5 mL	Glutamax (**Gibco; 35050-061**)
250 uL	Insulin (**cat# I9278, sigma**)
3.6 uL	BME (or use 1 mL of 1000x GIBCO/**ThermoFisher 21985023**)

B27 medium

500 mL	Component
477.5 mL	Neurobasal medium **(#21203-049, Gibco/Invitrogen**)
5 mL	NEAA (**11140-050, Thermo fisher**)
10 mL	B27 with Vitamin A (**Thermo fisher; 17504044**)
2.5 mL	Pen/Strep
5 mL	Glutamax (**Gibco; 35050-061**)

Mix 250 mL each and sterile filter

Freezing medium for D2 iNeurons:

10 mL	Component
6.5 mL	3N+A (65%) (in house made)
2.5 mL	KOSR (25%) (**cat# 10828-010 Invitrogen**)
1 mL	DMSO (10%)